A Study of In Situ Outer Hair Cells from the Adult Mammalian Cochlea

Sarah Jane Richmond

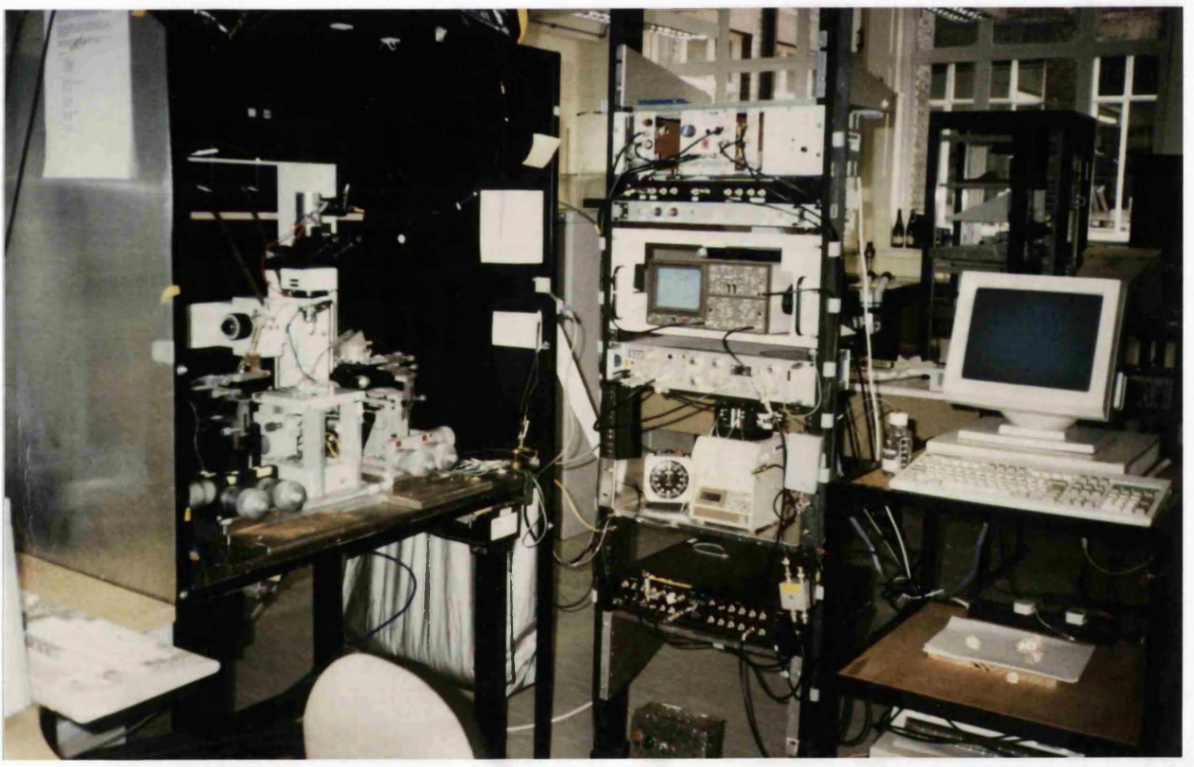

A thesis submitted to University College London in accordance with the requirements of the degree of Doctor of Philosophy in the Faculty of Science

Department of Physiology
1999

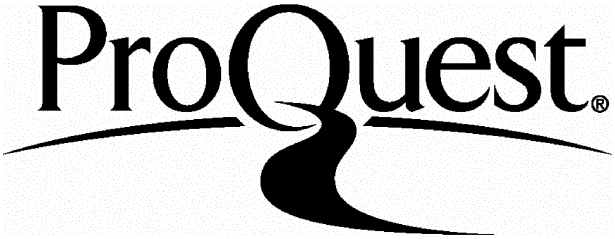

If.....

If you can keep you head when all about you
Are losing theirs and blaming it on you,
If you can trust yourself when all men doubt you,
But make allowances for their doubting too;
If you can wait and not be tired by waiting,
Or be lied about, don't deal in lies,
Or be hated, don't give way to hating,
And yet don't look too good, nor talk too wise:

If you can dream - and not make dreams your master;
If you can think - and not make thoughts your aim;
If you can meet with Triumph and Disaster
And treat those two imposters just the same;
If you can bear to hear the truth you've spoken
Twisted by knaves to make a trap for fools,
Or watch the things you gave your life to, broken,
And stoop and build 'em up with worn-out tools:

If you can make one heap of all your winnings
And risk it on one turn of pitch-and-toss,
And lose, and start again at your beginnings
And never breathe a word about your loss;
If you can force your heart and nerve and sinew
To serve your turn long after they are gone,
And so hold on when there is nothing in you
Except the Will which says to them: "Hold on!"

If you can talk with crouds and keep your virtue,
Or walk with Kings - nor lose the common touch,
If neither foes nor loving friends can hurt you,
If all men count with you, but none too much;
If you can fill the unforgiving minute
With sixty seconds' worth of distance run,
Yours is the Earth and everything that's in it,
And - which is more - you'll be a Man, my Son!

Rudyard Kipling
(1865-1939)

Abstract

This thesis investigates three characteristics of outer hair cells (OHCs) of the adult mammalian cochlea. The first investigation compared the basolateral membrane K^+ channel expression of turn 4 (T4) and turn 1 (T1) OHCs, cells that respond to low and high frequency sound respectively. The second and third studies investigated two further aspects of T4 OHCs, the equivalent concentration of endogenous Ca^{2+} buffer and the characteristics of the mechanoelectric transduction (MET) current. OHCs *in situ* were recorded from using the whole-cell patch-clamp technique.

For the first study, the kinetics, pharmacology and Ca^{2+} sensitivity of T4 and T1 OHC K^+ channels were investigated. This work demonstrated that T4 OHCs express at least three types of K^+ channels, termed I_{kss}, I_{kCa} and I_{kT4}. In contrast, T1 OHCs express different ion channels that exhibit faster onset kinetics, different pharmacology and an insensitivity to raised intracellular Ca^{2+} concentrations compared to those channels expressed in T4. These T1 channels have been termed I_{kT1} and $I_{k,n}$. The characteristics of these ion channels are discussed in relation to the particular sound frequency to which the OHC best responds.

The equivalent concentration of endogenous Ca^{2+} buffer in T4 OHCs was investigated by using the time constant of current onset as a tool to compare the effects of various concentrations of BAPTA, introduced into the cell via the patch pipette, with those of the endogenous buffer, assayed using the perforated-patch technique. The concentration of endogenous Ca^{2+} buffer was found to be equivalent to the Ca^{2+} binding capacity of 2.1 mM BAPTA. This value converts to a Ca^{2+} binding ratio of 10,500. These results indicate that OHCs posess an enormous Ca^{2+} buffering capacity, have a low free $[Ca^{2+}]_i$ and a huge pool of bound Ca^{2+} within their cytosol.

Finally, the biophysical properties of the MET current of T4 OHCs were investigated. The few recordings obtained were variable but indicated that MET currents *in situ* are small (60 pA), limited in their onset kinetics only by the kinetics of the fluid-jet stimulus and run-down over a period of 20 minutes in the whole-cell recording configuration. These currents were found to be physiologically effective in activating the motile response of the OHC.

Acknowledgements

I would like to thank Professor Jonathan Ashmore for the infectious enthusiasm he shows for his subject and for the unlimited encouragement and advice he has provided to me throughout my PhD.

I would also like to thank Doctors Daniel Jagger and Gwénaelle Géléoc for the many informative discussions I have had with them, for their support and friendship but above all for making the laboratory an enjoyable place to work.

I would like to thank the coaches and members of the University of Bristol and Imperial College, London Dancesport Teams who provided a lively, energetic environment where I could get away from my PhD and immerse myself in my friends and my dancing.

Finally, I would like to thank my Mum and Michael for their loving support and encouragement and for their continual belief in me.

Declaration

The investigations described in this thesis are my own work. The experiments were carried out in the Department of Physiology, University of Bristol and Department of Physiology, University College London between October 1995 and December 1998 under the supervision of Professor J.F. Ashmore FRS.

Sarah J. Richmond
1999

Contents

List of Figures and Tables

List of Equations

Abbreviations

4AP	4-aminopyridine
ADP	Adenosine diphosphate
ATP	Adenosine triphosphate
BAPTA	1,2-bis(2-aminophenoxy)ethane-N,N,N',N'-tetraacetic acid
C_m	Intrinsic membrane capacitance
C_{stray}	Stray capacitance of patch pipette and pipette holder
ε	Dielectric constant
E_k	Equilibrium potential for potassium
E_{rev}	Reversal potential
f_o	Corner frequency for a low pass filter
γ	Slope conductance
HBS	HEPES buffered saline
HEPES	N-(2-hydroxyethyl)piperazine-N'-(2-ethanesulphonic acid)
I_c	Capacitative current
IC_{50}	Half blocking concentration for a drug on its receptor
IHC	Inner hair cell
$I_{k,n}$	Current active around V_z in T4 and T1 OHCs
$I_{k(Ca)}$	Calcium-activated potassium current
$I_{k,L}$	Delayed-rectifier current found in Type 1 vestibular hair cells
I_{kT1}	Current activated above -30 mV in T1 OHCs
I_{kT4}	4AP-sensitive current activated about -40 mV in T4 OHCs
$I_{k,UR}$	Ultra-rapid delayed-rectifier potassium current
I_m	Membrane current
LJP	Liquid Junction Potential
K_A	A-type potassium channel
K(Ca)	Calcium-activated potassium channel
OHC	Outer hair cell
P_o	Open probability of a channel
Q	Electrical charge
PBS	Phosphate buffered saline
R_f	Feedback resistor
R_m	Variable membrane resistance
R_s	Series resistance
τ	Time constant for an exponential function
TEA	Tetraethylammonium
T4	Turn 4, apical, low frequency turn of the cochlea
T1	Turn 1, basal, high frequency turn of the cochlea
UV	Ultra violet light
V_{cmd}	Command potential
V_h	Holding potential
V_m	Cell membrane potential
V_p	Pipette potential
V_z	Zero current potential of cell

Chapter 1

General Introduction

1.1 The mammalian cochlea

The mammalian cochlea acts as a Fourier analyzer, decomposing sound-related vibrations in to individual time- and amplitude-varying frequency components. These vibrations are transduced in to electrical signals that are sent, via the auditory nerve, to the brain. The exquisite sensitivity of the mammalian cochlea to discriminate between individual sound frequencies is exemplified by the ability of young humans to differentiate between two sounds whose frequencies are just 0.2 % apart (Dallos, 1996).

The first part of this chapter demonstrates that the extraordinary sensitivity of the mammalian cochlea relies on outer hair cells (OHCs), specialized sensory and motor cells, acting as highly localized, micromechanical amplifiers. The second part of this chapter introduces the experiments undertaken on OHCs for this thesis.

1.2 The central role of OHCs in cochlear physiology - an historical perspective.

The cochlea is embedded within the temporal bone of the skull and consists of a three compartment tube coiled around a central axis, or modiolus. The three compartments are fluid filled and are known as the scala vestibuli, scala media and scala tympani (Figure 1.1). The scala media runs centrally through the coiled tube. It is bounded laterally by a membrane known as the stria vascularis and is separated from the overlying scala vestibuli by Reissner's membrane. It is further separated from the underlying scala tympani by the basilar membrane.

Sound-related vibrations are transmitted to the cochlea via the outer and middle ears. In the cochlea they are represented as pressure fluctuations of the cochlear fluids. The following section explains how the cochlea uses these

pressure fluctuations to decompose incoming sound in to its individual frequency components.

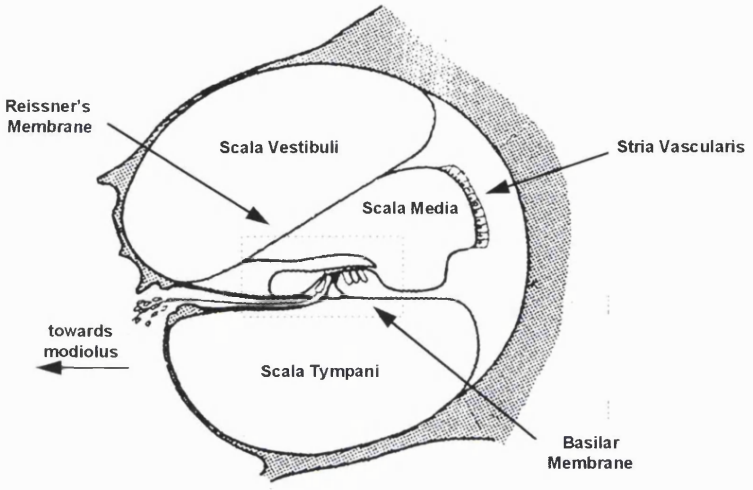

Figure 1.1 A cross-section of the cochlear duct showing the three scalae. The dotted line represent that pert of the cochlea shown in Figure 1.4. Amended from Figure 2, Chapter 1, Cochlear Nonlinearity, Kanis, (1995).

1.2.1 The Basilar Membrane: a passive frequency analyzer

The mechanism of hearing and the analysis of sound was little understood before the mid-nineteenth century. Herman Helmholtz was the first investigator to recognise the importance of the basilar membrane in the spectral analysis of sound. He proposed that the basilar membrane comprised a series of independent resonators that were distributed along the length of the cochlea according to their frequency. These would resonate independently of one another in response to a particular frequency of sound, much like the strings of a piano.

"The membrana basilaris...seems to me to furnish a very important mechanical relation, namely that this membrane in its natural connection admits of being tightly stretched in the transverse direction from the modiolus to the outer wall of the cochlea, but can have little tension in the direction of its length, because it could not resist a strong pull in this direction... If the tension in the direction of its length is infinitesimally small in comparison with the tension in the direction of the breadth, then the radial fibres of the basilar membrane may be approximately regarded as forming a system of stretched strings.... In that case, the laws of their motion would be the same as if every individual string moved independently of all others... Consequently any exciting tone would set part of the membrane in to sympathetic vibration"

extract from a translation of 'On the Sensations of Tone'
Herman Helmholtz (1885) pp 146

What Helmholtz could not understand was how sound communicated itself to these individual resonators.

It was not until the pioneering work of Georg von Békésy, working in the late 1930's and 40's, that the fundamental ideas of frequency analysis by the cochlea were developed (von Békésy, 1960). In a series of experiments using temporal bone specimens from human and animal cadavers, von Békésy monitored the movement of the cochlear partition to a series of pure tone, low frequency sounds. These experiments required that high sound intensity levels were used in order that vibrations of the partition could be seen with a light microscope. He observed that:

a) vibration of the stapes gave rise to a travelling wave of fluid displacement in the cochlea
b) for a pure tone, the displacement grew in amplitude as it travelled towards the apex of the cochlea , then beyond a certain point, it died out rapidly.
c) low frequency sounds peaked near the apex of the cochlea, that part of the coil furthest away from the middle ear, whereas low frequency sounds peaked near the base of the cochlea.

Figure 1.2 demonstrates these salient results of von Békésy's experiments.

These experiments confirmed the importance of the basilar membrane in the spectral decomposition of sound. They demonstrated that the basilar membrane could respond to different frequencies of sound with vibration patterns that peaked at different points along its length, according to the frequency of the incoming sound. This mechanism relied on hydrodynamic coupling between the incoming sound-related vibration and basilar membrane motion, the key factor not understood by Helmholtz.

The origins of the frequency-place map are heavily dependent on the graded changes in the shape and properties of the basilar membrane along the length of the cochlea. At its base, the basilar membrane is narrow and stiff whilst in the apex, it is wide and less stiff (Pickles, 1988). These changes reflect changes in the ratio of extracellular matrix material to ground substance fibres such as collagen and fibronectin (Slepecky, 1996). Thus, at the base of the

cochlea near the oval window, basilar membrane vibrations are stiffness limited whereas at the apex, they are mass limited. As a result, a given pressure wave will grow in amplitude towards the apex until it reaches a peak where the stimulus frequency matches the resonant frequency of one part of the basilar membrane. Beyond this point, the wave does not propagate significantly due to mass limiting forces within the partition and the vibrations die away.

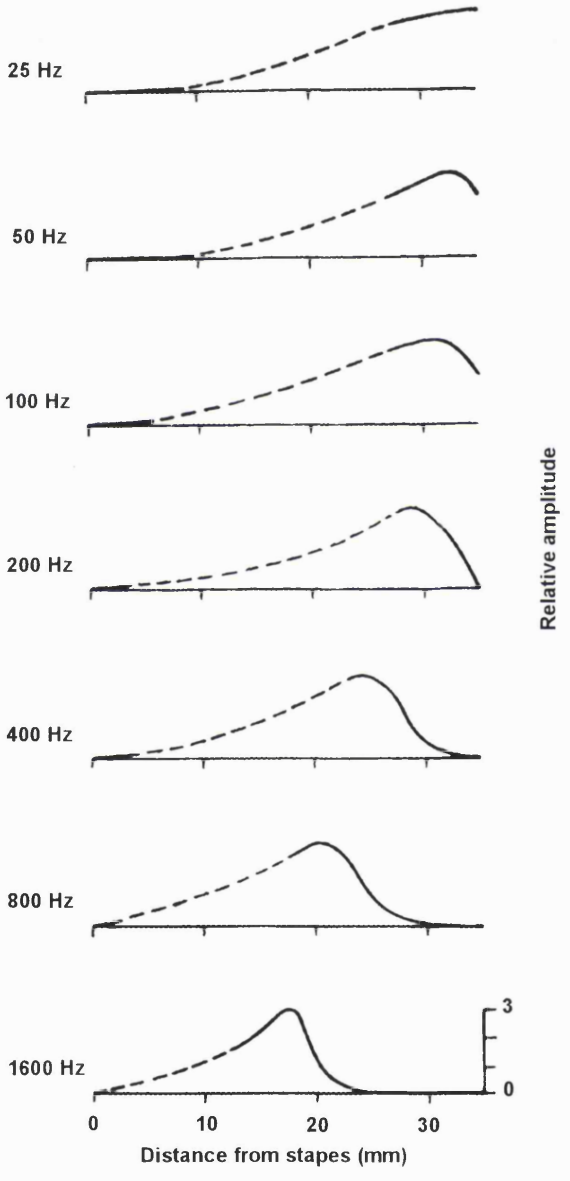

Figure 1.2 Travelling wave envelopes in the cochlea for tones of different frequency. Solid lines show the actual measurements made by von Békésy, the dashed lines are von Békésy's extrapolations. From Experiments in Hearing, von Békésy, (1960).

von Békésy's results made significant inroads in to understanding how the cochlea discriminates between different frequencies of sound. However, his

results suggested that the basilar membrane was not sharply tuned to one particular frequency as the peak of the travelling wave was very broad. These results did not explain the ability of subjects to discriminate between two sounds whose frequencies are very close together or the frequency selectivity observed in individual auditory neurones (Galambos and Davis, 1943).

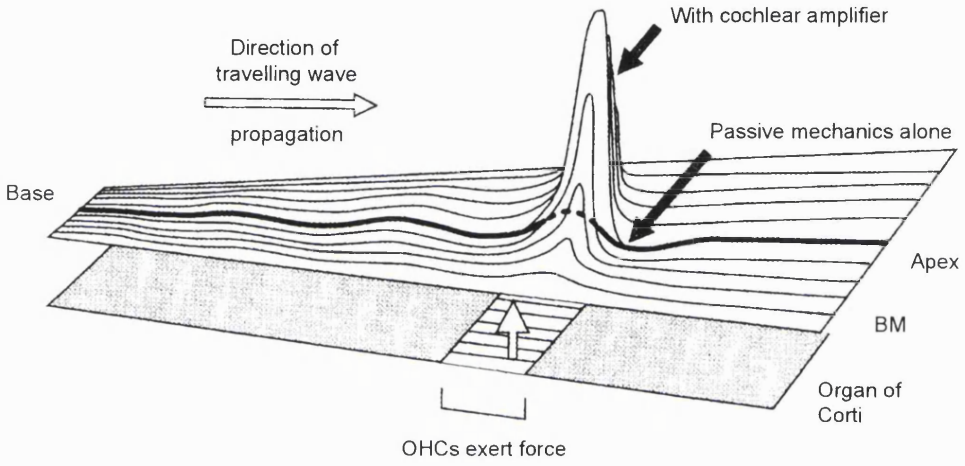

Figure 1.3 Wave motion in the cochlea. Sound entering the cochlea sets up a travelling wave that propagates along the basilar membrane from the stapes at the base. The motion at the peak is enhanced, up to 100 times by the effects of cochlear amplification (From Ashmore and Kolston, 1994).

The most recent advances in our understanding of cochlear mechanics have relied on the development of highly sophisticated experimental techniques such as the Mössbauer technique (Sellick, Patuzzi and Johnstone, 1982) and laser interferometry (Mammano and Ashmore, 1995). These allow nanometer deflections of the cochlear partition to be measured in response to very low sound pressure levels, rather than relying on the extrapolation of this information from much higher sound intensity levels, the mechanism relied on by von Békésy. These techniques have demonstrated that the travelling wave of a recently excised cochlea differs both qualitatively and quantitatively from the travelling waves observed by von Békésy. First, the wave was enhanced in amplitude and peaked over a very narrow (500 μm), sharply defined region of the basilar membrane (Figure 1.3). Second, the sharp tuning of the cochlea was critically dependent on the intensity of the incoming sound, disappearing at sound pressure leves beyond 60 dB (Johnston, Patuzzi and Yates, 1986, Khanna and Leonard, 1982, Sellick, Patuzzi and Johnston, 1982). Third, the above two characteristics depend critically on the physiological condition of the

cochlea, becoming less obvious the older the cochlea (Johnston, Patuzzi and Yates, 1986).

The above results demonstrated that within a recently excised cochlea, the basilar membrane is as sharply tuned as nerve fibres. These results provided auditory researchers with one of the most important findings of the last few decades which is that within the cochlea, there is some mechanism which enhances the motion of the basilar membrane to create larger, more sharply tuned vibration patterns than those observed by von Békésy. This mechanical enhancement of cochlear mechanics has become known as the 'cochlear amplifier' (Davis, 1983). By the early 80's, auditory research had obtained an additional focus, that of finding the cellular candidate responsible for this localized enhancement of basilar membrane motion. The most widely accepted candidate pinpoints the OHC of the organ of Corti as the basis of this amplification.

1.2.2 The organ of Corti

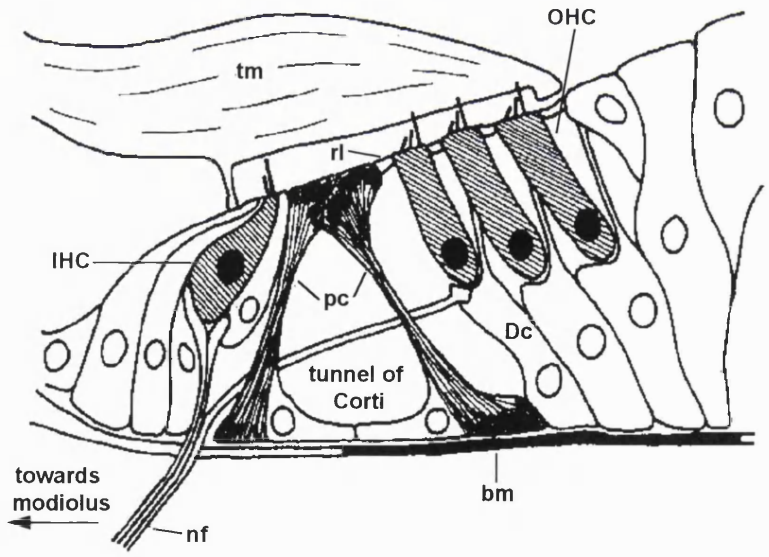

Figure 1.4 A cross-sectional representation of the organ of Corti. tm = tectorial membrane, rl = reticular lamina, Dc = Deiter's cell, pc = pillar cell, bm = basilar membrane, nf = nerve fibres. From Holley, 1990.

The organ of Corti is the sensory epithelium of the cochlea. It is a highly repeating structure attached to the basilar membrane. The main cellular components of the organ of Corti are hair cells, their nerve endings and supporting cells. These are most clearly observed in a cross-section of the

cochlear duct (Figure 1.4). The organ of Corti contains two distinct populations of hair cells, inner hair cells (IHCs) and OHCs. IHCs are aligned in a single row on the modiolar side of the tunnel of Corti and are innervated by 90-95% of afferent fibres of the auditory nerve (Brown, 1987a, Spoendlin, 1972). They are considered to be the true sensory cells of the cochlea, and fulfil the second role of the cochlea, that of sending time- and amplitude-varying information about individual frequency components of incoming sound to the brain. This is achieved by converting sound-related vibrations into electrical signals by a mechanism known as mechanoelectric transduction (Chapter 7).

OHCs form three parallel rows on the stria vascularis side of the organ of Corti. These cells are cylindrical and are supported by Deiter's cells. Their length varies both radially and longitudinally through the cochlear partition (Poujol, Lenoir, Ladrech, Tribillac, Rebillard, 1992). OHCs are mainly innervated by efferent nerve fibres (Kimura and Wersäll, 1962).

1.2.3 The outer hair cell: active frequency analysis

The key discovery that focused investigators on the idea that OHCs were the cellular basis of the cochlear amplifier was the demonstration that these cells changed length upon electrical stimulation (Brownell, Bader, Bertrand and de Ribaupierre, 1985). Isolated OHCs were observed to elongate on hyperpolarization and contract on depolarization. Subsequent investigations demonstrated that these length changes were effective at audio frequencies up to 25 kHz (Ashmore, 1987, Dallos, Evans and Halliworth, 1991, Gale and Ashmore, 1997). Thus, a new theory for cochlear mechanics was born that suggested OHCs function both as sensory and motor cells. In responding to sound-related vibrations of the basilar membrane, OHCs at the peak of the travelling wave change length and feedback forces to the system to further enhance and sharp tune the motion of the basilar membrane by overcoming the damping of the cochlear partition. Thus, while the BM is tuned according the mechanism of von Békésy, OHCs alter the mechanical impedance of the basilir membrane leading to enhanced tuning that affects the mechanical input to the IHCs.

This fundamental work on OHCs explained a great deal or research conducted in the 70's and early 80's that demonstrated the necessity of OHCs

for normal cochlea function. In the absence of OHCs, either through mechanical damage or pharmacological manipulations, cochlea tuning and sensitivity was lost (Dallos, Billone, Durrant, Wang, Raynor, 1972; Ryan and Dallos, 1975; Schmiedt, Zwislocki and Hamernik, 1980). However, at the time, it was not clear why this should occur since OHCs received only 5% of afferent neurones and were clearly not the primary sensory cell of the cochlea.

For the proposed amplification process to be effective, length changes by OHCs must be sufficient to produce forces that will overcome damping within the cochlear partition. Although mathematically it appears that OHCs can generate sufficient forces *in vivo* to affect cochlear mechanics (Ashmore, 1992, Iwasa and Chadwick, 1992), such calculations cannot take in to account all of the mechanical constraints that contribute to the inherent damping of the cochlear partition.

Direct evidence demonstrating the OHC are a realistic component of this un-damping mechanism have been provided in a series of experiments where electrical stimulation across the organ of Corti was observed to generate displacements of the basilar membrane (Nuttall and Dolan, 1993, Xue, Mountain and Hubbard, 1993). Such electrical stimulation was designed to specifically activate OHCs, the only cochlear cells that have so far been reported to respond mechanically to changes in voltage across their membrane. More detailed experiments investigated the simultaneous movement of the basilar membrane and the reticular laminar (Mammano and Ashmore, 1993). This work demonstrated that electrical stimulation causes the basilar membrane and the reticular lamina to move simultaneously together or apart. This implies that a force within the organ of Corti can alter the geometry of the partition, a result most easily explained by OHC length changes. OHC length changes within the organ of Corti were observed more directly by digital subtraction of images before and during a step change in potential in OHCs patched using the whole-cell patch-clamp techniqe (Mammano, Kros and Ashmore, 1995). One shortfall with these experiments is that by opening up the cochlea, the mechanical behaviour of the system will inevitably be altered.

The above experiments suggest that whilst the basilar membrane is tuned according the mechanism proposed by von Békésy, its motion can be modified by changes in OHC length. These changes are both fast enough and

strong enough to sharpen the sound-induced displacements of the basilar membrane. This enhanced frequency selectivity affects the input to IHCs and the information relayed to the auditory nerve via afferent synapse. The direct effect of OHC action on the input to IHCs has been demonstrated in a series of experiments by Brown and Nuttall (1984) who recorded from IHCs whilst stimulating the crossed olivocochlear bundle. Thus, the OHC can be considered the cellular basis of the cochlear amplifier.

1.2.4 The molecular basis of OHC motility

Considerable effort is now being invested in to establishing how OHCs perform their function. Central to this issue is the identification of the molecule responsible for OHC motility. The speed of motility in itself suggests that the molecule works independently of intermediate biochemical steps such as the binding of Ca^{2+} or the hydrolysis of ATP. Thus, actin based motility is ruled out. The voltage-dependence of the process suggests that the molecule is located in the plasma membrane where it will be able to experience the electric field across the membrane. A high density of integral membrane proteins in the lateral plasma membrane is a distinguishing feature of OHCs (2500 - 6000/μm^2). A major fraction of these proteins are suggested to account for the motor elements (Kalinec, Holley, Iwasa, Lim and Kachar, 1992). The most likely candidate molecules for the motor protein that work at the necessary speeds are modified ion channels or transporters that can effect voltage-dependent shape changes in OHCs. Based on this theory, gating currents have been recorded from OHCs when most of the basolateral and stereocilial ion channels have been blocked. Gating currents follow a very similar time course and have a similar voltage dependence to that of the cell length changes (Ashmore, 1990, Gale and Ashmore, 1997, Santos-Sacchi, 1992). Gating currents can be mapped to the basolateral membrane of OHCs (Huang and Santos-Sacchi, 1993). Both the gating currents and OHC length changes are simultaneously inhibited by extracellular gadolinium ion, experimental evidence that the two may be linked. One of the most recent theories being pursued is the idea that the motor molecule may constitute a modified glucose transporter (Géléoc and Ashmore, 1998).

1.3 Experiments undertaken on OHCs

1.3.1 A focus on three characteristics of OHCs

The work presented in this thesis focuses on OHCs at the cellular level. It exploits the use of an *in situ* preparation that maintains hair cells within the organ of Corti, allowing the precise location of the hair cell to be identified. This preparation provides a valuable bridge between isolated OHC preparations and the intact system *in vivo*. This thesis is outlined in the following manner. Chapter 2 describes the general methods used in these investigations. Chapters 3 to 5 describe the voltage-dependent ion channel expression in turn 4 (T4) and turn 1 (T1) OHC basolateral membranes. The characteristics of these ion channels are discussed in relation to the frequency of sound to which the respective OHC best responds. Chapter 5 investigates the equivalent concentration of endogenous Ca^{2+} buffer in T4 OHCs. Finally, Chapter 6 describes an investigation in to the characteristics of T4 OHC mechanoelectric transduction (MET) currents. Individual results chapters present a more detailed introduction to each of these investigations.

The work presented in this thesis aims to improve our understanding of how OHCs in the adult mammalian cochlea perform their function as amplifiers of basilar membrane motion. This function is thought to provide adult mammals with the ability to discriminate clearly between the different components of a complex sound and thus distinguish environmentally and biologically significant sounds.

Chapter 2

General Materials and Methods

2.1 The *in situ* preparation

2.1.1 Removal of the temporal bone

Adult male and female albino guinea-pigs weighing 200-300g were killed by rapid cervical dislocation and decapitated. The right and left temporal bones (bullae tympanica), containing the middle and inner ear regions, were removed from the head by leverage with a pair of scissors. Connective tissue and muscle tissue still attached to the temporal bones were removed using bone nibblers. Only the temporal bone from the left side of the head was used in these experiments as the equipment was optimally positioned for recording from one particular coil. This also ensured that preparations were fresh.

2.1.2 Mounting in the recording chamber

The bony outer shell of the cochlea was exposed by cracking open and peeling back the ventral surface of the bulla with a pair of bone nibblers. With the apex of the cochlea facing upwards, the bulla was firmly mounted on the end of the rotating arm of the recording chamber (Figure 2.1) using wax (L'atelier du Vin, France). This was melted on to the dorsal surface of the bulla before transferring the bulla to a screw (M2 stainless steel machine screws, RS, UK) at the end of the rotating arm. As the wax cooled and hardened, small adjustments to the position of the bulla could be made to ensure optimal orientation of the epithelium under the microscope. The recording chamber was then filled with standard phosphate buffered saline (standard PBS) (Section 2.2.1 and Table 2.1) and viewed under a dissecting microscope (Wild L7A, Switzerland).

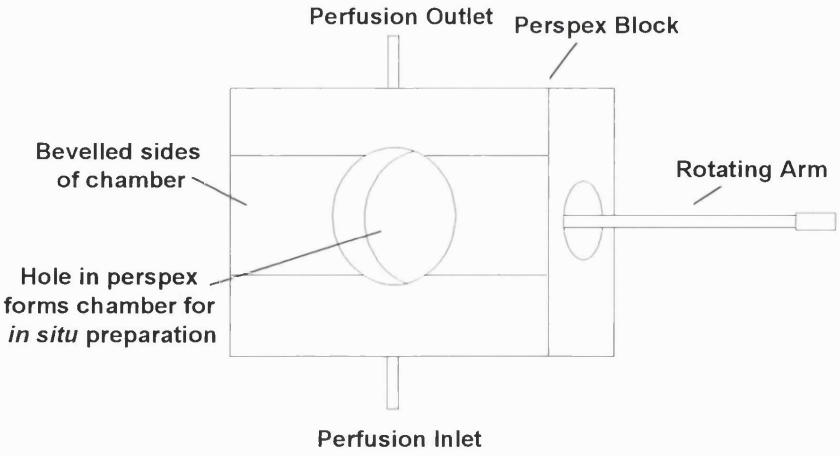

Figure 2.1 The Recording Chamber. The rotating arm to the right of the figure allowed 3D rotation of the preparation which was important to obtain good visualization of the organ of Corti. Bevelled sides to the chamber improved access of the patch and puff pipette to the preparation.

2.1.3 Microdissection of the organ of Corti

Cochleae were dissected to expose either the most apical turn (T4) or the most basal turn (T1) of the sensory epithelium. In both cases, the bony shell of the cochlea was scored using a scalpel and gently peeled away with a pair of fine forceps to a level just below the turn of interest. The underlying organ of Corti was easily recognizable, particularly in the more apical turns of the cochlea, due to the reflection of light by lipid globules in the Hensens's cells. Access to the sensory epithelium in T1 was obtained by removing the overlying turns by cutting through the modiolus between turns 1 and 2.

For both T4 and T1 preparations, the organ of Corti was exposed by gently peeling away the stria vascularis using a pair of very fine, curved tip forceps (T 5014, Dumont, UK) thus allowing Reissner's membrane to be peeled back from the sensory epithelium towards the modiolus. Finally, the tectorial membrane was removed using an etched tungsten wire (TW10-3, Clark Electromedical Instruments, UK). This process was most successful if begun at a point either more apical or more basal to the section of cells to be recorded from, as raising the membrane sometimes damaged the underlying epithelium. However, once lifted, large sections of membrane tended to free themselves. The dissection was completed within 10 minutes of removing the bulla from the guinea-pig.

2.1.4 Visualization of the organ of Corti

The recording chamber was mounted on the adjustable stage of a hybrid, upright microscope (Zeiss, Germany; M-2A, Microinstruments, UK). The epithelium was illuminated by light from a 1 mm optical fibre that was positioned next to the Hensen's cells of the organ of Corti. Careful positioning of the fibre was permitted by mounting it on a manipulator that was mobile in the x, y and z-planes. The light was filtered below 510 nm to avoid burning the cells. The epithelium was located using a X5 objective (0.15, Cooke) but the magnification was increased to X40 (Achroplan 0.75 NA, water immersion, working distance 1.6 mm, Zeiss, Germany) for patch-clamp experiments. Light captured by the objective passed through a CCD camera (Watec, USA) linked to the microscope and an image enhancer (CE-3, BRSL, UK) before being displayed on a black-and-white monitor (VM-902, Hitachi, Japan). Critical positioning of the optical fibre caused light to sweep over the epithelium giving a clear view of the cell boundaries and their stereocilia on the monitor. This method of cell visualization was vitally important because of the poor quality of the image observed through the eye pieces alone due to the random scattering of incident light off an epithelium that is poorly optically reflective (Khanna, Willemin & Ulfendahl, 1989).

2.1.5 Removal of Hensen's Cells

In all experiments, except during the investigation of mechanoelectric transduction, Hensen's cells were removed to improve access to the basolateral membranes of OHCs. This was achieved using a slight variation on the technique developed by Edwards, Konnerth, Sakmann and Takahashi (1989) for accessing cells in tissue slices. Oversized patch pipettes (tip diameter ~5 mm) filled with PBS were placed in a normal patch pipette holder and brought down to rest on the outer edge of the Hensen's cells using a Huxley-type micromanipulator (Huxley-Bertram, Cambridge, UK). Gentle suction was applied to the back of the pipette by mouth to secure the supporting cells in the tip of the pipette. Using the fine controls on the micromanipulator, the pipette was gently pulled away from the organ of Corti at an angle parallel to the long axis of the OHCs. Hensens's cells could be clearly seen

to detach themselves from the underlying hair cells after ~10 μm of movement. This process was continued until a section of the sensory epithelium approximately 100 μm long had been cleared of Hensen's cells. This process greatly improved the probability of patching an OHC and reduced the probability of cell debris adhering to the tip of the patch pipette. These supporting cells were not removed during mechanoelectric transduction experiments to avoid damaging the transduction apparatus.

2.1.6 Determining the quality of a preparation.

The quality of the preparation could be determined morphologically by observing the overall structure of the sensory epithelium and the shape, optical reflectivity and durability of OHCs.

In good preparations, all three rows of OHCs were clearly visible with high contrast. Cells were cylindrical, had an apparently smooth surface and basally located nuclei. This was true of OHCs over a great length of the organ of Corti, the highly organized structure of which was undisturbed. Cells maintained this appearance for up to 4 hours in T4 preparations. These cells formed high resistance seals very rapidly and stable whole-cell patch-clamp recordings (Sections 2.3.4 and 2.3.5).

Certain cochlear features presented an unfavorable prognosis for the experiment. A rippling of the whole organ of Corti was often the first sign of an unhealthy preparation. This effect was often associated with OHCs shortened to about half their normal length and swollen at their basal pole. Although these cells tended to form very high resistance seals, they were lost immediately on trying to break through into the whole-cell configuration. However, flat, organized organs of Corti did not always represent healthy preparations. On closer inspection, OHCs that were clearly cylindrical sometimes exhibited a rather "ghost-like" appearance and more apically located nuclei. This optical reflectivity could not be improved by adjusting the position of the fibre optic. These cells were not durable *in situ* and often swelled and burst within an hour or so of opening up the cochlea. Swelling was speeded up when a patch pipette containing a standard intracellular solution

and with very slight positive pressure approached the cell. These cells rarely formed high resistance seals.

2.2 Solutions

2.2.1 Extracellular solutions

The dissection of and experiments on T4 *in situ* OHCs were carried out in an artificial perilymph-like solution. The standard solution was a Na^+Cl^- based phosphate buffered saline (standard PBS), titrated to pH 7.3-7.4 with <1ml NaOH (1 mM). The osmolarity of the solution was measured using a freezing point depression osmometer (Roebling, Germany) and adjusted to 325-332 mOsm/kg by the addition of D-glucose. Details of this solution can be found in Table 2.1. A HEPES buffered saline (standard HBS) was used in some experiments but only if the intracellular solution was also buffered with HEPES (Section 2.2.3) or if the test solution to be applied to the cell was buffered with HEPES (Section 2.2.2). This was not the preferred pH buffer as the survival time of OHCs tended to be shorter in HBS rather than PBS.

The composition of the standard PBS was modified in experiments conducted on T1 OHCs in an attempt to slow the rapid cell deterioration usually observed in these preparations (Isolation PBS, Table 1). To minimize Ca^{2+} entry either through the transduction apparatus or through basolateral membrane ion channels or exchangers, the extracellular Ca^{2+} concentration was reduced from 1 mM to 0.05 mM. 200 μM DH-streptomycin was also added to the solution to prevent Ca^{2+} entry through the transducer channels. Finally, the osmolarity of the solution was increased from 225 mOms/kg to 232 mOsm/kg in order to try and minimize the swelling of the cells.

2.2.2 Test Solutions

In many of the experiments described, various pharmacological agents were added to the external medium and applied to the cell either by whole bath perfusion or by a puffer pipette (section 2.2.6). When the concentration of the drug

External Solutions

	Na^+	K^+	Ca^{2+}	Mg^{2+}	Cl^-	DH-strep.	H_2PO_4	HPO_4	HEPES	D-Glucose
Standard PBS	152	4	1	1.5	143	--	2	8	--	25
Standard HBS	142	4	1	1.5	151	--	--	--	5	25
Isolation PBS	152	4	0.05	1.5	141.1	0.2	2	8	--	30

Internal Solutions

	Na^+	K^+	Ca^{2+}	Mg^{2+}	Cl^-	F^-	BAPTA	H_2PO_4	HPO_4	HEPES	D-Glucose
Basic PBS	17	144	--	2	148	--	5	1	8	--	20
Basic HBS	--	144	--	2	148	--	5	--	--	5	20
Photolysis	--	144	1	--	146	--	--	--	--	5	20
KF	17	144	--	2	4	144	0.5	1	8	--	20

Table 2.1 Ionic composition of basic extracellular and intracellular solutions (mM)

was less than 1 mM, it was added directly to the solution. However, at concentrations greater than 1 mM, the drug was substituted for an equal concentration of an ion of the same valence (usually Na^+). The pH of the solution was then readjusted where necessary. Drugs were added to standard PBS (Table 2.1.). However, occasionally it was observed that at high concentrations of a drug, eg 4AP at $\geq$ 1 mM, a white precipitate would appear in the solution. Under these circumstances, drugs were dissolved in standard HBS.

2.2.3 Intracellular Solutions

A phosphate buffered potassium chloride solution was used as the standard intracellular solution. In experiments where HEPES was used as the eternal pH buffer, so it was also used as the internal buffer. The pH of these solutions was adjusted to 7.25 with KOH solution and the osmolarity adjusted to 323 mOsm/kg with D-glucose. The pipette solution was slightly hypo-osmotic to the extracellular solution as it has been suggested that this facilitates giga-seal formation (Hamill, Marty, Neher, Sakmann and Sigworth, 1981). Free concentrations of Ca^{2+} and Mg^{2+} were calculated for all intracellular solutions using the computer software WinMAXC (Version 1.2, Stanford University, USA) so that free Ca^{2+} was buffered to <100 nM. This concentration was chosen as it reflected the experimental estimates of resting intracellular Ca^{2+} concentrations using fluorescent dyes in isolated mammalian hair cells (Ashmore and Ohmori, 1990). The total concentration of intracellular Ca^{2+} was estimated to be 1.4 μM from the contamination in the various other salts added to the solution. All solutions were filtered through a 0.2 μm filter (Sartorius, Germany) before use.

The experiments described in Chapter 6 used the basic PBS intracellular solution as standard with 2.5 mM Mg-ATP added. These were the only experiments were nucleotides were consistently used in the intracellular solutions. Other experiments where ATP was added to the pipette solution are noted at the appropriate points in the text. GTP was not used in any experiments.

In early experiments on T1 OHCs, the standard PBS was used as the intracellular solution. However, in later experiments the internal solution was

changed to a phosphate buffered potassium fluoride solution which was observed to steady the zero current potential during recording.

2.2.4 Storage

The extracellular solution was made up from stock solutions. Stock A was a 25X concentrate of NaCl and KCL. This solution was stored at 0-4 ^{0}C. Stock B was a 25X concentrate of Na_2HPO_4 and NaH_2PO_4 or of HEPES. These solutions along with concentrates of $CaCl_2$ and $MgCl_2$ were kept at room temperature in the dark.

Intracellular solutions were filtered and aliquotted into 1.5 ml eppendorff tubes. The solutions were stored at -20 ^{0}C and kept for up to 6 months. Intracellular solutions containing ATP were filtered, aliquotted and snap frozen in liquid nitrogen immediately after they had been made to avoid breakdown of ATP to ADP and adenosine. These aliquots were stored at -80 ^{0}C and kept for 3 months.

2.2.5 Sources

Chemicals and drug were obtained from either BDH or Sigma except for DM-Nitrophen which was obtained from Calbiochem.

2.2.6 Perfusion of preparation and test solution administration

For all experiments except for mechanoelectric transduction, the preparation was continuously perfused using a multi-channel peristaltic pump (Minipuls 3, Gilson, France) at a rate of 450 µl/min. The total volume of the recording chamber was 8 ml and that of the inlet and outlet tubes combined, 2 ml. Solution entered at the base of the chamber and was removed at the top on the opposite side. This ensured a good exchange of solutions in the bath which was particularly important during drug application and washout. Except for times when pharmacological agents were being applied to the preparation, the extracellular solution was reperfused. This was done to try and avoid leaching of factors vital for the survival of the cells from the preparation (Paton, 1996). In reality, it is questionable whether

this really made a difference as the volume of the reservoir (10 ml) probably diluted any factors too much and no significant difference was observed between preparations that were and were not reperfused.

Test solutions were applied to the preparation either via a puffer pipette or by whole bath perfusion. Puffer pipettes were fabricated as a patch pipette (Section 2.3.3) but with a tip diameter of ~1 μm. Clearly, the puffer pipette system offers the advantage of speed. However, it was a logistically more difficult method of drug administration, particularly in T1 preparations and thus, the whole bath method was preferred.

2.3 Recording techniques

2.3.1 Voltage-clamp theory

Experiments were conducted using the whole-cell patch-clamp technique (Hamill, Marty, Neher, Sakmann and Sigworth, 1981). Used in voltage-clamp mode, this technique allows ion flow across a cell membrane to be measured as current whilst the membrane voltage is held under experimental control with a feedback amplifier.

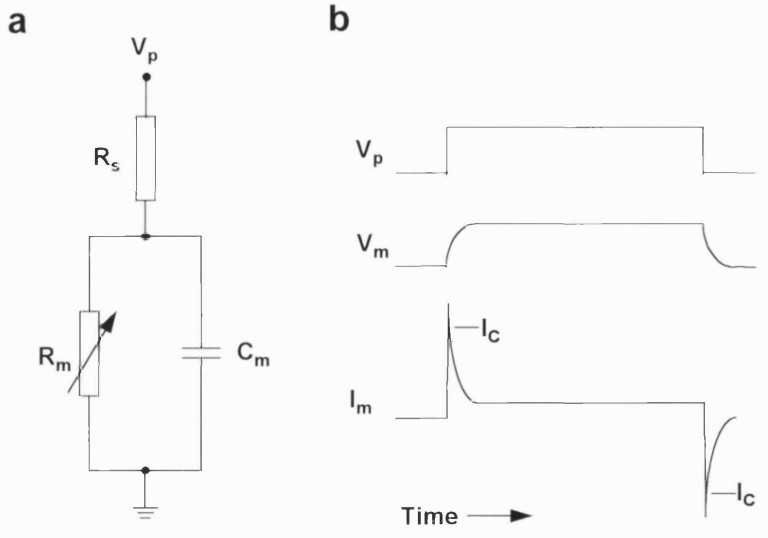

Figure 2.2 Whole-cell recording configuration. a, Equivalent electronic circuit. b, Time course of changes of V_m, I_m and I_c following a step change in V_p

Voltage clamp theory is best understood by considering an equivalent circuit for a biological membrane (Figure 2.2a). This considers a membrane as a capacitor and a variable resistor in parallel. The capacitor represents the total cell membrane capacity (C_m) and the variable resistor (R_m) the current flow through ion channels in the membrane. The voltage inside the cell can be controlled by applying a current from the pipette through an additional resistance (R_s) that represents the resistance of the pipette tip. Corrections for voltage drops across the series resistance must be made (Section 2.4.2) to yield the true potential inside the cell. This change in voltage is usually applied in a step-like fashion. Under these conditions, the applied current will charge the membrane capacitance before it changes the membrane voltage as capacitance is the ability to store charge when a change in voltage occurs. Thus, the change in intracellular potential is not achieved immediately but with a time constant given by:

$$\tau = C_m \frac{R_s \cdot R_m}{R_s + R_m}$$

Equation 2.1

However, the charging of the membrane capacitance is generally completed within 1 ms and thus ionic current can be recorded free from capacity current once the change in intracellular voltage is over (Figure 2.2b). Ions flowing into or out of the cell via the membrane as a result of this change in voltage can be recorded. By convention, cation movement out of the cell (eg K^+) is represented by upward going current deflections and cation movement into the cell is represented by downward going current deflections. Conversely, outward movement of negative ions (eg Cl^-) is represented by downward deflections.

Intracellular voltage is maintained at the new steady state level by means of a high gain operational amplifier with a feedback resistor (R_f). Any difference in potential between the command potential, V_{cmd}, and V_p is feedback into the pipette so that the difference between the two potentials is negligible (Figure 2.3).

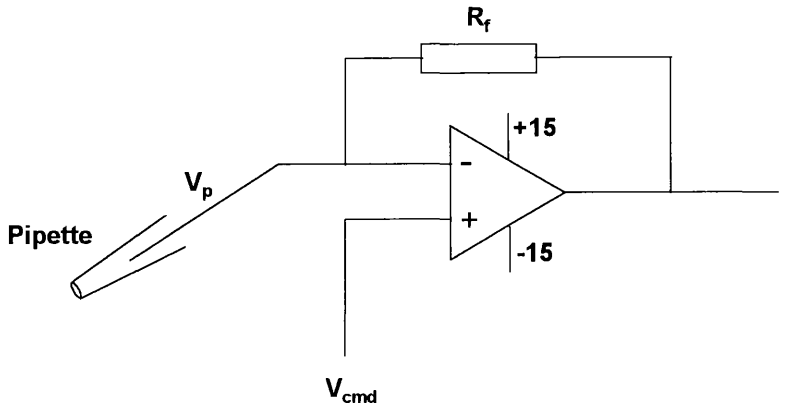

Figure 2.3 Simplified voltage clamp circuit. V_p, pipette potential, V_{cmd}, command potential R_f, feedback resistor that determines the sensitivity, background noise level and range of current measurements of amplifier.

2.3.2 Experimental apparatus

The arrangement of the recording equipment is shown diagrammatically in Figure 2.4. The microscope was mounted on an anti-vibration table (Ealing Electro Optics plc, USA) within a plate metal Faraday cage. This was located in the corner of the laboratory where building vibrations were generally smaller. Membrane potential was controlled by a patch amplifier (L/M-PC, List Medical, Germany). The head stage of the amplifier was mounted adjacent to the microscope on a Huxley micromanipulator (Huxley-Bertram, Cambridge, UK) in order to position the attached patch pipette. All potentials were measured relative to the bath potential which was grounded by means of a silver/silver chloride bath electrode (E206, Clark Electromedical Instruments, UK). However, during mechanoelectric transduction experiments, an agar salt bridge (1% agar in PBS) was used to connect bath solution with the reference electrode to avoid any toxic effects of Ag^+ ions on the transduction channels. The output of the patch amplifier was controlled by voltage protocols designed using C.E.D. 'Patch and Voltage Clamp Software' version 6.0 run from a PC (Genie PCi, Viglen, USA). Specific protocols used will be described in the appropriate sections. An analogue to digital/digital to analogue converter (Cambridge Electronic Design 1401, UK) interfaced between the PC and the patch amplifier. Current responses to changes in membrane potential were digitized and recorded on to the hard disc of a PC using the software mentioned above. Data were filtered at 3 kHz by the filter internal to the patch-clamp amplifier. Online monitoring of the membrane current and potential was possible using a two channel

oscilloscope (PM3302, Philips, UK). In addition, a record of the experiment was also taken with a chart recorder (Graphic 1002, Lloyd Instruments, UK). All equipment was grounded with low resistance copper cables to the high quality ground in the patch amplifier unit.

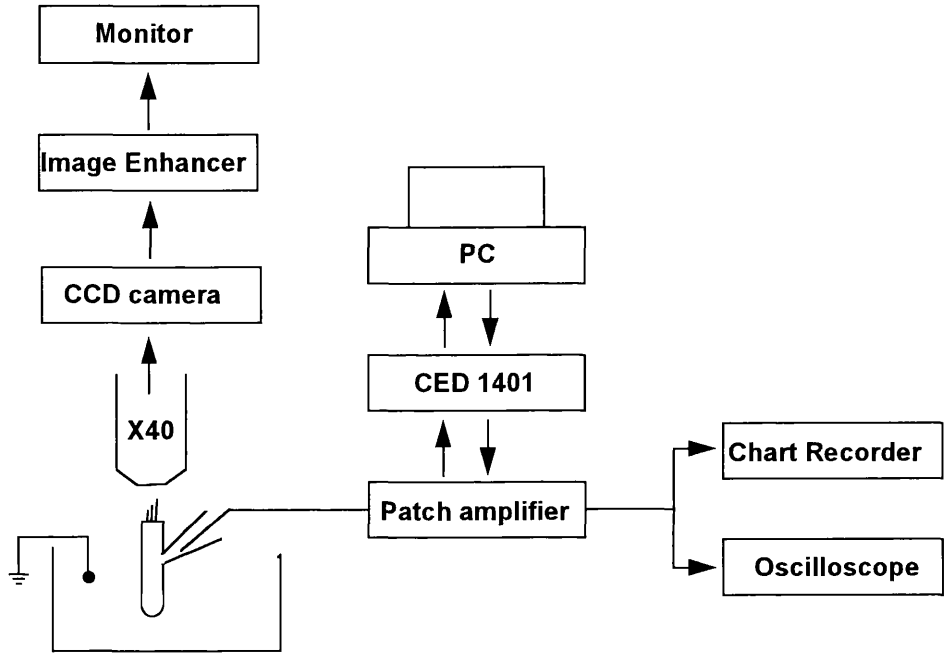

Figure 2.4 Diagrammatic representation of the electrophysiological recording apparatus

2.3.3 Glass pipettes

Patch pipettes were fabricated from soda glass capillaries (SG150T-10, Clark Electromedical Instruments, UK). These were pulled on a two stage vertical puller (PP-83, Narishinge, Japan) to a resistance of 4 MΩ ± 1 MΩ as measured with standard solutions. In order to reduce the stray capacitance between the pipette interior and the bath, pipettes were coated with ski wax (Swix, Norway) using a clean soldering iron tip heated to 180 ^{0}C. Heat polishing these pipettes was not necessary as they tended to pull into smooth, conical shaped tips. Pipettes were stored for up to 3 hours in a sealed container before they were used. Pipettes were filled by dipping the tip into the chosen intracellular solution for up to 5 seconds and then back filling the pipette with up to 2 cm of the same solution. Care was taken not to overfill the pipettes and cause solution to spill into the pipette holder to

increase thermal noise. Any bubbles were removed by gently tapping on the side of the pipette. Pipettes were inserted into a pipette holder (PC-53-1.5, Clark Electromedical Instruments, UK) and mounted on to the headstage of the patch amplifier.

2.3.4 Seal formation

Before insertion into the bath, gentle positive pressure was applied to the back of the pipette via an inlet on the side of the holder. This was important to keep the tip of the pipette clean whilst maneuvering it through the air-water interface and down to the cell for seal formation. The process of seal formation was monitored by observing the pipette currents on the oscilloscope while applying voltage pulses of 10 mV to the pipette. Before the pipette was inserted in to the bath, the current trace was flat. Before sealing on to the cell, any off sets between the pipette and the reference electrode were cancelled. With the positive pressure still on, pipettes were pushed up against the side of the outer row OHC around the basal pole causing the resistance of the pipette to increase and the total amount of current to decrease. The pipette pressure was then released. This was sometimes sufficient to initiate giga seal formation ($\geq 10^9\ \Omega$) also known as the cell-attached configuration of the patch-clamp technique. However, more often than not, gentle suction was required before a giga seal was achieved. In some instances where seal formation did not progress rapidly with negative pressure, it could be encouraged by making the inside of the pipette more negative (by up to -20 mV). However, if this did not improve the seal, the cell was abandoned and an attempt on another cell would be made. Seal resistances ranged between 1-10 GΩ although any seal in excess of 1 GΩ was accepted. If pipettes were sufficiently waxed, fast capacitative transients ($\tau < 100\ \mu s$) associated with the charging and discharging of the stray capacitance of the pipette and the pipette holder were cancelled using the fast capacitance control on the patch amplifier.

2.3.5 Whole-cell configuration

After a giga seal had been formed, the whole-cell configuration of the patch-clamp technique was achieved by further short suctions applied to the pipette. In

order not to depolarize the cell when breaking the patch, the holding potential of the cell was set to -40 mV. Electrical access to the cell's interior was indicated by the appearance of further transients on the current trace at the beginning and end of the seal pulse. This was caused by the charging of the membrane capacitance and could be removed by C-slow and G-series controls on the amplifier. These dials estimated the membrane capacitance and series resistance respectively.

On achieving a whole-cell configuration, OHCs fell into one of two categories. Either the whole-cell zero-current potential (V_z) was immediately around -60 mV or the whole-cell V_z changed over a period of 20-30 seconds from approximately -10 mV to -60 mV. The latter observation was probably due to Na^+ and Ca^{2+} loading of the OHC (Liu, 1997) through the transduction apparatus. Only cells that had a V_z less than -50 mV were accepted for analysis.

Whole-cell recordings from T4 cells *in situ* could be maintained for up to one hour. However, the duration of an individual experiment was typically between 10 and 40 minutes.

Occasionally, cell attached seals would break down prematurely. This generally resulted in a leaky or loose whole-cell configuration. The data from these cells was discarded.

All experiments were conducted at room temperature (20-22 ^{0}C).

2.4 Analysis of Data

2.4.1 Cell capacitance

A capacitor is formed when two parallel plates of area A are separated by an insulator with a dielectric constant ε and thickness d. Capacitance is given by

$$C = (A.\varepsilon)/d \qquad \textbf{Equation 2.2}$$

Biological membranes form good capacitors as the lipid bilayer acts as an insulator separating two conductive solutions. Thus, cells possess an intrinsic membrane capacitance, C_m, that is directly proportional to the cell's surface area.

When the voltage across a biological membrane is forced to change by providing a current from a patch amplifier, transient capacitative currents flow to charge both the stray capacitances of the pipette and pipette holder (C_{stray}) and the membrane capacitance. In addition, the steady-state currents flow through ion channels (Figure 2.2b). These large transients can seriously compromise the high-frequency performance of the patch amplifier and need to be minimized. This is achieved by supplying the capacitances with current from a capacitor at the summing input of the headstage amplifier rather than via the feedback resistor of the operational amplifier. The size and shape of this current is determined by dials on the patch amplifier that have been calibrated to give C_m, C_{stray} and R_s values. Thus, not only are the capacitative currents not seen by the amplifier headstage but the current dialed up can be used to measure the membrane capacitance and thus the size of the cell.

2.4.2 Series resistance

In whole-cell patch-clamp experiments, the membrane potential of the cell is controlled by the potential applied to the pipette electrode. This control depends critically on R_s, the resistance of the pipette itself and cellular debris that lie in series with the membrane resistance (Figure 2.2a). Series resistance causes a number of detrimental effects on whole-cell recordings. In particular, it causes a discrepancy between the command potential and the true membrane potential. The voltage error, V_{error}, is defined as

$$V_{error} = V_p - V_m = I_m.R_s \qquad \textbf{Equation 2.3}$$

Thus, the error is more serious when large membrane currents flow.

80-90% series resistance compensation may be achieved on-line by the patch-clamp circuitry. This not only improves the discrepancy between V_{cmd} and V_p,

but it also improves the effective speed of the voltage clamp. However, because series resistance compensation employs positive feedback, it has a tendency to oscillate out of control with small changes in R_s during an experiment. For this reason, it was decided that series resistance compensation would be conducted off-line using Microsoft Excel (Microsoft Office, Microsoft Corporation, USA) having determined a value for R_s using the capacitance compensation dials on the patch amplifier. This allowed 100% series resistance compensation to be achieved at the steady-state current and thus an accurate measure of the membrane potential to be calculated, particularly in T1 cells that exhibited very large currents (up to 9 nA). R_s compensation was conducted on all cells used for analysis in this thesis.

2.4.3 Liquid junction potentials

The potential difference formed at the interface between two solutions of different ionic composition due to the mobility of anions and cations in solution is known as a liquid junction potential (LJP). LJPs occur between the intracellular solution and the bath solution when the patch pipette is lowered into the bath and when the bath solution is changed during an experiment. LJPs can cause apparent shifts in the voltage dependence of ionic currents and compensations for these potentials should be made.

LJPs were measured off-line using a programme integral to Clampex 7.0 (Axon Instruments, Inc, USA) that uses the Henderson equation (Barry and Lynch, 1991) to calculate LJPs. This equation requires a knowledge of both the valency and mobility of each of the ions in the solution. LJPs between standard PBS and each of the intracellular solutions listed in Table 2.1 and LJPs between standard PBS and each of the major test solutions used were calculated.

An estimate of the true membrane potential, V_m, can be calculated from the recorded potential, V_p, as follows

$$V_m = V_p + V_{i\text{-}b} \qquad \textbf{Equation 2.4}$$

where V_{i-b} represents the voltage between the intracellular solution and the bath solution and V_{t-b} represents the voltage between the test solution and the bath solution. In cases where a solution change occurred

$$V_m = -V_p + (V_{i-b} + V_{t-b}) \qquad \textbf{Equation 2.5}$$

Corrections for LJPs were made when values exceeded ±1 mV.

Bath Solution	Intracellular Solution	V_{i-b} (mV)
Standard PBS	Basic PBS	-4.7
Standard PBS	KF	-8.8
Standard PBS	Basic HBS	-4.4
Standard PBS	Photolysis	-4.6

Table 2.2 Liquid junction potentials formed between standard PBS and standard intracellular solutions

Bath Solution	Test Solution	V_{t-b} (mV)
Standard PBS	3 mM 4AP	0.0
Standard PBS	30 mM TEA	0.6
Standard PBS	5 mM Cs^+	-0.2
Standard PBS	4AP, TEA + Cs^+	-0.4
Standard PBS	Isolating PBS	0.0

Table 2.3: Liquid junction potentials formed between standard PBS and test solutions bath-perfused on to cells

2.4.4 Subtraction of currents

Occasionally, it was necessary to subtract test currents from control currents in order to observe either the current blocked by a particular pharmacological agent or a very small biological effect that could not otherwise be seen in the raw data. Such subtractions were only conducted if the following criteria were met;

1. No large time dependent changes were observed during the recording eg due to R_s.
2. The recording was stable through the experiment.

2.4.5 Data presentation

Data were initially analyzed on a PC after experimentation using the C.E.D. electrophysiology package 'Patch and Voltage Clamp Software' (Version 6.0, Cambridge Electronic Design Ltd, UK) and were then exported either to Origin (Microcal™ Software, Inc, USA) or Fig P (Fig P Software Corporation, Version 6.0c, Durham, NC, USA) for presentation. Voltage protocols show the maximum and minimum step changes in voltage. Intermediate voltage steps are not shown. Pooled data are presented as means ± S.D. Equations used in fitting the data are presented in the text and were fitted to the data in Fig P. Statistical significance was examined using a two-tailed Student t-test. P values are presented in the text and in Table 1, Appendix 1.

Chapter 3

Basolateral Membrane Currents of T4 OHCs

3.1 Introduction

3.1.1 Voltage-dependent ion channel expression in the basolateral membrane of OHCs

The size and shape of the OHC receptor potential generated by the MET current (see Chapter 7) is determined not only by the properties of the transduction current but also by the characteristics of the low-pass filter of the cell. OHC filtering is determined by the cell's parallel capacitance and resistance according to the following equation for a low-pass filter:

$$f_c = 1/(2\pi R_m C_m) \qquad \textbf{Equation 3.1}$$

where f_c represents the corner frequency passed by the low-pass filter before the signal is attenuated and R_m and C_m are the membrane resistance and capacitance respectively.

Hair cells located along the tonotopic gradient of the cochlea will be required to transduce sound-induced vibrations from 20 Hz to 20 kHz or more depending on the species. To be effective amplifiers and influence the basilar membrane motion on a cycle-by-cycle basis, OHCs will have to change length at speeds equal to the stimulus frequency. This will require that the corresponding changes in the receptor potential are large enough to activate OHC motility without being attenuated by the OHC low-pass filter. Thus, the properties of the OHC filter are critical to ensure that the change in potential induced by the MET current is sufficient to activate the OHC motor.

The resistive properties of the OHC are determined by the properties of voltage- and ligand-gated ion channels in the basolateral membrane of the cell. Previous studies have investigated variations in the voltage-dependent ion

channel expression of OHCs along the tonotopic axis of the cochlea (Art and Fettiplace, 1987; Housley and Ashmore, 1992; Mammano, Kros and Ashmore, 1995; Mammano and Ashmore, 1996; Raybould and Housley, 1997). However, they have not been satisfactorily completed due to the paucity of information regarding true T1 OHCs.

3.1.2 Investigating four variables of T4 OHCs

The aim of this study is to characterize T4 OHCs according to their morphology and the currents that pass through the voltage-activated ion channels in their basolateral membrane. A number of studies have already looked at some elements of this work (Housley and Ashmore, 1992; Santos-Sacchi and Diliger, 1988). However, only one other study has used *in situ* OHCs that seem to provide a good estimate of the properties of OHCs in the intact cochlea (Mammano and Ashmore, 1996).

T4 OHC currents were characterized by their kinetics, pharmacology and sensitivity to raised intracellular Ca^{2+} concentrations. The term kinetics was used in this thesis to describe a number of current characteristics that were not necessarily dynamic, but that did not fit well into the other two categories of pharmacology and Ca^{2+} sensitivity, for example, the voltage-dependence and amplitude of the current. Separation and characterization of currents by their kinetic properties is appropriate if the properties are very different. However, if the differences are more subtle, other means of separation will be necessary.

Pharmacological reagents provide a very powerful means of categorizing currents. Ion channel antagonists prevent ions permeating the channel either by binding within the pore and occluding it or by an allosteric interaction that affects the channel gating. These effects may be highly specific. For example, neurotoxins such as tetrodotoxin and saxitoxin are effective in blocking Na^{+} channels at nanomolar concentrations (Hille, 1992). Other antagonists may be less specific, requiring micro- or millimolar concentrations to be effective. For example, tetraethylammonium (TEA) must be present at millimolar concentrations to be an effective antagonist of delayed-rectifier K^{+} channels (Hille, 1992).

Finally, currents may be separated by observing their response to raised intracellular Ca^{2+} concentrations. Ca^{2+} has been shown to alter the gating of ion channels. For example, it can activate K^+ (Marty, 1981; Maruyama, Gallacher, Petersen, 1983; Meech, 1974) and Cl^- channels (Barnes and Hille, 1989; Miledi, 1982) and is involved in Ca^{2+} channel inactivation (Eckert and Chad, 1984). This ubiquitous second messenger may provide a further means of distinguishing kinetically similar currents.

3.1.3 Control of intracellular Ca^{2+} concentration with caged compounds

Caged compounds are molecules whose activity is controlled by light, usually by conversion from an inactive to an active form. They are useful biologically because illumination can be easily controlled in timing, location and amplitude. However, they must satisfy several criteria:

a) When caged, the active species should be inert to the biological system under study.
b) The active species should be released by photolysis at high yield and at sufficient speed by wavelengths of light that are non-detrimental to the preparation.
c) Any photoproducts other than the active species should not affect the biological system.

Photochemical release of Ca^{2+} was made possible with the development of caged Ca^{2+} chelators such as the Nitr series of compounds (Adams, Kao, Grynkiewicz and Tsien, 1988) and DM-Nitrophen (Kaplan and Ellis-Davis, 1988). The basic properties of these compounds reflect those of the parent chelator molecules from which they were derived. Thus, the Nitr compounds, which are based upon BAPTA, show a high selectivity for Ca^{2+} over Mg^{2+}, whereas DM-Nitrophen, which is based on EDTA, discriminates less well for Ca^{2+} over Mg^{2+} and protons. Additional differences between these molecules relate to the mechanism by which photolysis results in a decrease in their Ca^{2+} affinity. Nitr compounds rely on the photochemical conversion of a 2-Nitrobenzyl substituent. For Nitr-5, the most commonly used of the Nitr series of compounds, conversion of this group causes a 40 fold decrease in its Ca^{2+} affinity upon photolysis. In contrast, photolysis of DM-Nitrophen results in the chemical disintegration of the Ca^{2+} binding site yielding a 600,000 fold decrease

in Ca^{2+} affinity (Figure 3.1). A comparison of the properties of Nitr-5 and DM-Nitrophen can be found in Table 3.1.

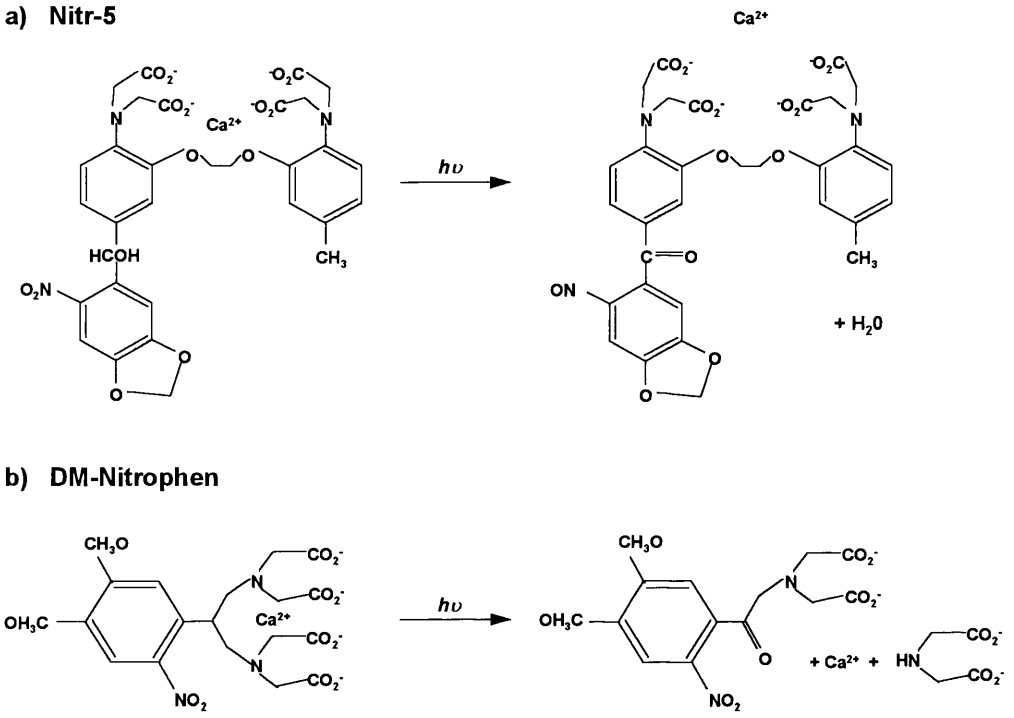

Figure 3.1 Photochemical reaction schemes proposed to account for the photolysis of a) Nitr-5 and b) DM-Nitrophen leading to the release of Ca^{2+}.

DM-Nitrophen was finally chosen as the preferred chelator for these investigations because of its:

a) very high affinity for Ca^{2+}.

b) high quantum efficiency, particularly for the Ca^{2+} bound form of the molecule.

c) enormous change in K_d for Ca^{2+} on photolysis, leading to large changes in $[Ca^{2+}]_i$.

Property	Unit	Nitr-5	DM-Nitrophen
K_d for Ca^{2+} before photolysis	nM	145	5
K_d for Mg^{2+} before photolysis	mM	>8.5	0.0025
K_d for Ca^{2+} after photolysis	mM	0.0063	3
K_d for Mg^{2+} after photolysis	mM	>8.5	2
Selectivity for Ca^{2+} over Mg^{2+} before photolysis		>6900	500
Quantum Efficiency		0.035	0.18
Binds H^+ in physiological pH range		No	Yes
Time constant of Ca^{2+} release	ms	0.23	0.13
Absorption maximum	nm	369	345

Table 3.1 A comparison of the properties of Nitr-5 and DM-Nitrophen. Data sources: Product Data Sheets, Calbiochem and Gurney, 1991.

3.2 Methods

3.2.1 Photochemical control of $[Ca^{2+}]_i$ by caged compounds.

3.2.1.1 Photolysis equipment

UV light, required for the photochemical conversion of DM-Nitrophen, was provided by a mercury-xenon arc lamp (307-143.004, Leitz Wetzlar GMBH, Germany). This produced an emission spectrum that was bell-shaped between 250 nm and 400 nm with a tail extending past ~500 nm. Light from this lamp passed to the microscope via a water filled light guide (Cairn Research, UK) and was focused on to the preparation via the objective (x40 Achroplan 0.75 NA, water immersion, working distance 1.6 mm, Zeiss, Germany). A dichroic mirror located within the epillumination port of the microscope, ensured that light below 400 nm passed down to the preparation to photolyse the Ca^{2+} chelator, whilst light at all wavelengths was able to pass up to the microscope eye pieces and/or the camera (Figure 3.2) allowing visualisation of the preparation. UV illumination was controlled via a manual shutter located at the junction between the UV lamp and the water filled light guide. Typically, UV illuminations were 5 seconds long.

DM-Nitrophen was incorporated into cells via the intracellular solution of the patch pipette during whole-cell patch clamp experiments. To avoid the premature photolysis of DM-Nitrophen, the pipette solution was protected from light by:

a) coating the patch pipette with ski wax (Swix, Norway) to reduce the transmittance of light to the solution inside the pipette.

b) filtering the light from fibre optic illuminating the preparation below 510 nm and reducing the intensity of this light by half.

At least 5 minutes were allowed to elapse between achieving the whole-cell configuration and photolysing DM-Nitrophen to ensure complete dialysis of the cell with the intracellular solution.

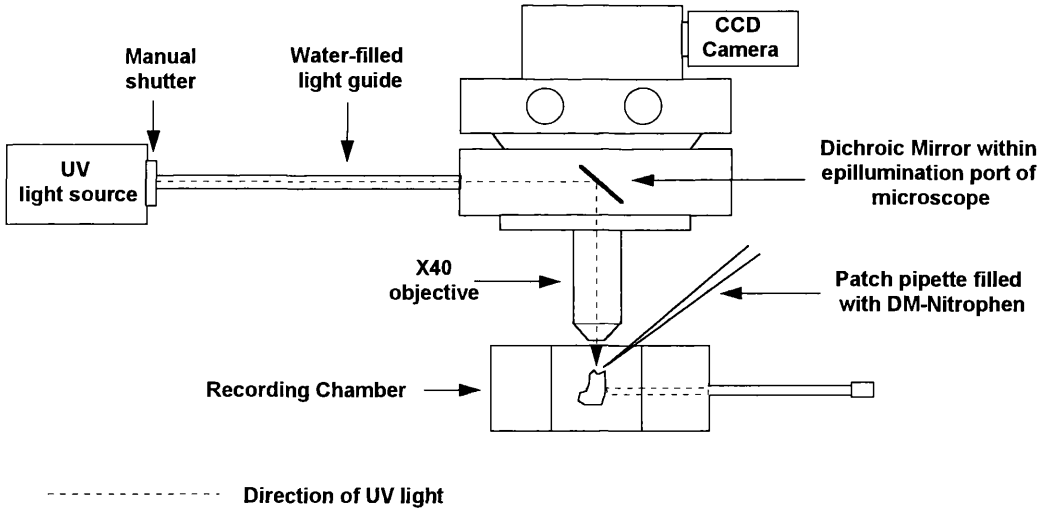

Figure 3.2 Experimental set-up used for photolysis experiments. The UV light source was a mercury-xenon arc lamp. The dichroic mirror reflected light below 400 nm down through the microscope objective to the cell and allowed light at all wavelengths up to the eye pieces or the camera. UV light shining on to the preparation was controlled by a manual shutter located at the junction between the light source and the light guide.

The photolysis of a caged compound by a timed, short duration, high intensity exposure of UV light is known as flash photolysis. It is the most common method of photolysing caged compounds (eg, Currie, Wootton and Scott, 1995; Jagger and Ashmore, 1999; Lancaster and Zuker, 1993; Parsons Ellis-Davies and Almers, 1996). Flash photolysis was not possible with this experimental set-up because of the absorption of UV light by the glass within the objective. Although the UV light source used in these experiments was of a

low light intensity, the use of a manually operated shutter allowed much longer exposures and therefore the amount of UV light exceeded that of a single flash allowing photolysis of the caged compound.

3.2.1.2 Drug preparation

DM-Nitrophen is only available as a tetrasodium salt (Calbiochem). It was dissolved in a HEPES buffered saline rather than a phosphate buffered saline (Table 2.1) as small crystals that inhibited gigaseal formation were observed at the tip of the pipette in the latter solution. Care was taken to ensure minimal exposure of the salt to light prior to use. Thus, DM-Nitrophen solutions were always made in rooms with dimmed lighting and the aliquots of solution used during the experiments were kept wrapped in aluminium foil and sat on ice.

Using the following equation (Gurney, 1991), a prediction of the free calcium concentration in the solution can be estimated:

$$C_{freeCa2+} = \frac{- (C_{DMN}-C_{totalCa2+}+K_d) \pm \sqrt{[(C_{DMN}-C_{totalCa2+}+K_d)^2 - 4K_dC_{totalCa2+}}}{2}$$

Equation 3.2

$C_{free}\,Ca^{2+}$	free Ca^{2+} concentration in solution before photolysis
C_{DMN}	total DM-Nitrophen concentration
$C_{total}\,Ca^{2+}$	total concentration of added Ca^{2+}
K_d	dissociation constant for Ca^{2+} binding to DM-Nitrophen before photolysis.

Thus, the free Ca^{2+} concentration in a solution with a DM-Nitrophen:Ca^{2+} ratio of 3:1 is 2.5 nM. This is in close agreement with the free Ca^{2+} concentration obtained with WinMaxC (Version 1.2, Stanford University, USA) of 6.3 nM when stating the Ca^{2+} chelator as EDTA.

The proportion of DM-Nitrophen that was complexed with Ca^{2+} before photolysis was calculated to be 99.99% using the following equation (Gurney 1991):

$$[C_{DMNCa2+}] = \frac{[C_{totalCa2+}] \cdot [C_{DMNtot}]}{K_d + [C_{totalCa2+}]}$$ **Equation 3.3**

$[C_{DMNCa2+}]$	concentration of buffer present as a Ca^{2+} complex
$[C_{totalCa2+}]$	total concentration of added Ca^{2+}
$[C_{DMNtot}]$	total DM-Nitrophen concentration
K_d	dissociation constant for Ca^{2+} binding to DM-Nitrophen before photolysis

Therefore, the majority of DM-Nitrophen photolyzed on UV illumination would release Ca^{2+}.

3.2.1.3 Control Experiments

In order to be biologically useful, photolabile Ca^{2+} buffers should be physiologically inert both before and after photolysis, should act simply as buffers for Ca^{2+} and should be photolysed by wavelengths of light that do not affect the cell. Control experiments for each of these requirements were conducted.

The effects of UV light were investigated by exposing an OHC, patched with standard HBS, to 5 seconds of UV light. To test for the effects of unphotolysed DM-Nitrophen on OHCs, basolateral membrane currents recorded immediately after achieving the whole-cell configuration and then again 5 and 10 minutes later were compared. To ensure that the photoproducts of DM-Nitrophen did not affect OHCs, photolysis of the unbound chelator was observed. These control experiments did not affect OHCs.

Finally, to ensure that there was no appreciable Mg^{2+} release during photolysis of DM-Nitrophen, the maximum Mg^{2+} contamination of the solution was calculated and found to be 145 μM. In the absence of Ca^{2+}, most of this Mg^{2+} would be bound to DM-Nitrophen. However, due to the higher K_d of DM-Nitrophen for Ca^{2+} over Mg^{2+}, only 0.014 mM of Mg^{2+} are likely to be bound to the chelator (WinMaxC). Thus, the major divalent cation released from DM-Nitrophen will be Ca^{2+}.

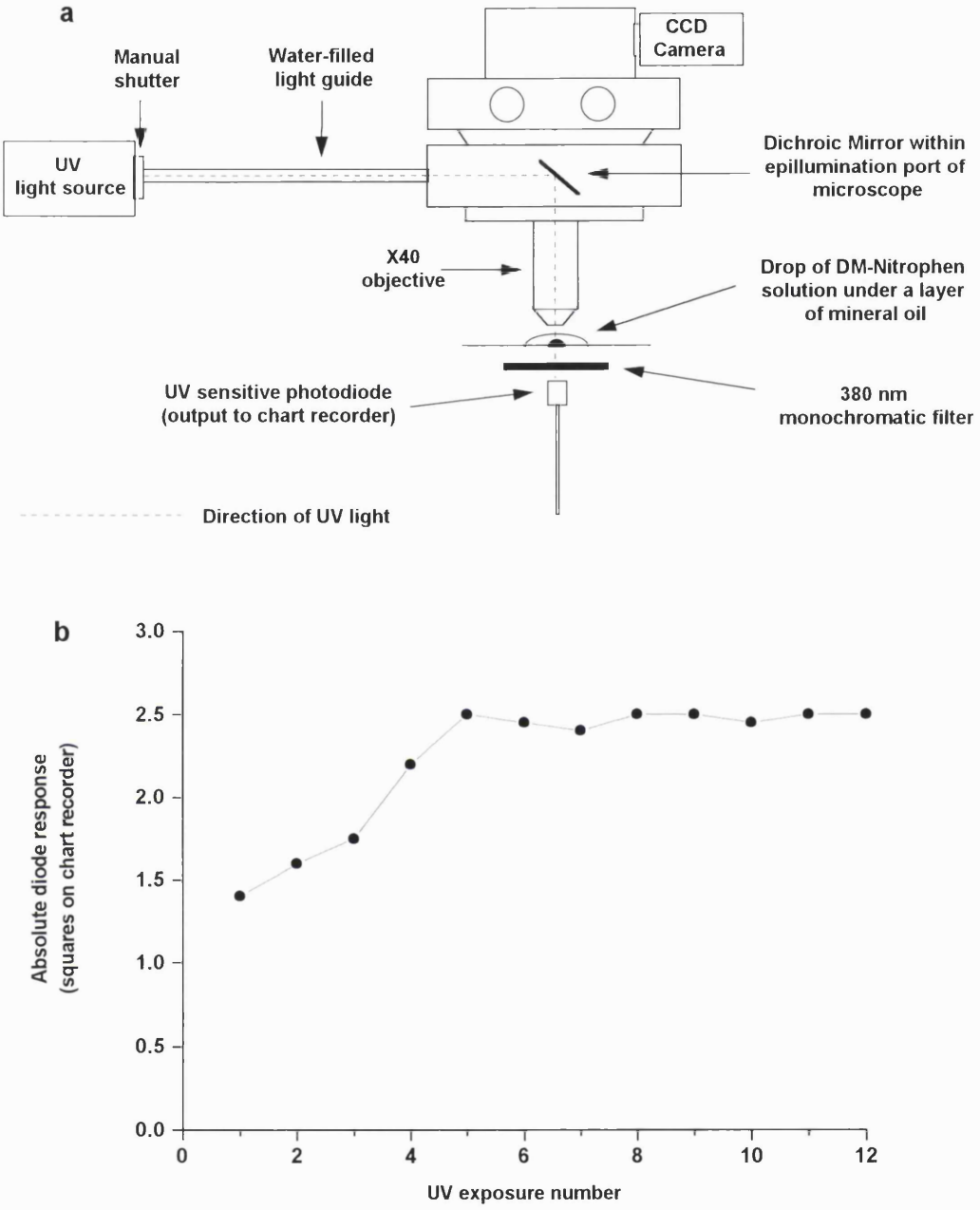

Figure 3.3 Cell free calibration of Ca^{2+} release from DM-Nitrophen. a, The change in absorbance of 380 nm light by the photolysis of DM-Nitrophen was monitored by a photodiode, held in place by the microscope condenser. b, The change in absorbance was quantified by measuring the photodiode current on a chart recorder after each 1 second UV exposure.

3.2.1.4 Calibration of calcium release from DM-Nitrophen

The amount of Ca^{2+} released from DM-Nitrophen during a 5 second UV exposure was estimated using a cell free calibration method outline in Gurney (1991). This method exploits the fact that the absorbance spectrum for DM-Nitrophen changes upon photolysis. Thus, by monitoring the change in absorption of DM-Nitrophen with each UV exposure, the fraction of molecules photolysed by a single exposure can be extrapolated from the rate at which the absorbance change reaches a maximum

The calibration was performed on a droplet of DM-Nitrophen solution located on a microscope coverslip. Changes in the absorbance of the droplet were monitored by a UV sensitive photodiode located underneath the droplet of solution (Figure 3.3a). Light reaching the photodiode was filtered by a 380 nm monochromatic filter. At this wavelength of light, DM-Nitrophen decreases its absorbance with photolysis (Kaplan and Ellis-Davis, 1988). Thus, the amount of light reaching the photodiode with each UV exposure increases as DM-Nitrophen photolyses. The change in absorbance of DM-Nitrophen with photolysis was quantified by measuring the photodiode current on a chart recorder after each exposure. The diameter of the droplet was smaller than the diameter of the spot of UV light irradiating it, ensuring that all the DM-Nitrophen molecules were exposed to the light. Such small droplets were formed by advancing a patch pipette, containing the DM-Nitrophen solution, through a layer of mineral oil (to prevent evaporation of the solution) and applying gentle pressure to the back of the pipette to eject a small bubble of solution. This procedure could be controlled so that bubbles of ~20 μm diameter could be formed.

Initially, DM-Nitrophen droplets were exposed to a series of 5 second UV exposures. However, no significant change in the photodiode current could be observed. When the duration of the UV exposure was reduced to 1 second, changes in the photodiode current could be seen over the course of the first 5 exposures, after which time there was no further measurable change to the peak current (Figure 3.3b). These results indicate that complete photolysis of DM-Nitrophen is achieved in one, 5 second UV exposure. Thus, all caged Ca^{2+} is released. Knowing that 99.99% of the DM-Nitrophen in this solution is present

in the Ca^{2+} bound form and that after photolysis, it is unable to re-chelate Ca^{2+}, these results indicate that 1 mM of Ca^{2+} is released from the chelator during a 5 second UV exposure. However, this result does not take into account the fact that within a cell, this Ca^{2+} release must overcome the endogenous Ca^{2+} buffering of the cytoplasm before it can be effective. In OHCs, the endogenous Ca^{2+} buffer has been calculated to be equivalent to 2.1 mM BAPTA (Chapter 6). On this basis, a Ca^{2+} release of 1 mM from DM-Nitrophen would create a rise in cytoplasmic Ca^{2+} of 0.1 μM after overcoming the endogenous Ca^{2+} buffering of the cell (WinMaxC).

3.3 Results

3.3.1 The morphology of the apical organ of Corti

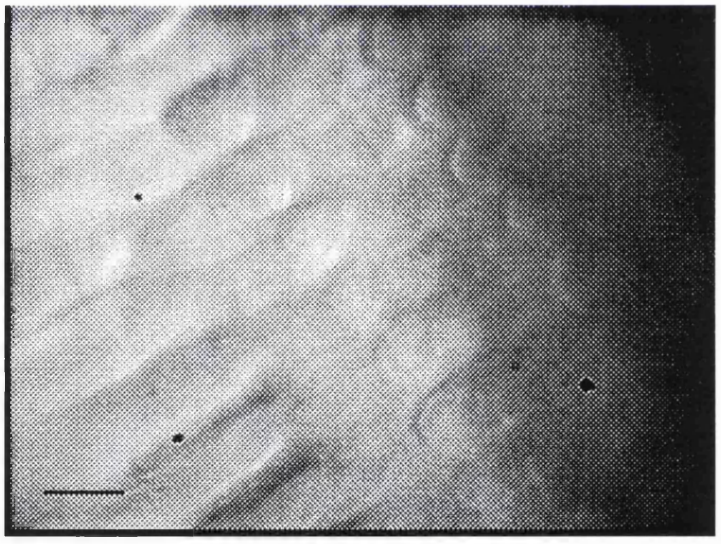

Figure 3.4 Digital image of the organ of Corti in the isolated temporal bone preparation. Scale bar - 10 μm. At this focal depth, the mid-region of the outer row OHCs can be seen to the left of the picture, the cuticular plate of the middle row OHCs can be seen in the centre and the V-shapes of the stereocilia of the inner row OHCs can be seen to the right of the picture. Hensen's cells have been removed. Outer row OHCs were patched at their basal end around the nucleus.

Figure 3.4 shows the organ of Corti from the apical turn of the guinea-pig cochlea. The Hensen's cells, normally located to the left of the image, have been removed to improve access to outer row OHCs for whole-cell patch-clamp recordings. The length of OHCs in the apex of the cochlea varies across the width of the organ of Corti (Lim, 1980). Outer row OHCs located furthest away from the modiolus are 70 μm long, whereas those nearest the modiolus (inner

row OHCs) are shorter, 60 μm. This gradient in OHC length tilts the apical sensory epithelium (Spoendlin, 1972) and thus, the plane of focus for each row of OHCs is different. The recording location in the apex of the cochlea was 2.2 mm from the helicotrema. This correlates to the site along the basilar membrane tuned to ~400 Hz (Greenwood, 1990). The ability to clearly locate the position of the hair cell within the organ of Corti is a major advantage of this preparation, as it allows hair cell characteristics to be closely correlated with their frequency response.

3.3.2 The kinetics of apical OHC basolateral membrane currents

Whole-cell currents recorded from apical outer row OHCs patched using basic PBS are shown in Figure 3.5a. These currents are characteristic of apical turn OHC currents for three reasons:

a) the zero-current potential, (V_z), of the cells is -65 mV.
b) whole-cell currents are strongly outwardly rectifying.
c) a fast, transient current is observed at the onset and offset of the step change in voltage.

a) On achieving the whole-cell configuration, the zero-current potential of the cell was often around -30 to -40 mV but shifted to more negative potentials over the first minute of recording (-65 ± 8.85 mV, n = 20). It has been shown that isolated OHCs have a high concentration of Na^+ and Ca^{2+} ions in their cytosol on isolation (Liu, 1997). Assuming this is also true of *in situ* OHCs, the observed shift in potential over the first minute of the experiment was presumably caused by the dialysis of the cell with the K^+-based pipette solution. Command steps were not applied to the cells until the zero-current potential had stabilized. The averaged, stabilized zero-current potential recorded was significantly more depolarized than the resting potential of OHCs recorded *in vivo* using microelectrodes (Dallos, 1986) (P = 0.002), was comparable to previous studies using this *in situ* preparation (Mammano and Ashmore, 1996) (P = 0.05), but was significantly more hyperpolarized than that observed *in vitro* (Housley and Ashmore, 1992). In fact, a comparison of the mean zero-current potential *in vitro* and *in situ* using a two-tailed Student t-test showed that the standard deviations of the two populations were significantly different (P = 0.004) that a comparison of the means was not warranted. This result suggests

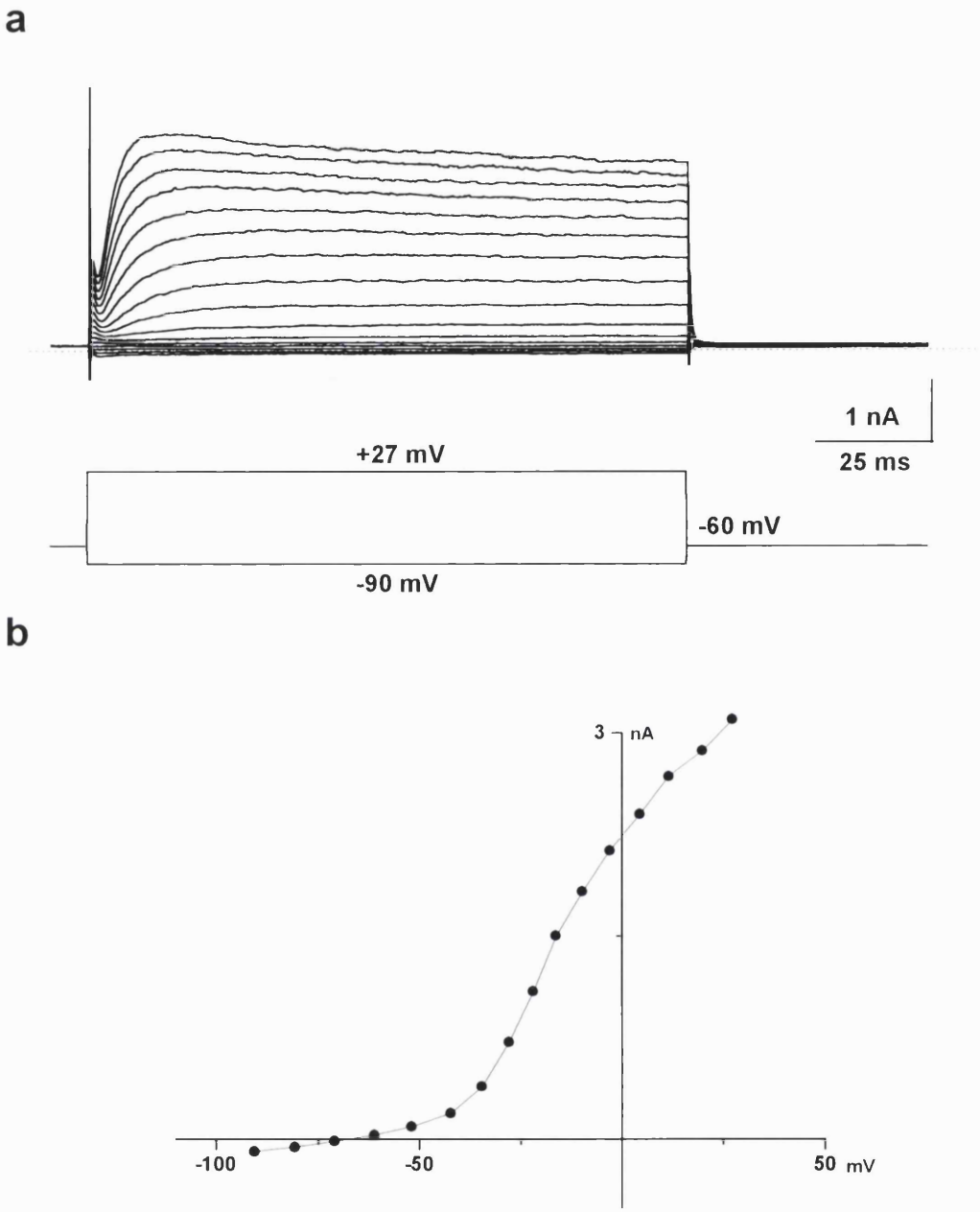

Figure 3.5 Whole-cell currents from a T4 outer row OHC of the intact adult organ of Corti. a, currents recorded in response to the series of voltage commands shown immediately below. V_h -60 mV. Voltage was stepped from -90 mV to +27 mV in 10 mV steps. The dotted line in this and subsequent figures represents the position of zero current. Data was sampled at 3 kHz. b, steady-state current-voltage relationships obtained from data in a. Data measured 10 ms before voltage command offset and corrected for series resistance errors (11 MΩ).

that the cells in this preparation were significantly closer to the quality of *in vivo* OHCs than OHCs *in vitro*. The cell capacitance, as measured using the capacitance compensation circuitry on the patch amplifier was 35.5 ± 5.08 pF (n = 20) at -60 mV, a value consistent with other T4 outer row OHC recordings

(Mammano and Ashmore, 1996) (P = 0.09). For more information regarding the above significance tests, see tests a, b, c and d, Table 1, Appendix 1.

b) T4 OHCs exhibit currents that are strongly outwardly rectifying. Stepping the membrane potential negative to the holding potential elicited small inward currents of -0.297 ± -0.08 nA at -110 mV (n = 20). Voltage commands positive to the holding potential elicited much larger outward currents that measured 1.335 ± 0.34 nA at 0 mV (n = 20). The holding potential of -60 mV was chosen for T4 OHCs as it was close to the zero-current potential of the cell and avoided depolarization of the cell membrane.

When plotting the current-voltage (I-V) relationship for these currents, two distinct gradients to the curve are observed (Figure 3.5b). This may represent the activation of two different channel types, the first component being active around the zero-current potential of the cell, (I_k), the second component activating around -40 mV, (I_{kout}), as indicated by the substantial increase in the gradient of the I-V curve at this potential.

OHCs act as low-pass filters due to the parallel resistance and capacitance of their membrane (Section 3.1.1, Housley and Ashmore, 1992; Santos-Sacchi, 1992). Such filters progressively reduce the amplitude of high frequency signals, but pass low frequency signals unattenuated. The time constant for a this low-pass filter can be calculated from the following equation:

$$\tau = R_m.C_m \qquad \textbf{Equation 3.4}$$

where R_m is the resistance of the cell membrane, the reciprocal of the slope conductance of the membrane at V_z and C_m is the membrane capacitance. Averaged slope conductances of 2.92 ± 1.73 nS (n = 20) at the zero-current potential of the cell were measured. Using Equation 3.3, the time constant for a T4 OHC is 12 ms. The corner frequency (f_o) for a low pass filter can be calculated from the following equation:

$$f_o = 1/(2\pi\tau) \qquad \textbf{Equation 3.5}$$

For a cell with a time constant of 12 ms, signals of frequencies above 13 Hz will be progressively attenuated. Thus, receptor potentials in T4 OHCs, generated as a result of the transducer conductance, will be filtered by the OHC basolateral membrane capacitance if the frequency of the transducer conductance is greater than 13 Hz.

The maximum slope conductance (g_{in}) of these cells was observed at -35 mV and measured 22.0 ± 6.9 nS (n = 20). The slope conductance at -110 mV was 2.7 ± 0.8 nS (n = 10).

The above data is summarised in Table 3.2.

Property	V_z (mV)	C_m (pF)	g_{in} -110 mV (nS)	g_{in} V_z (nS)	g_{in} max (nS)	I_{max} 0 mV (nA)	τ_{onset} 0 mV (ms)	τ_{inact} 0 mV (s)
mean	-65.6	35.5	2.7	2.92	22.01	1.335	8.13	0.41
SD	8.85	5.08	0.88	1.73	6.90	0.34	2.60	0.15
n	20	20	10	20	20	20	20	4

Table 3.2 Properties of T4 outer hair cells. V_z, zero current potential; C_m, membrane capacitance; g_{in}, slope conductance measured at -110 mV, V_z and at the point of maximum slope on the IV curve; I_{max}, maximum current measured at 0 mV; τ_{onset}, time constant of current onset measured at 0 mV; τ_{activ}, time constant of current inactivation at 0 mV during a maintained depolarization.

c) An important characteristic of currents recorded under voltage-clamp from OHCs is the fast, transient current observed at the start and end of a voltage step (Figure 3.5a). This current is thought to arise from the voltage dependent movement of a molecule located in the basolateral membrane of OHCs believed to be associated with OHC motility (Ashmore 1987). The observed current is not a true current where ions pass through the membrane via ion channels, but is more like a capacitative current, arising from charge displacement within the molecule when the membrane potential is changed (Gale and Ashmore, 1997). Estimates of cell membrane capacitance from controls on the patch amplifier were not heavily contaminated by this motor transient. At -70 mV, the maximum contamination of the membrane capacitance by the motor is 20 % (Tunstall, Gale and Ashmore, 1995). A comparison of the maximum charge transfer for a change in membrane potential between isolated

and *in situ* OHCs was not possible, due to the substantial K^+ currents contaminating the motor activity.

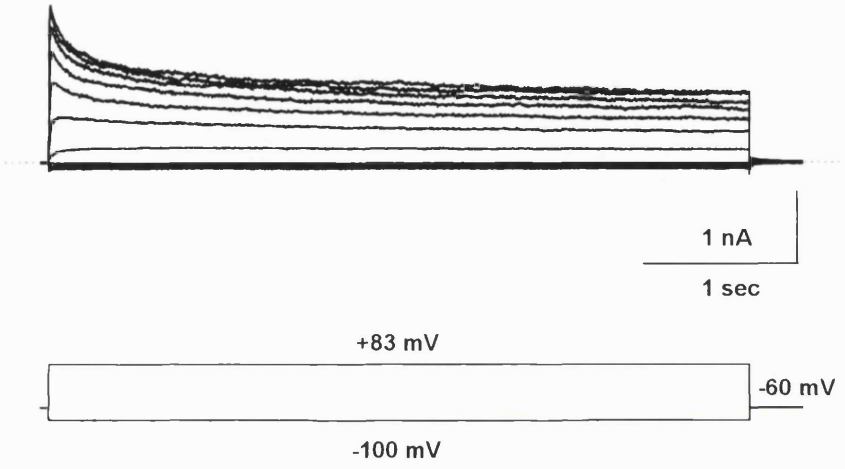

Figure 3.6 Inactivation of the outward current in T4 outer row OHCs. Upper traces show the current response of an OHC to prolonged step changes in potential (bottom panel). All voltages corrected for series resistance errors (8 MΩ).

Outward currents inactivated during a prolonged depolarization (Figure 3.6). Currents peaked 20 ms after the step change in potential but decreased slowly to a steady-state level over the following 3 seconds. Due to the slow time course of this process, very little current inactivation was observed during the much shorter potential changes shown in Figure 3.5. Inactivation was not due to the depletion of $[K^+]_i$ during the maintained voltage step. Potassium movement out of the cells during depolarization amounted to a reduction in $[K^+]_i$ of 11 μM at +20 mV (see Appendix 2). This change in $[K^+]_i$ does not alter E_k from -90 mV and does not significantly decrease the efflux of K^+ from the cell. Current inactivation was not complete and was observed to stabilize at a level 58 ± 7.6 % (n = 4) of the maximum at 0 mV. This observation adds extra support to the hypothesis that there are at least two types of channels carrying the outward current in these cells, one that inactivates, the other being non-inactivating.

It is unlikely that the inactivating current is the classical A-type K^+ current for two reasons:

a) Current inactivation is too slow in these cells compared to the conventional A-type potassium current I_{kA} that inactivates within 30 ms at 20 °C (Hoshi, Zagotta, Aldrich, 1990).

b) It was not possible to separate out the inactivating component of the current by holding the cell at -80 mV and repeating the experiment. At this potential, K_A is almost completely inactivated (Hille, 1992) thus removing this component of the current.

The time constant of both current activation and inactivation was voltage dependent, although very weakly so in the latter case (Figure 3.7). With more positive voltage steps, the time constant decreased. For voltage steps from -60 to 0 mV, the time constant of current activation was 8.13 ± 2.60 ms (n = 20) and for inactivation, was 0.41 ± 0.15 s (n = 4). The smooth curves fitted to both sets of data are monoexponential decays of the following form:

$$\tau = Ae^{(-kV)} + B \qquad \textbf{Equation 3.6}$$

where k defines the steepness of the voltage dependence and V is the test potential in volts. Curves were generated in Fig P and for the time constant of activation, A = 7.9 ms, k = 0.018 and B = -1.1 ms and for the time constant of inactivation, A = 0.6 ms, k = 0.006 and B = -0.006 ms.

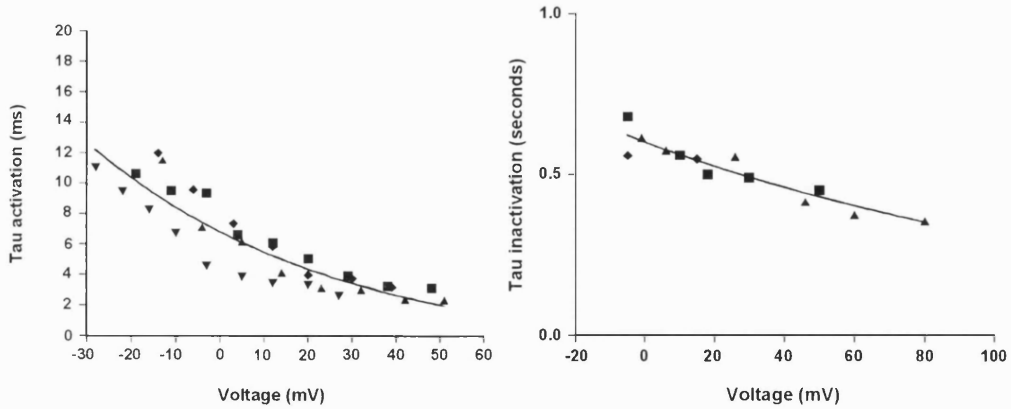

Figure 3.7 Time constants of current activation and inactivation. a, Time constant of current activation in 4 cells when stepping from the holding potential (-60 mV) to a more positive, fixed potential (x-axis). b, Time constant of current inactivation observed in response to a maintained, depolarized voltage step. Each cell is represented by a different symbol. All voltages are corrected for series resistance errors.

The ionic species carrying the outward current was determined from the reversal potential (E_{rev}) of the tail currents shown in Figure 3.8a. The reversal

potential of the I-V relationship following a depolarization to a constant potential represents E_{rev}, since the conductance of the membrane immediately after the step is constant and only the driving force across the membrane varies. Currents were measured at the point indicated by the arrow in Figure 3.8 as this represented a point where currents were uncontaminated by the motor transient. The reversal potential for the currents depicted in Figure 3.8a was -70 mV (Figure 3.8b). The equilibrium potential for a K^+ selective membrane can be calculated using the Nernst equation:

$$E_k = \frac{RT}{zF} \ln \frac{[K^+]_o}{[K^+]_i}$$

Equation 3.7

where R is the gas constant, T, the absolute temperature, z, the valency of the ion, F, Faraday's constant and $[K^+]_o$ and $[K^+]_i$, the extracellular and intracellular concentrations of K^+ respectively. E_k was calculated to be -90 mV for the standard PBS and basic PBS solutions used when recording the currents depicted in this figure (Table 2.1). Thus, the outward current in T4 OHCs must be carried mainly by K^+ ions, due to the very negative value of E_{rev} that tends towards E_k.

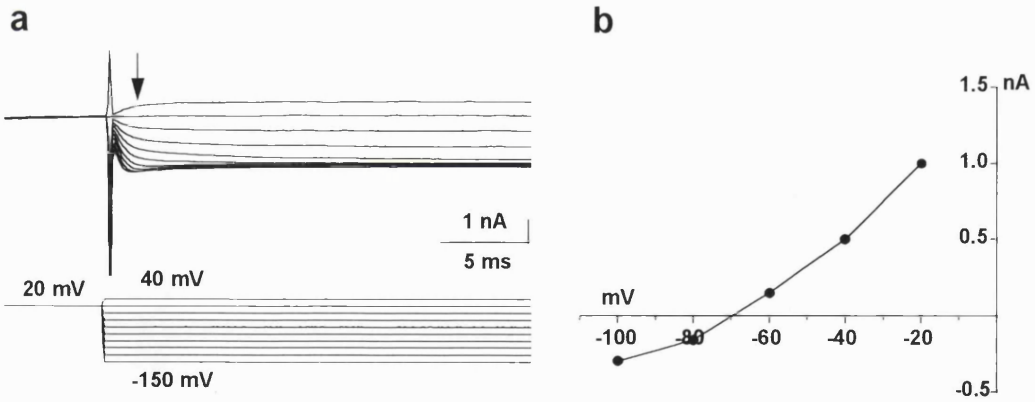

Figure 3.8 Reversal potential measurement. a, tail currents recorded at various potentials following a 10 ms step to +20 mV. b, I-V relationship for the data in part a plotted for the currents recorded at the arrow in part a. Tail currents reversed at -70 mV. Values corrected for R_s and LJPs.

3.3.3 Pharmacology of T4 OHC currents.

3.3.3.1 Dose-response curves for 4AP and TEA

Having demonstrated the possible existence of two different channels carrying the outward current in T4 OHCs through kinetic evidence, attempts were made to distinguish these two components pharmacologically. 4-aminopyridine (4AP) and tetraethylammonium (TEA) were chosen as the K^+ channel antagonists that would be used to attempt to separate the currents. This experimental design relied on the fact that most potassium currents are sensitive to either one or other of these agents (Hille, 1992).

The blocking mechanisms of 4AP and TEA are quite different. TEA exists as a charged molecule and will not cross the membrane. Therefore, inhibition of the channel by TEA is from the outside, possibly via a binding site for the ion (Hille, 1994). 4AP on the other hand is likely to have a far more complex mechanism of action for two reasons:

a) it is a weak organic base which can exist in cationic and uncharged forms at physiological pH
b) its binding to K^+ channels appears to be dependent on the kinetic state of the channel

A consensus opinion on the mechanism of inhibition of K^+ channels by 4AP has not yet been reached. However, the working hypothesis seems to be that the uncharged form of the molecule crosses the membrane and subsequently, the cationic form acts intracellularly to block the open state of the channel (Hille, 1992).

Single-cell dose-response curves for 4AP and TEA were constructed for T4 OHC currents (Figure 3.9). Cells were held at -60 mV and the blockade of the outward current at +40 mV was determined by measuring the instantaneous current recorded in response to ramping the voltage from -100 to +70 mV. Increasing concentrations of the drugs were applied to the cell by whole-bath perfusion. Blockage at each concentration was allowed to reach a steady-state level before a higher concentration of the drug was applied. The

effects of 4AP on OHC currents were not reversible and the effects of TEA, only partially so.

T4 OHC currents are very potently blocked by 4AP. The averaged IC_{50} (half-blocking concentration) for 4AP on these currents at +40 mV was 6.9 ± 2.2 μM (n = 5). The averaged Hill co-efficient was 0.726 ± 0.23 (n = 5) suggesting an approximately 1:1 stochiometry for the number of 4AP molecules required to block one channel. The blocking effects of 4AP saturated after blocking ~70 % of the total current

Outward currents showed very little sensitivity to TEA. Concentrations of TEA in excess of 1 mM were required before any significant inhibitory effects were observed. Even at 100 mM, only 48 ± 5.6 % (n = 4) of the current was blocked at +40 mV. The effects of TEA did not saturate.

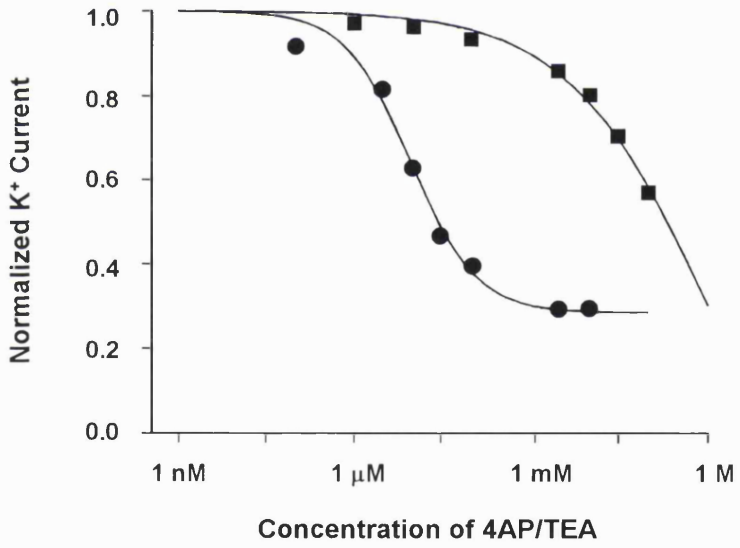

Figure 3.9 Single-cell dose-response curve for 4AP (■) and TEA (●) on the outward currents of T4 outer row OHCs. Inhibition of current measured at +40 mV. Current was normalized to the control level of current. Curve fits to the data produced on FigP using the asymmetric sigmoid fit with allosteric Hill kinetics. The equation was of the following form: y = min + (max-min)/(1 + ((X/X50) - P)).

3.3.3.2 Effects of 4AP on the outward currents of T4 OHC currents

At a concentration of 500 μM, 4AP almost completely removed the current activated in addition to I_k above -40 mV (Figure 3.10a & b). However, it had no effect on the inward current or on the zero-current potential of the cell.

At 0 mV, 77.1 ± 13.1 % (n = 8) of the outward current was blocked by concentrations of 4AP equal to or in excess of 500 μM.

The residual current left in the presence of 4AP exhibited an almost linear relationship with voltage. It was virtually impossible to analyse the onset time constant of these residual currents due to their contamination by the motor transient. Removal of the motor transient with salycilate was not possible as this does not completely block the motor transients (Tunstall, Gale and Ashmore, 1995) and their removal by leak subtraction was not satisfactory as motor activity is not linear with voltage. A component of the onset kinetics of this residual current can be seen after the motor activity has subsided. This could either be due to complex onset kinetics of the 4AP insensitive current or due to a residual number of 4AP sensitive channels that have been left unblocked at this concentration of the antagonist.

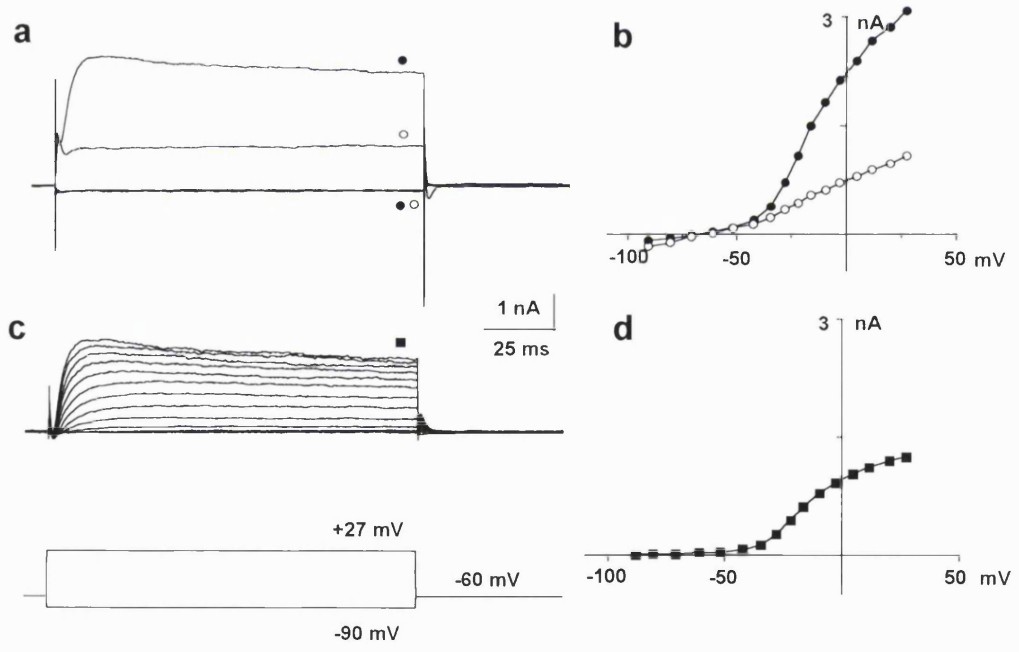

Figure 3.10 Effect of 500 μM externally applied 4AP on T4 outer row OHC currents. a, ● - control current at +27 mV and -90 mV, ○ - current at the same two potentials recorded after application of 500 μM 4AP. Voltage commands shown bottom left. b, steady-state I-V relationship for the family of currents recorded in a. All voltages are corrected for series resistance errors. 4AP completely blocked the current activated above -40 mV whereas it did not affect either the inward current or the zero current potential of the cell. c, family of 4AP sensitive currents obtained by subtraction of residual current ● from control current ○. d, steady state I-V relationship for currents in c.

The 4AP sensitive current, obtained by subtracting the residual traces from the control traces, exhibited a voltage dependence consistent with it being the current described in the previous section that activated above -40 mV, I_{kout} (Figure 3.10c & d). These subtracted currents were delayed in their activation by 1 ms from the start of the voltage step. The time constant of activation for this current at 0 mV was 7.78 ± 0.85 ms (n = 5). This is approximately the same time constant for the whole-cell currents. Therefore, it appears that either the whole-cell time constants are dominated by the 4AP sensitive current, perhaps because the residual current is almost completely activated by the time the 4AP sensitive current is activating, or because both current components activate with the same time constant at approximately the same time and cannot be separated by their time constants alone.

4AP provided a means of uncovering the inactivating component of the outward current. In the presence of 500 μM 4AP, the inactivating component of the current , as well as some of the steady-state current, was removed (Figure 3.11a). The residual current showed absolutely stable steady-state currents throughout the duration of the voltage step. Thus, the 4AP sensitive current is the inactivating component of the outward current. Inactivation can be clearly seen in Figure 3.11b.

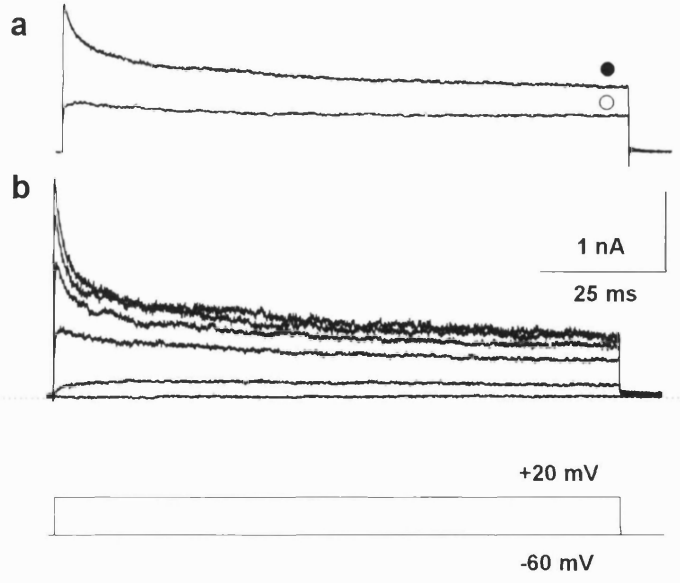

Figure 3.11 Inactivation of the 4AP sensitive current. a, ● - control current; ○ - residual current recorded at 0 mV in the presence of 500 μM 4AP. b, family of 4AP sensitive currents obtained by subtracting the control currents from the residual currents. Voltage was stepped from -60 mV to a series of potentials from -60 to +20 mV in steps of 10 mV.

Finally, the contribution of a calcium-activated potassium conductance (I_{kca}) to T4 OHC currents was investigated by observing the combined effects of 4AP and TEA on OHCs. Calcium-activated potassium channels have been found in a variety of hair cells (Ohmori, 1984; Ashmore and Meech, 1986; Hudspeth and Lewis, 1988; Sugihara, 1994; Fuchs and Evans, 1990; Kros and Crawford, 1990) to activate at potentials more positive than -35 mV with an I-V relationship above this potential very similar to the 4AP sensitive conductance observed in these hair cells. After the application of 3 mM 4AP to T4 OHCs, further addition of 30 mM TEA did reduce the outward currents. TEA reduced the currents remaining after the addition of 4AP by 0.06 nA or 10 % at +40 mV and by 0.03 nA or 9 % at 0 mV. These small changes are not due to rundown of currents with time in the whole-cell recording configuration. Control experiments demonstrated that the current amplitude and the zero-current potential of the cell changed by less than 5 % over a 50 minute recording period (data not shown). No additional effect of TEA to 4AP was observed at -60 mV (Figure 3.12). Thus, the contribution of a TEA-sensitive conductance to these T4 OHCs currents is small but obvious. T4 OHCs appear to express two currents that are only activated a voltages above -40 mV.

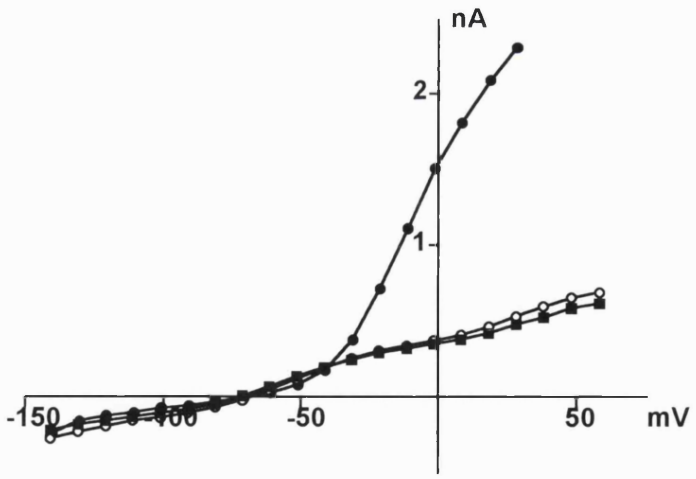

Figure 3.12 The combined effects of 3 mM 4AP and 30 mM TEA on T4 OHC currents. ● - control current-voltage relationship, ○ - current-voltage relationship in the presence of 4AP alone. ■ - current-voltage relationship in the presence of 4AP and TEA. Although 4AP was able to remove most of the extra current activated above -40 mV, TEA was able to remove 10 % of the remaining current at +50 mV. Data have been corrected for voltage errors due to uncompensated series resistance.

Together, 4AP and TEA are clearly able to distinguish between the currents activated above -40 mV and those activated around the zero-current potential of the cell. Thus, the 4AP-sensitive current will now be referred to as

I_{kT4} the TEA-sensitive current as I_{kca} and the 4AP and TEA-insensitive current, that is active around the zero-current potential of the cell, as $I_{k,n}$.

3.3.3.3 Pharmacology of I_k in T4 OHCs

The predominant current activated around the zero-current potential of the cell was a K^+ dependent conductance, as the mean zero-current potential of -65 mV was unaffected by the presence of 4AP and TEA. This current showed an almost linear relationship to voltage (Figure 3.10b) and no signs of saturating its response to voltage below -100 mV as observed in other studies (Mammano and Ashmore, 1996). Inward currents did not exhibit the very significant transient component observed in isolated OHCs (Housley and Ashmore, 1992). However, in 37 % (n = 7) of T4 OHCs, some inactivation of the inward current was observed at all potentials below -70 mV (Figure 3.13). In this sub-population of cells, inward currents relaxed by 0.12 ± 0.01 nA over 35.6 ± 5.2 ms (n = 5) at -140 mV. This transient component of the inward current could be completely removed by 5 mM extracellular Cs^+. Cells exhibiting this transient inward current did not show significantly different zero-current potentials from

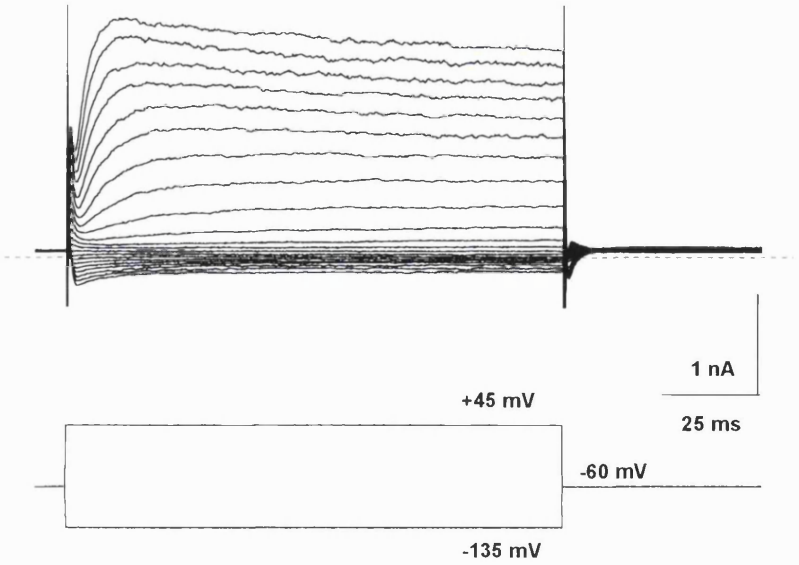

Figure 3.13 The transient component of the inward current in T4 OHCs. Relaxation of the inward current could be observed in 37% (n = 7) of *in situ* OHCs. This feature was generally associated with larger steady-state inward currents. All voltages were corrected for series resistance errors and may be due to the activation of a K^+-independent conductance.

cells without the transient (P = 0.04, test e, Table 1, Appendix 1). However, this test does not rule out the possibility that this transient current results from a K^+-

independent conductance, such as a non-specific cation conductance, that may shift V_z towards 0 mV.

The pharmacology of the steady-state component of I_k is extremely unusual. Data in the previous section demonstrated that this current is unaffected by 4AP or TEA. Thus, the effects of Cs^+ were investigated. Previous work on isolated OHCs has shown that the current active around V_z is slightly Cs^+ sensitive (Housley and Ashmore, 1992). However, the application of 5 mM external Cs^+ to OHCs via a puffer pipette had almost no effect on the steady-state current, except below -80 mV where a 0.06 nA reduction in current was observed (Figure 3.14). These effects were fully reversible. No further investigations into the pharmacology of the steady-state current were conducted.

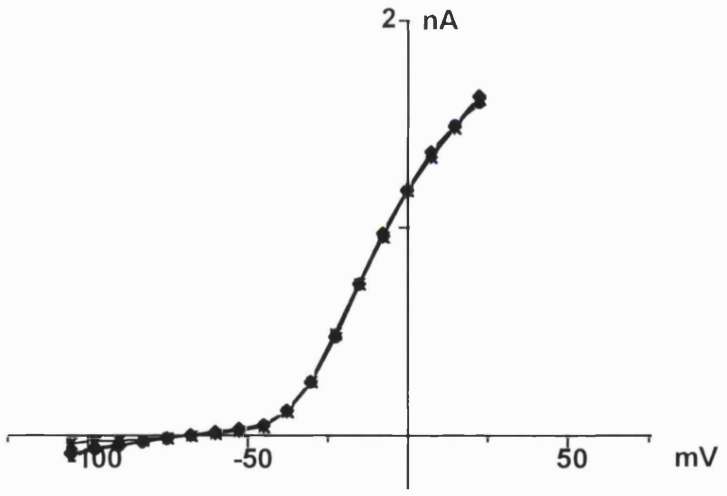

Figure 3.14 Effects of Cs^+ on the steady-state component of T4 OHC currents. I-V curve plotted for data, before ●, during ✳ and after ■ the puff application of 5 mM extracellular Cs^+ on T4 OHCs. Data have been corrected for voltage errors due to uncompensated series resistance.

These results suggest that the inward current in T4 OHCs may be made up of a transient and a steady-state component. These will now be referred to as I_{kt} and $I_{k,n}$ respectively. Expression of the transient component is variable, being seen in just over one third of all the cells. Its time course and pharmacology closely resemble the transient current observed in isolated OHCs. Its expression may indicate some deleterious effects to OHC such as the activation of a non-specific cation conductance. However, the difference between the zero-current potential of the two populations of cells is not

significantly different, indicating that those cells with and those cells without the transient components are from the same population of cells.

The steady-state component of the outward current in T4 OHCs exhibits extremely unusual pharmacology, being almost completely insensitive to three, broad spectrum K^+ channel antagonists. However, this result does not imply that $I_{k,n}$ is not a potassium current as the zero-current potential of the cell in the presence of 4AP is still close to E_k. This component is responsible for the resting conductance in OHCs.

3.3.4 Sensitivity of basolateral membrane currents to increases in intracellular Ca^{2+}

The regulatory effects of intracellular Ca^{2+} on T4 OHC currents were investigated using the photolabile Ca^{2+} chelator DM-Nitrophen. Whole-cell currents recorded before and during Ca^{2+} release from this chelator were compared. Currents were recorded at -110 mV and at 0 mV. The former voltage was chosen to investigate the effects of increased intracellular Ca^{2+} on I_k alone. The latter voltage was chosen to allow the Ca^{2+} sensitivity of I_{kT4} to be investigated without contamination by a non-selective cation current, observed in isolated OHCs (Housley and Ashmore, 1992). The maximum response of the cells to the photolysis of DM-Nitrophen was compared to the pre-photolysis level.

T4 outer row OHC currents can be modulated by raised intracellular Ca^{2+} levels (Figure 3.15a). The maximum effect was reached ~3 seconds after the start of the UV exposure. Raised intracellular Ca^{2+} concentrations resulted in seven of the nine cells tested showing a very slight reduction of their outward current at the holding potential of -60 mV (0.025 ± 0.008 nA). The other two cells showed no change in their current at this voltage. In all the cells recorded, outward currents at 0 mV increased in amplitude by 0.17 ± 0.12 nA (n=9). No significant difference was observed in the time constant of current onset at 0 mV between control and test traces ($P = 0.15$, test f, Table 1, Appendix 1). Only one of the nine cells tested showed a change in the current level at -110 mV. For this one cell, the increase in current was very small, being just 0.02 nA. The effects of photolysis were fully reversible within 2 minutes.

To attempt to correlate the observed Ca^{2+} sensitivity with one of the currents described above, the experiments were repeated in the presence of millimolar concentrations of 4AP. 4AP blocks the outward current activated above -40 mV and may therefore help to discriminate between the Ca^{2+} effects on the currents activated above and below -40 mV. In the presence of 4AP, the responses of the cells were variable. Three out of six cells showed an increase in the inward current at the holding potential of -60 mV of 0.093 $\pm$ 0.049 nA. The other three cells showed no change in the holding current. Four of the six cells tested showed a response to raised intracellular Ca^{2+} at 0 mV of 0.221 $\pm$ 0.15 nA. Five showed an increase in their inward current of 0.123 $\pm$ 0.098 nA. At 0 mV, current activation did get faster with raised intracellular Ca^{2+} (Figure 3.15b). However, this change in the time constant of current onset was unmeasurable due to the contamination of the current by the motor transient. The highly variable responses observed in this set of experiments may reflect:

a) the different loading of chelator between different cells
b) the increased age of the cells by the time intracellular Ca^{2+} was increased compared to control cells due to the time required to bath perfuse the cells with 4AP.

The effects of photolysis were not always fully reversible. 32% of all the cells investigated exhibited some permenant change following photolysis.

These results indicate that I_{kT4} is unlikely to be Ca^{2+} sensitive as the Ca^{2+} responses of the OHCs are maintained in the presence of millimolar concentrations of 4AP. Ca^{2+} could be activating the TEA-sensitive conductance. However, this conductance must play a very small part in the Ca^{2+} response, as significant increases in current with the photolysis of DM-Nitrophen were still observed in the presence of TEA (data not shown). The increase in the inward current at -60 mV is not consistent with the activation of a K^+ conductance. Thus, it seems unlikely that $I_{k,n}$, the potassium conductance activated around the zero-current potential of the cell, would contribute towards this response. However, the Ca^{2+} sensitivity of this current cannot be ruled out as a decrease in the extracellular Ca^{2+} concentration of the perfusate did, in one experiment, cause a decrease in the conductance of the cell both above and below -50 mV,

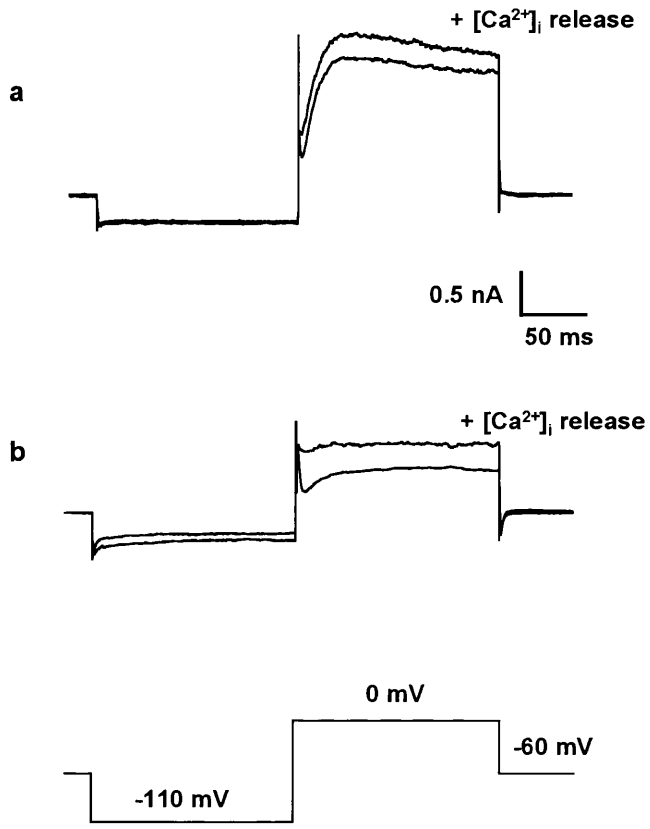

Figure 3.15 Effects of increasing intracellular Ca^{2+} by photolysis of DM-Nitrophen on T4 OHC currents. a, control currents recorded before and during photolysis. b, currents recorded before and during photolysis in the presence of 3 mM 4AP. Voltage protocol shown in the bottom panel.

a result also observed by Raybould and Housley (1997). Additionally, Jagger and Ashmore (1999) have shown the current activated around the zero-current of the cell to be Ca^{2+} sensitive. Finally, these results could be explained by the activation of a cation conductance which, as well as increasing the inward and outward conductances, would also increase the inward current at the holding potential of the cell. Although the aim of recording the current at 0 mV was to minimize the effect of such a current, voltage errors due to uncompensated series resistance would keep the voltage just below 0 mV, allowing the effect of raised intracellular Ca^{2+} on this current to be observed . It is unlikely that the cation conductance in question is associated with the transducer current as Ca^{2+} responses could also be obtained from OHCs in the presence of 100 μM DH-streptomycin. However, a Ca^{2+} sensitive cation conductance, associated with the basolateral membrane of the hair cell, has been observed in isolated preparations (Housley and Ashmore, 1992, Van den Abbeele, Tran Ba Huy, Teulon, 1994). The amount of current carried through the channels associated

with this conductance increases with time after isolation and time in the whole-cell configuration possibly due to intracellular Ca^{2+} accumulation. The latter effect could certainly explain why increased and more variable responses were observed in the presence of 4AP, as these cells had been patched longer before photolysis to allow for the bath perfusion of 4AP. However, in a freshly excised cochlea, a cation conductance was not obvious (Figure 3.5) which may indicate that the channel carrying this cation conductance is expressed, but not functioning in T4 OHCs unless the concentration of intracellular Ca^{2+} is increased.

It seems highly unlikely that these results can be exclusively explained by the Ca^{2+} activation of a cation conductance when there is also evidence for Ca^{2+} activation of $I_{k,n}$ (Housley and Ashmore, 1992; Jagger and Ashmore, 1999; Raybould and Housley, 1997). Therefore, the story is probably far more complex than the explanation given above and most likely involves the combined activation of $I_{k,n}$ and the cation conductance, the observed changes being the net effect of the two currents.

3.4 Discussion

This preparation provides an ideal means of examining the physiological characteristics of OHC for two reasons:

a) the significantly more negative zero-current potential of *in situ* OHCs compared to *in vitro* OHCs, that tends towards the zero-current potential for *in vivo* OHCs indicates that this preparation provides an ideal physiological environment in which to study OHCs without the complications of an *in vivo* preparation.

b) it allows the recording site along the basilar membrane to be unequivocally identified and thus, the electrophysiological characteristics of OHC to be closely correlated with the best tuning frequency for that point along the cochlear length

The identity of the ion channels carrying the basolateral membrane currents of mammalian T4 OHCs has been examined by characterizing the

currents according their kinetics, pharmacology and Ca^{2+} sensitivity. The results are summarized in Figure 3.16. These results are grossly similar to previous studies, in so far as they demonstrate that *in situ* OHCs exhibit a negative zero-current potential and express at least two K^+-dependent membrane currents, one active around the zero-current potential of the cell, the other above -40 mV. However, these results extend previous observations by suggesting that there are at least two components to each of these previously identified conductances. These conclusions help to bring together the results from other studies.

3.4.1 Basolateral membrane conductances activated above -40 mV

Investigations into the basolateral membrane conductances of adult mammalian OHCs first started with Meech and Ashmore (1986). They provided evidence for a calcium-activated potassium conductance at the synaptic pole of isolated OHCs and concluded that the basolateral membrane conductances of these cells are dominated by I_{kca}. This is feasible in the cells used in this study that exhibited resting membrane potentials of -15 to -40 mV and large input conductances of up to 40 nS. However, such a conductance would not be able to dominate the basolateral membrane of *in situ* OHCs as these channels would be shut at the zero-current potential of -65 mV. Other authors have also confirmed that adult mammalian OHCs express calcium-activated potassium channels by demonstrating the TEA sensitivity of the currents activated above -40 mV (Housley and Ashmore, 1992; Santos-Sacchi and Dilger, 1988). However, the extreme 4AP sensitivity of the same current was not demonstrated until 1995 by Mammano, Kros and Ashmore, working on OHCs from the *in situ* cochlea. Calcium-activated potassium conductances are not known for their sensitivity to 4AP (Hille, 1992). Therefore, previous assumptions that I_{kca} dominated the basolateral membrane conductances above -40mV had to be reviewed. The experiments described in this thesis show that the additional current activated above -40 mV comprises of at least two conductances, one that is 4AP sensitive, making up 90 % of the current activated above -40 mV, (I_{kT4}), the other being TEA sensitive and comprising the final 10 % of the outward current activated above -40 mV. Similar result to these have been obtained by Nenov, Norris and Bobbin (1997).

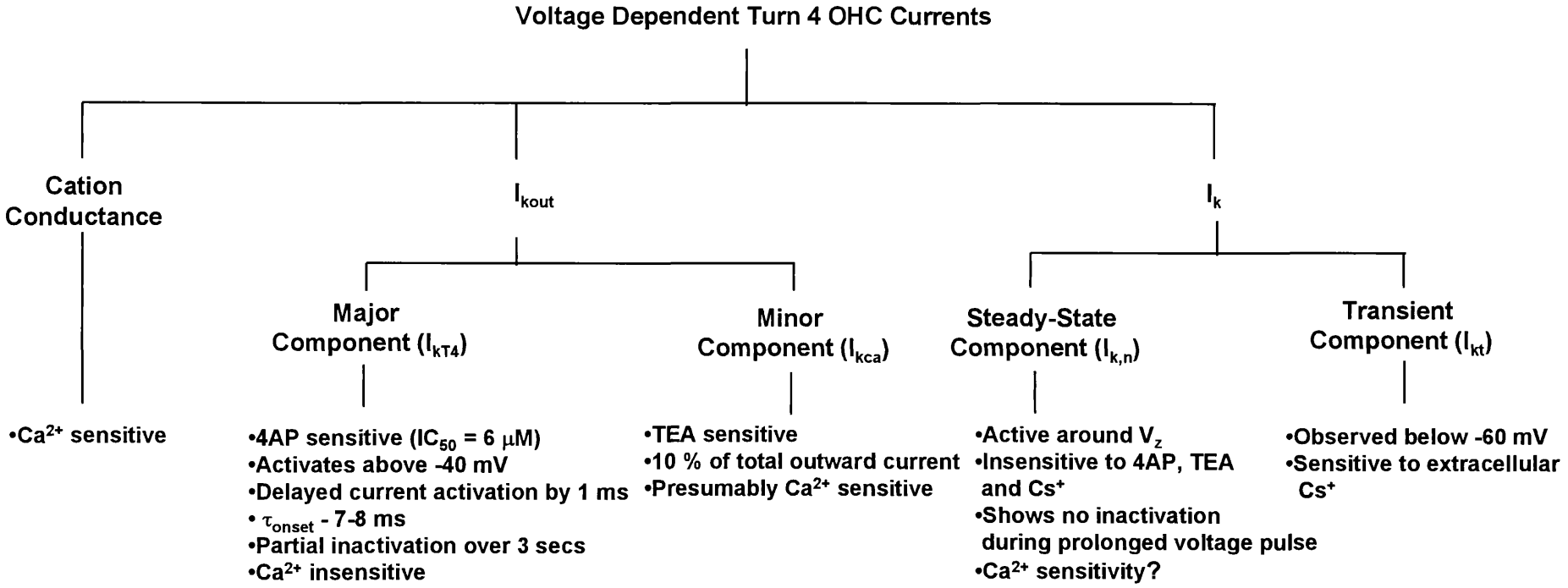

Figure 3.16: Ionic currents in turn 4 *in situ* OHCs

To try and identify the type of current that is blocked by 4AP in adult mammalian OHCs, a comparison has been made between I_{kT4} and other, well defined potassium currents that are either 4AP sensitive or exhibit kinetics similar to I_{kT4} (Table 3.3). I_{kT4} is characterized by several distinctive biophysical and pharmacological features such as rapid onset kinetics, sensitivity to micromolar concentrations of 4AP and insensitivity to TEA. These characteristics are not consistent with I_{kT4} being an A-type potassium current. This current exhibits more negative voltage activation and less sensitivity to 4AP in comparison to I_{kT4}. In addition, the properties of I_{kT4} are inconsistent with it being a classical delayed rectifier current, which is 4AP insensitive, or an L-type potassium current, which is very sensitive to block by TEA. Instead, I_{kT4} appears to show the greatest similarity to the D-type potassium current (I_{kD}) (Locke and Nerbonne, 1997; Wu and Barish, 1992; Storm, 1988) and the ultra-rapid delayed rectifier current ($I_{k,UR}$) (Feng, Wible, Li, Wang, Nattel, 1997; Guo, Kamiya, Liu, Toyama, 1997; Yue, Feng, Li, Nattel, 1996). Both currents exhibit extremely high sensitivity to 4AP, delayed onset kinetics and a time constant of current activation very similar to that observed in this preparation. However, unlike I_{kT4}, $I_{k,UR}$ exhibits submillimolar sensitivity to TEA, a more positive voltage activation threshold and sensitivity to increased intracellular calcium concentrations. I_{kD} on the other hand shows no TEA sensitivity and little sensitivity to raised intracellular calcium concentrations, unless intracellular solutions contain minimal BAPTA, ATP and GTP concentrations (personal communication, M. Barish). Thus, I_{kT4} appears to most closely resemble I_{kD}.

The molecular architecture of I_{kD} channels is not yet known. However, being part of the delayed-rectifier family, the subunits that make up the channel are most likely to be of the Kv2 sub-type. Immunocytochemical studies on hippocampal pyramidal neurones that exhibit D-type potassium currents express Kv1.4 at high levels (M. Barish, personal communication). Thus, it may be that I_{kD} is not part of the classical delayed-rectifier family, but is derived from one of many splice variants produced from *Shaker* genes. These splice variants all have highly conserved core structures that determine features such as the voltage dependence of activation. However, they vary in their amino terminal domains that form the cytoplasmic, inactivation gate of the ion channel. This non-conserved region of the protein is responsible for the highly variable inactivation kinetics seen among the *Shaker* subfamily (Jan and Jan, 1992; Salkoff, Baker, Butler, Covarrubias, Pak and Wei, 1992). Such variations in the

channel protein may also affect the 4AP sensitivity of the channel. This prediction could be confirmed or disproved using single cell RT-PCR profiling to identify the cellular mRNA coding for voltage-dependent potassium channels (Baro, Levini, Kim, Willms, Lanning, Rodriguez, Harris-Warrick, 1997).

I_{kT4} is clearly well designed to restore the membrane potential after a depolarization. It would be easily activated by a maximum receptor potential of 30 mV (Dallos, 1986). Once activated, this conductance would also help to shape the receptor potential in OHCs.

Current	Channel Subunit	Activation voltage (mV)	4AP (mM)	TEA (mM)	τ_{onset} (0 mV) (ms)	$\tau_{Inactivation}$ (0 mV) (s)	Ca^{2+} sensitive	Ref
Shaker **A-type**	Kv1/4	-50	>0.5	n/a	1.5 V.D.	0.02 (full) V.I.	No	a
D-type	Kv1.4?	-70 to -30	<0.1	n/a	4 V.D.	0.6 (partial) V.D.	?	b
Delayed Rectifier	Kv2	-40	n/a	>5	30 V.D.	0.4 and 3.1 (partial) V.I.	?	c
Ultra-Rapid Delayed Rectifier	Kv1.5	-30 to -20	0.01	0.3	15 V.D	0.6 and 5.5 (partial) V.I.	Yes	d
L-type	Kv3.1	-20	<0.1	0.2	5 V.D.	5.2	?	e
I_{kT4}	?	>-40	<0.06	n/a	8.13 V.D.	0.41 (partial) V.D.	No	

Table 3.3 Characteristic of a sample of K^+ channels. These channels either show a high sensitivity to 4AP and/or kinetics very similar to those observed for the 4AP sensitive current in T4 OHCs. References used for data: a) Locke and Nerbonne, 1997; Song, Tkatch, Baranauskas, Kitai, Surmeier, 1998, b) M. Barish, personal communication; Locke and Nerbonne, 1997; Wu and Barish, 1992; Storm, 1988 c) Locke and Nerbonne, 1997 d) Feng, Wible, Li, Wang, Nattel, 1997; Guo, Kamiya, Liu, Toyama, 1997; Yue, Feng, Li, Nattel, 1996 e) Grissmer, Nguyen, Aiyar, Hanson, Mather, Gutman, Karmilowicz, Auperin, Chandy, 1994, Massengill, Smith, Son, O'Dowd, 1997; Wang, Gan, Forsythe, Kaczmarek, 1998 V.D. = Voltage Dependent, V.I. = Voltage Independent

The calcium-activated potassium channel of adult mammalian OHCs is very likely to be encoded by the *Slo* gene, named after the *'slowpoke'* gene from Drosophila that codes for K_{ca} channels in the fruit fly (Atkinson, Robertson, Ganetzky, 1991). Homologous genes have been identified in mammals (Bulter, Tsunoda, McCobb, Wei, Salkoff, 1993) and certainly the single channel conductance of *cSlo* (224 pS) is comparable to the single channel conductance of 233 pS, observed in guinea-pig OHCs, that was identified as a calcium-activated potassium conductance (Ashmore and Meech, 1986). Although the calcium-activated potassium conductance is well designed for the same role as I_{kT4}, its relatively minor expression in these cells may implicate it in a different role, perhaps in controlling the synaptic activity of the cell. The expression of I_{kca} and I_{kT4} are restricted to the basal pole of the OHC (Santos-Sacchi, Huang and Wu, 1997).

3.4.2 Basolateral membrane conductances activated around the zero-current potential of the cell

The current activated around the zero-current potential of the cell was first investigated in detail by Housley and Ashmore (1992) who termed it $I_{k,n}$ to signify its negative activation potential. They found it comprised of two parts, a transient component and a steady-state component, the former and to some extent the latter, being sensitive to extracellular Cs^+. This was interpretated as a desensitization of the conductance that was fully or substantially activated at the zero-current potential of the cell (Housley and Ashmore, 1992; Mammano and Ashmore, 1996; Nenov, Norris and Bobbin, 1997). The residual current remaining in the presence of extracellular Cs^+ was hypothesised to be due to a non-selective cation conductance. Both the transient and the steady-state components of $I_{k,n}$ have been shown to be activated by calcium (Jagger and Ashmore, 1999). $I_{k,n}$ is not a classical inward rectifier current as it contributes to the outward current in response to depolarizing steps and the inward current in response to hyperpolarizing steps (Mammano, Kros and Ashmore, 1995). Further, significant characterization of $I_{k,n}$ has not been published.

This study indicates that the two components to the inward current in T4 OHCs may be separate currents. The transient component (I_{kt}) was smaller and less often observed *in situ* compared to isolated OHCs. It was completely removed by extracellular Cs^+, an agent that had no effect on $I_{k,n}$. As the

expression of I_{kt} is limited to isolated OHCs and a sub-population of *in situ* OHCs, it is tempting to suggest that its expression is associated with less healthy hair cells, perhaps ones with a raised cytoplasmic Ca^{2+} concentration. *In situ* OHCs may have a lower cytoplasmic Ca^{2+} concentration if their transducer channels are more in tact, if there is less Ca^{2+} channel degradation in a preparation that does not require enzymes or if the endogenous Ca^{2+} buffering of the cell has been not been saturated or deteoriated (Chapter 6). Although the zero-current potential of OHCs exhibiting I_{kt} is not significantly different from cells without I_{kt}, it is nevertheless more positive. This may implicate I_{kt} as a cation conductance whose functional expression increases with increasing intracellular Ca^{2+} concentrations.

Most of the steady-state current ($I_{k,n}$) remains in the presence of Cs^{+}. It is unlikely that this current is the same as $I_{k,L}$, a delayed rectifier conductance that has been observed in Type 1 hair cells of the mouse utricle (Rüsch and Etock, 1996) because although $I_{k,L,}$ like $I_{k,n}$ has an unusually negative activation voltage, it is 4AP sensitive (IC_{50} = 43 μM) and Ca^{2+} independent. Thus, $I_{k,n}$ is an extremely unusual K^{+}-dependent conductance that exhibits a very negative voltage dependence and extraordinary pharmacology.

One function for $I_{k,n}$ may be to clamp the cell close to the potassium equilibrium potential to maximize the inward driving force for cations across the transduction channels at the apical surface. However, it is also responsible for controlling the electrical properties of the OHCs at the zero-current potential of the cell where it controls the membrane time constant and the corner frequency of the hair cell. Paradoxically, although the characteristic frequency for OHCs located at this point along the length of the cochlea is 400 Hz (Greenwood, 1990), the membrane time constant for T4 OHCs was calculated to be 12 ms, giving rise to a corner frequency of 13 Hz (Equations 3.3 and 3.4). This implies that at the characteristic frequency for OHCs located at that point along the length of the cochlea, most of the current passing through the transducer channels will pass through the membrane capacitance, attenuating the size of the receptor potential. Incomplete charging and discharging of the OHC membrane at high frequencies will reduce the magnitude of the OHC-length changes by half for each doubling of the stimulus frequency (Kolston, 1995). Therefore, a maximum receptor potential of 30 mV (Dallos, 1986), will be attenuated to 0.973 mV which will generate a maximum length change of 1.9 nm

based on a motor sensitivity of 2 nm/mV (Santos-Sacchi, 1989). At the threshold of the OHCs response (20 dB s.p.l.), T4 OHCs will change length by 0.124 nm. The implications of this are discussed in Chapter 5.

One interesting point to note about the cation conductance is that if it is functional *in vivo*, when activated it would increase the corner frequency of the basolateral membrane thus allowing higher frequency signals to pass before being attenuated. However, this would be at the expense of reducing the resting membrane potential of the cell and reducing the transduction current. The two would therefore end up negating one another. Activation of this cation conductance requires micromolar levels of Ca^{2+} for its activation. Such levels may only conceivably be reached *in vivo* during loud noise exposure. This conductance may be a marker for unhealthy hair cells.

3.4.3 Model and summary

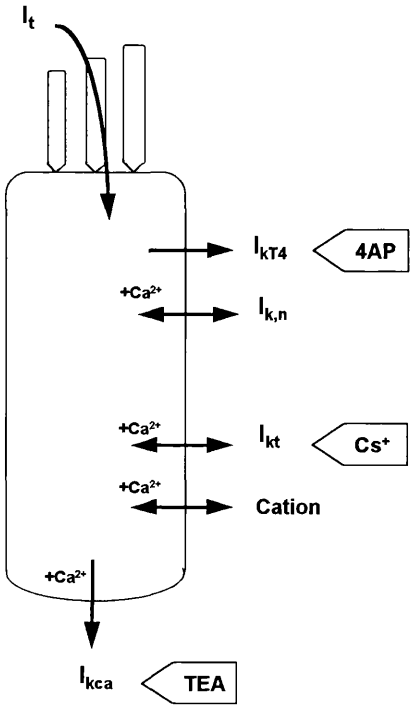

Figure 3.17 Proposed model for the ionic conductances present in T4 *in situ* OHCs. I_{kT4} represents the 4AP-sensitive current activated above -40 mV. Additionally, there is a calcium-activated potassium conductance also activated above -40 mV that is sensitive to millimolar concentrations of TEA. This current is termed I_{kca}. I_k has been separated into the transient, I_{kt}, and steady state, $I_{k,n}$, components which make up the total current activated around the zero-current potential of the cell. A cation conductance also appears to be expressed, but not functioning in T4 OHCs unless intracellular Ca^{2+} is increased.

A model of the ionic currents thought to be present in T4 OHCs is presented in Figure 3.17. Experiments described in this chapter demonstrate the presence of three types of potassium channels in the basolateral membrane of these cells. It is proposed that only $I_{k,n}$ and I_{kT4} contribute to the functional properties of the basolateral membrane of the OHCs and that I_{kca} is more likely involved in the synaptic activity of T4 OHCs. I_{kt} and a cation conductance may be one in the same current and may act as markers for unhealthy hair cells.

Chapter 4

Basolateral Membrane Currents of T1 OHCs

4.1 Introduction

4.1.1 Investigating four variables of T1 OHCs

The aim of this study is to characterize T1 OHCs according to their morphology and the currents that pass through the voltage-activated ion channels in their basolateral membrane. T1 OHCs are some of the most fascinating mammalian cells, as they have evolved to respond to stimulus frequencies beyond 10 kHz (Greenwood, 1990). However, there is a paucity of information regarding these cells, possibly due to their high morbidity outside the cochlea and the logistical difficulty of accessing these cells at the base of the cochlea. The information gleaned so far has almost exclusively come from *in vivo* preparations where their receptor potential has been investigated with intracellular recordings from these cells (Cody and Russell, 1987). Only one study has attempted to explore the membrane currents of basal turn OHCs that underlie the receptor potential (Raybould and Housley, 1997). However, the main focus of this study was the examine the change in the OHC response to ATP along the length of the cochlea. Thus, no detailed description of the kinetics or pharmacology of the voltage-dependent currents in the basolateral membrane of T1 OHCs was given. The results presented in this chapter start to fill this gap. The basolateral membrane currents of T1 OHCs were characterized by their kinetics, pharmacology and sensitivity to raised intracellular Ca^{2+} concentrations.

4.2 Methods

T1 OHCs *in situ* survived for just 40-45 minutes following the removal of the temporal bone from the guinea-pig. During this time the cells changed morphologically, swelling around their basal pole and losing their

optical reflectivity. These changes gave the cells a 'ghost-like' appearance and were often followed by the cell bursting. Electrophysiological recordings from T1 OHCs also caused problems. Giga-seal formation was difficult to achieve anywhere on the basolateral membrane, the cell-attached configuration was rarely stable, breaking down to the whole-cell configuration almost immediately. Finally, when patching using the basic intracellular solution used in T4 OHC recordings, the zero-current potential of the cell rapidly deteriorated from ~-80 mV towards 0 mV over a period of 5-7 minutes. These changes were accompanied by a loss of the current activation kinetics and a linearization of the I-V relationship. Clearly, the standard protocol used for T4 OHC preparations was not suitable to obtain stable whole-cell recordings from T1 OHCs. Thus, alterations to this protocol had to be made to improve the quality of basal turn OHCs for electrophysiological recordings. These alterations are discussed below.

4.2.1 Mounting the bulla in the recording chamber

T1 OHC preparations were mounted in the recording chamber at an angle ~45^0 relative to a T4 preparation. Once the overlying turns had been removed, this significantly improved the illumination, visualization and access to hair cells in the basal turn of the cochlea (Figure 4.1).

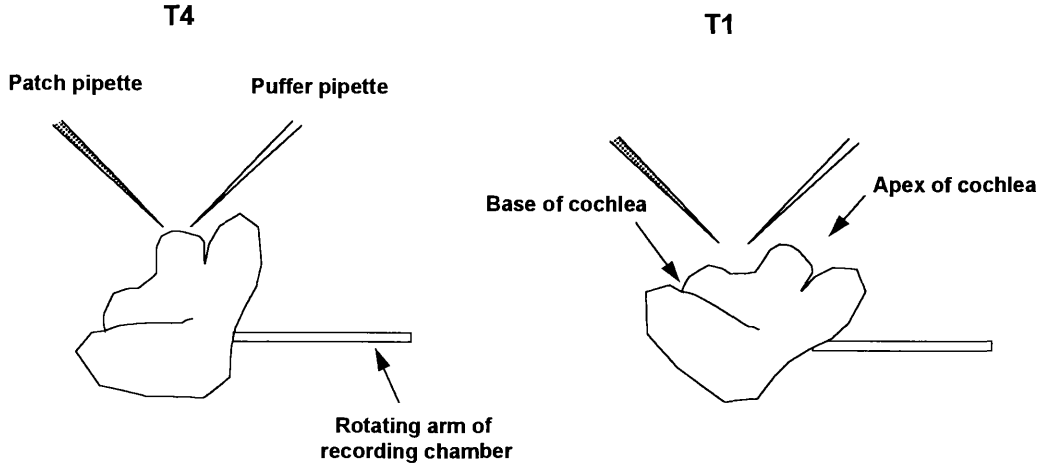

Figure 4.1 Schematic, comparing the mounting of the temporal bone on the rotating arm of the recording chamber for a T4 and a T1 preparation. T4 organ of Corti is easily illuminated by the fibre optic and accessed by the patch and puffer pipettes as it sits proud of the bulla. The lower turns of the cochlea are less easily illuminated and accessed as they are more encased within the bulla. These preparations must be tilted to improve visualization of and access to the basal sensory epithelium.

4.2.2 Maximizing the survival time of T1 OHCs

It was critical that the time from decapitation of the guinea-pig to the start of recording from OHCs was kept as short as possible (ideally < 15 minutes), maximizing the time window available to work on the preparation. However, an efficient dissection was not necessarily a prerequisite for healthy basal turn OHCs. Below are a list of alterations made to the standard protocol that significantly improved the quality of T1 OHCs and prolonged their life-span.

a) OHC swelling was reduced by increasing the osmolarity of the extracellular solution from 325 to 332 mOsm/kg, by the increased addition of D-glucose. Although this did not remove the swelling of the OHCs, it did significantly slow the process.

b) The concentration of extracellular Ca^{2+} was reduced from 1 mM to 50 μM, reducing the electrochemical gradient for Ca^{2+} movement into the hair cell either via the transducer channels or via putative Ca^{2+} channels (Isolation PBS, External Solutions, Table 2.1). This concentration was chosen as it reflects the concentration of Ca^{2+} thought to bathe the stereocilia *in vivo* (Boscher and Warren, 1978). As a ubiquitous second messenger, Ca^{2+} overloading of the cytoplasm has the potential to activate a whole variety of biochemical cascades that may have deleterious consequences on the OHCs. A low concentration of extracellular Ca^{2+} may also have helped to reduce swelling by preventing the insertion of synaptic vesicles into the basolateral membrane of the OHC. Ca^{2+} movement through the transducer channels was further reduced by the addition of 200 μM DH-streptomycin to the extracellular solution.

c) T1 OHCs survived longer when the extracellular solution was pH buffered with phosphates rather than HEPES. This effect was also observed in T4 OHCs but over a much longer time course. It is unclear why HEPES is not a favourable pH buffer to use. One hypothesis might be that if phosphate transporters are expressed in OHCs, phosphates may be able to cross the OHC membrane and effect the intracellular as well as the extracellular environment of the cell. Although there is no evidence for such transporters in OHCs of the cochlea, their existence cannot be ruled out. Phosphate transporters have been

observed in kidney epithelial cells (Miyamoto, Tatsumi, Sonoda, Yamamoto, Minami, Taketani, Takeda, 1995).

d) Supporting cells, that surround OHCs *in vivo,* may regulate the extracellular environment of the OHC by sequestering or releasing ions. Hensens's cells that overlie the outer row OHCs were removed in order to improve access to the basolateral membrane of the OHC for patching. As a result of the large, basolateral membrane conductances of T1 OHCs, K^+ may accumulate in the extracellular spaces immediately surrounding the OHC causing depolarization. To try and avoid this problem, T1 OHC preparations were dissected and initially bathed in a low K^+-concentration extracellular solution (0.4 mM), otherwise identical to the isolation PBS detailed in Table 2.1. This was exchanged for normal extracellular solution ($[K^+]_o$ = 4 mM) having achieved the whole-cell patch-clamp configuration.

e) To reduce the metabolic activity of the OHC and thus to slow the degradative processes and the oxygen demand of the tissue, the bulla was placed in ice-cold saline within 1 minute of decapitation and maintained in solution of this temperature throughout the dissection.

Together, the five procedures listed above improved the quality of basal turn OHCs for patching and increased their lifespan from 40-45 minutes to 1-1$\frac{1}{4}$ hours. Although these modifications eased the time pressures of the experiment, they clearly did not conquer the problem of rapid cell death, as the survival time of these cells was still significantly less than that of T4 *in situ* OHCs. Other amendments to the protocol were attempted, but they did not significantly improve the experiment. For completeness, these amendments are listed below:

a) As OHC integrity could be seriously damaged by free radical production within the cell itself (Hirose, Hockenbury and Rubel, 1997), a free radical scavenger, was added to the extracellular solution. However, 10 mM glutathione did not slow down or remove T1 OHC degradation.

b) Substitution of extracellular Na^+ for an equal concentration of NMDG did not prolong the lifespan of the preparation. Thus, depolarization of the OHC through Na^+ loading does not seem to contribute to T1 OHC death.

c) The quality of the preparation was not improved if either superglue or dental acrylic was used as an alternative to wax for mounting the preparation in the recording chamber.

d) To increase the oxygen saturation of the perfusate and thus minimise OHC hypoxia, the reservoir was bubbled with air. Although this did not improve the quality of the preparation, the possibility of hypoxia being a problem immediately after decapitation of the guinea-pig cannot be ruled out.

4.2.3 Preventing run-down of T1 OHC currents.

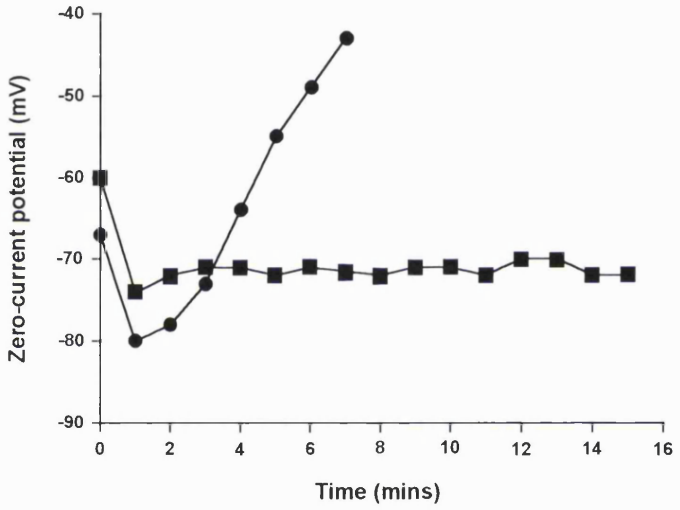

Figure 4.2 The change in zero-current potential of a T1 OHC patched with either standard intracellular solution (●) or a potassium fluoride based intracellular solution (■). 7 minutes after the start of the experiment, the cell patched with standard intracellular solution had died. For the cell patched with potassium fluoride, the cell was still healthy 15 minutes into the patch, after which time the experiment was terminated.

The zero-current potential of T1 OHCs patched with basic PBS solution (Table 2.1) deteoriated from ~-80 mV to 0 mV over the first 5-7 minutes of a whole-cell recording (Figure 4.2). Without a stable baseline, experimentation on these cells was impossible. The addition of 2.5 mM Mg-ATP to the pipette solution was unable to prevent this run-down. However, when the main intracellular anion was changed from Cl^- to F^- (KF, Internal Solutions, Table 2.1), the zero-current potential of the cell remained absolutely steady for upto 15 minutes and often for much longer. The most straightforward explanation for the effect of F^- would be to suggest that it relieved the cells of Cl^- regulation, a process that was otherwise overloaded, causing the cells to die. Alternatively, as F^- is known to interact with a number of different proteins such as G-proteins,

phosphatases and phospholipases (Duszyk, Liu, Kamosinska, French and Paul Man, 1995), it may have indirectly influenced the activity of ion channels perhaps by inhibiting L-type Ca^{2+} channels and reducing Ca^{2+} influx into the cell (Todorovic and Lingle, 1998) or by maintaining potassium channels, open around the zero-current potential of the cell, in an open state (Gofa and Davidson,1996). Finally, F^- may inhibit the activation of a non-selective cation conductance, a conductance observed in isolated OHCs (Housley and Ashmore, 1992).

4.2.4 Measuring C_m and R_s in T1 OHCs

It was not possible to estimate the membrane capacitance (C_m) and series resistance (R_s) of basal turn OHC recordings using the compensation circuitry on the patch-clamp amplifier. These dialled values suggested that T1 OHCs had no capacitance and an unrealistically high series resistance. Attempts were made to overcome these problems by using different software packages that measured these variables on-line. However, the software either required specific hardware that was unavailable (Clampex 7.0 software, Axon Instruments) or only measured one of the two variables (Whole-cell analysis programme, Version 2.1, Strathclyde Electrophysiology Software, University of Strathclyde).

Off-line estimates of the membrane capacitance were made by calculating the area underneath the charging transient curve, according to the following equation:

$$C_m = Q/\Delta V_m \qquad \textbf{Equation 4.1}$$

The area underneath the charging transient represents the charge transferred (Q) to the membrane capacitance upon a step change in potential (ΔV_m). Transients were recorded with a high sampling rate, little filtering and with the stray capacitance fully compensated. R_s can then be calculated from Equation 2.1. However, this method seriously underestimated C_m compared to the value expected from the trends of Mammano and Ashmore (1996) who measured the capacitance of OHCs in turns 4, 3 and 2 or the cochlea.

The problems encountered in measuring C_m and R_s either on-line or off-line may be explained as follows. As the cell-attached configuration of T1 OHCs was unstable, fast capacitance transients could not be accurately cancelled before a whole-cell configuration was achieved. Thus, the fast capacitance cancellation dial was left unchanged from the averaged setting for a T4 OHC recording where similar pipettes were used. However, if the stray capacitance was slightly reduced during a T1 recording, either through increased waxing of the pipette or a lower level of solution in the bath, the fast transient cancellation would be over compensated and would start to cancel the total membrane capacitance of the OHC. Changes in the stray capacitance of just 1-2 pF would have a significant affect on the estimate of a total membrane capacitance of just 10 pF.

The problems of estimating membrane capacitance for a T1 OHC were eventually overcome by modelling the cell on a series of cylinders (Figure 4.3). The surface area of a T1 OHC was calculated to be 1310 μm^2 on the basis that an OHC has 100 stereocilia with the dimensions shown below. Knowing that the specific capacitance of a biological membrane is 1 $\mu F/cm^2$, the capacitance of the model cell was calculated to be 13 pF. This method slightly overestimates the size of the OHC because stereocilia are graded in height and not uniform as suggested by the model. Nevertheless, this value fits well with the relationship between C_m and OHC length observed by Housley and Ashmore (1992) and with the predicted C_m of a T1 OHC according to the data in Mammano and Ashmore (1996) and will therefore be used where necessary as the capacitance of a T1 OHC.

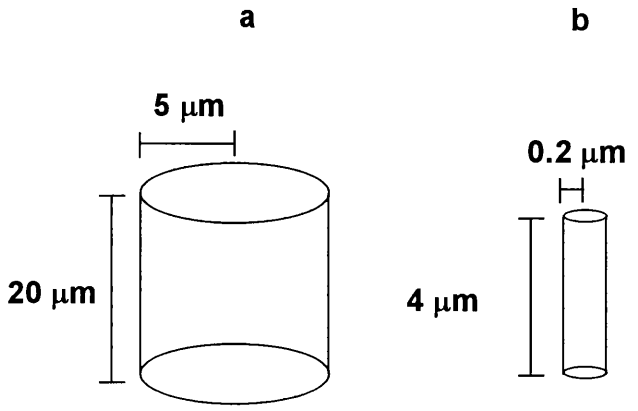

Figure 4.3 Modelling a T1 OHC. a, the basolateral membrane, b, the averaged stereocilia. Data obtained from measurements of OHC made during experiments and from Lim, 1980.

The series resistance of T1 OHC recordings were estimated as follows. As the pipettes used in this series of experiments were identical in shape and resistance to those used for T4 OHC recordings, it was assumed that the whole-cell configuration formed by these pipettes on either T4 or T1 OHCs would be similar. Thus, the series resistance value used for T1 OHC recordings was an averaged series resistance value was calculated from T4 OHC recordings. This averaged value was 8.58 $\pm$ 2.2 MΩ (n = 10).

4.3 Results

4.3.1 The morphology of the basal organ of Corti

T1 OHCs are extremely short, measuring just 20 μm in length (Figure 4.4). In this turn of the cochlea, the length of the OHC does not change across the width of the sensory epithelium and thus, the reticular lamina is flat. T1 OHCs, located 16.5 mm from the helicotrema, were used in this study. This site corresponds to a position along basilar membrane tuned to 12.5 kHz (Greenwood, 1990).

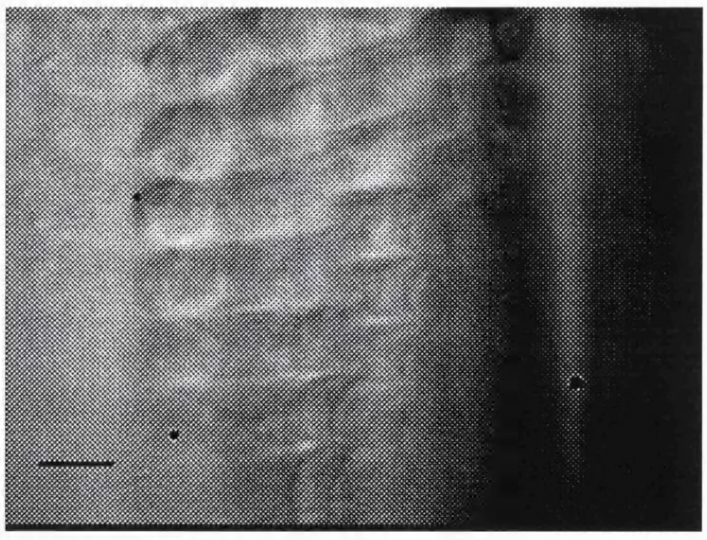

Figure 4.4 Digital image of the basal turn organ of Corti in the isolated temporal bone preparation. Scale bar - 10 μm. By tilting the preparation to improve access to the basal turn organ of Corti, the whole of the basolateral membrane of the outer row OHCs can be seen. The base of the outer row OHCs are to the left of the picture. In the centre are the V-shapes of the stereocilia of the outer and middle row OHCs. The modiolus is to the right. Hensen's cell that normally overlie the OHCs have been removed. However, the Deiter's cells that support the basal pole of the OHCs can just be made out to the far left of the picture.

4.3.2 The kinetics of basal OHC basolateral membrane currents.

Whole-cell currents recorded from basal turn OHCs are shown in Figure 4.5a. Currents recorded from hair cells in this turn of the cochlea exhibit three distinct characteristics:

a) very negative zero-current potentials (V_z)
b) outwardly rectifying currents
c) currents with very fast onset kinetics

The zero-current potential of T1 OHCs was -76.7 ± 11.2 mV (n = 12). This value was reached upto one minute after the whole-cell configuration had been achieved. This result suggests that the cells were initially loaded with Na^+, having been maintained in a high Na^+ concentration medium, but were gradually dialyzed with K^+ from the pipette solution (Liu, 1997). The zero-current potential of the cell was measured at least 5 minutes into a whole-cell recording allowing enough time for the bath solution, containing a low concentration of K^+ ions, to be exchanged with an otherwise identical solution containing 4 mM K^+. The very negative V_z recorded in these cells is close to the equilibrium potential for K^+, calculated to be -90 mV, indicating that the basolateral membrane conductances of T1 OHCs are carried by K^+. The averaged, stabilized zero-current potential recorded from T1 OHCs *in situ* was not significantly different to the averaged steady-state resting membrane potential of -83 ± 12.8 mV (n = 20) recorded *in vivo* (Cody and Russell, 1987) (P = 0.08, test g, Table 1, Appendix 1). It was also very similar to the averaged zero-current potential of -78 mV recorded from T1 OHCs *in vitro*. However, no standard deviation or standard error of the mean was quoted to allow the significance of the difference to be tested.

T1 OHCs exhibit outwardly rectifying currents. Voltage steps positive to the holding potential of -70 mV elicited large outward currents of 8.7 ± 2.1 nA (n = 12) at 0 mV. In two cells, this value had to be extrapolated from the current-voltage curve as the currents had saturated the amplifier by -6 and -10 mV (extrapolated values (nA): 12.5 and 11.9). Voltage steps in the opposite direction elicited much smaller, inward currents, measuring just 0.83 ± 0.62 nA (n = 12) at -110 mV. The holding potential of -70 mV was chosen for T1 OHCs as it was close to the zero-current potential of the cell and avoided depolarization of the cell membrane.

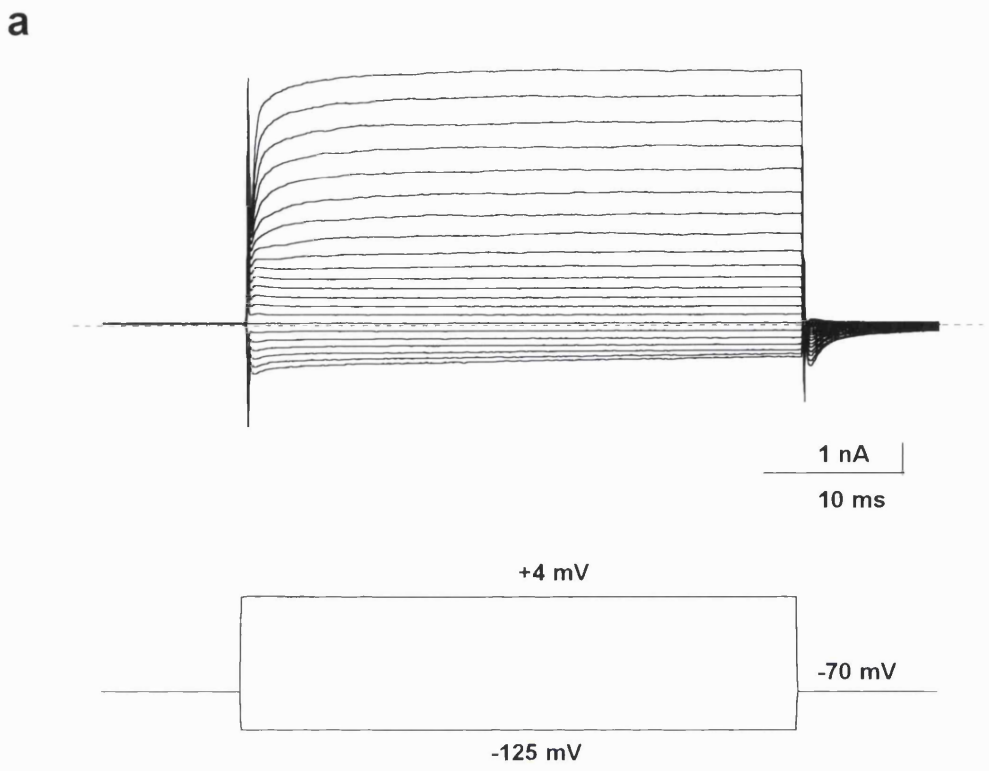

Figure 4.5 Whole-cell currents recorded from T1 outer row OHCs of the *in situ* cochlea. a, currents recorded in response to the series of voltage commands shown immediately below. The dotted line represents the position of zero current. Data was sampled at 3 kHz. b, steady-state current-voltage relationships obtained from the data in a. Data were measured 10 ms before command off-set. ○ - voltage uncompensated for series resistance errors. ● -voltage corrected for series resistance errors (8.5 MΩ).

The tail currents observed in T1 OHCs at the end of a step change in voltage were extremely unusual for a cell whose currents appeared to be dominated by potassium (V_z = -76 mV). Stepping the potential back to V_h from more negative potentials elicited very small outward currents, whilst changes in the opposite direction elicited large inward currents. These currents did not saturate, took upto 6 ms to decay at 0 mV and reversed at -74 ± 10 mV (n = 10). This reversal potential ruled out the possibility that the current was being carried exclusively by chloride (E_{Cl} = 0 mV), Ca^{2+} (E_{Ca} = +100 mV) or a cation current (E_{cation} = 0 mV). Instead, it appears that this is a K^+-based phenomenon. Such tail currents may be observed if the reversal potential for K^+ is shifted significantly during the voltage pulse. This may occur if K^+ accumulates around the extracellular face of the basolateral membrane as a result of K^+ efflux being greater than the rate of perfusion of new solution around the hair cell. *In vivo*, this may be less likely to happen if Hensen's cells buffer the concentration of extracellular potassium within the space of Nuel (Mammano, Goodfellow and Fountain, 1996). This would be particularly important in basal turn OHCs that must recover fast enough to respond to sounds in the kHz range, which would not be possible if the cell takes milliseconds to recover.

Figure 4.5b shows the current-voltage relationship for a T1 OHC measured at the steady-state level, 10 ms before command offset. The effects of R_s compensation on the voltage dependence of the currents and on the slope conductance are clearly demonstrated. Although the method outlined in Section 4.2.4 to estimate R_s is not ideal, some attempt at compensation was clearly required due to the enormous currents in these cells causing a large voltage drop over the series resistance. The main characteristic of the current-voltage relationship plotted in the above figure is the distinct change in the slope of the relationship at -40 mV. This indicates that at least two currents, with different voltage dependence are active in T1 OHCs, one around the zero-current potential of the cell, the other at potentials greater than -40 mV. It was not possible to examine the currents activated in response to voltage steps beyond 0 mV as currents were so large that they saturated the amplifier. Inward currents did not increase in size if the potential was stepped beyond -110 mV.

The slope conductance at -110 mV, V_z and at the point of maximum slope were calculated. At -110 mV, the slope conductance was 16.1 ± 4.9 nS (n

= 11). Larger conductances of 37.4 ± 21.0 nS (n = 12) were observed at the zero-current potential of the cell. However, the maximum slope conductance of the cells was observed at -15 ± 9 mV (n = 12) and measured 291.0 ± 102.5 nS (n = 12). The slope conductance measured at V_z is a particularly important value as it allows the time constant of the basolateral membrane to be calculated using Equation 2.1. The time constant of the basolateral membrane of T1 OHC was calculated to be 65 μs based on a membrane capacitance and series resistance as calculated in section 4.2.4. Using this value, the corner frequency of the membrane was calculated to be 2.4 kHz. At all frequencies above this value, the receptor potential will be attenuated by half for each doubling of the stimulus frequency (Kolston, 1995) as most of the transducer current will flow through the membrane capacitance of the OHC. This is a particularly low corner frequency value compared to the best frequency of the basilar membrane at this point along its length (12.5 kHz, Greenwood, 1990). The implications of this are discussed in the next section.

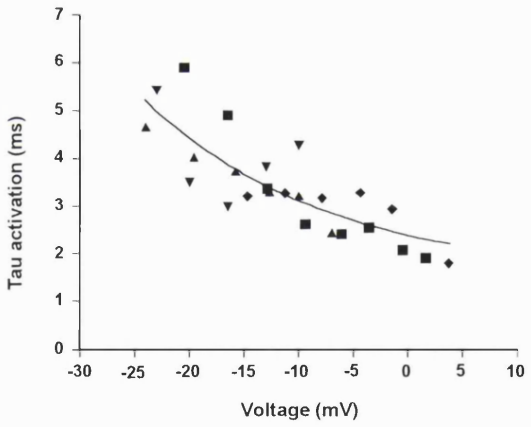

Figure 4.6 Voltage dependence of the time constant of current activation in 4 cells. Each cell is represented by a different symbol. The voltage was stepped from a holding potential of -70 mV to a more positive potential (x-axis). All voltages are corrected for series resistance errors.

c) Outward currents in T1 OHCs exhibited fast, complex onset kinetics, the slowest time constant of which measured 1.51 ± 0.72 ms (n = 10) at 0 mV. The time constant of current onset at each individual voltage was measured using the single exponential fitting procedure in C.E.D. "Patch and Voltage Clamp Software" package. The time constant of current onset was voltage dependent, decreasing with more positive voltages (Figure 4.6). The smooth curve fitted to the data in Figure 4.6 is a monoexponential decay of the following form:

$$\tau = Ae^{(-kV)} + B \qquad \textbf{Equation 4.2}$$

where k defines the steepness of the voltage dependence and x is the test potential in volts. The curve was generated in Fig P (Version 6.0c) where A = 0.912 ms, B = 1.467 ms and k = 0.058.

The above data is summarized in Table 4.1 below.

Property	V_z (mV)	g_{in} -110 mV (nS)	g_{in} V_z (nS)	g_{in} max (nS)	I_{max} 0 mV (nA)	τ_{onset} 0 mV (ms)	τ_{inact} 0 mV (s)
mean	-76.7	16.1	37.4	291.0	8.77	1.05	1.44
SD	11.2	4.9	21.0	102.5	2.1	0.72	--
n	12	11	12	12	12	8	1

Table 4.1 Properties of T1 outer hair cells. V_z, zero current potential; g_{in}, slope conductance measured at -110 mV; V_z and at the point of maximum slope on the IV curve; I_{max}, maximum current measured at 0 mV; τ_{onset}, time constant of current onset measured at 0 mV; τ_{activ}, time constant of current inactivation at 0 mV during a maintained depolarisation.

Outward currents in T1 OHCs inactivated in response to prolonged step changes in voltage (Figure 4.7). Inactivation proceeded with a time constant of 2.4 ms at -10 mV to a steady-state level 50 % of the maximum current level. Due to the slow time course of this process, inactivation was not observed during the much shorter potential changes in Figure 4.5. The possibility that inactivation was due to the depletion of intracellular K^+ cannot be ruled out. At -10 mV, the intracellular K^+ concentration would have been completely depleted if a constant current level of 5 nA had been maintained throughout the 4.5 sec voltage pulse. The delay of 10 seconds between each voltage pulse was apparently sufficient to replenish the intracellular K^+ concentration. However, recovery of the cell is clearly prolonged as is obvious from the duration of the tail currents following the most positive step changes in potential in Figure 4.7.

Finally, the transient current, thought to be associated with the activity of the motor protein in the basolateral membrane of OHCs, was not observed at the beginning and end of a voltage step applied to T1 OHCs. Some indication of such a current preceding the onset of K^+ channel activity was observed. However, these currents almost completely overshadowed the transient current

making calculations of its amplitude and duration impossible. Such fast activity would fit with the role of the motor protein in this turn of the cochlea, which would have to work on a microsecond time scale to be effective at encoding sound frequencies in the kilohertz range.

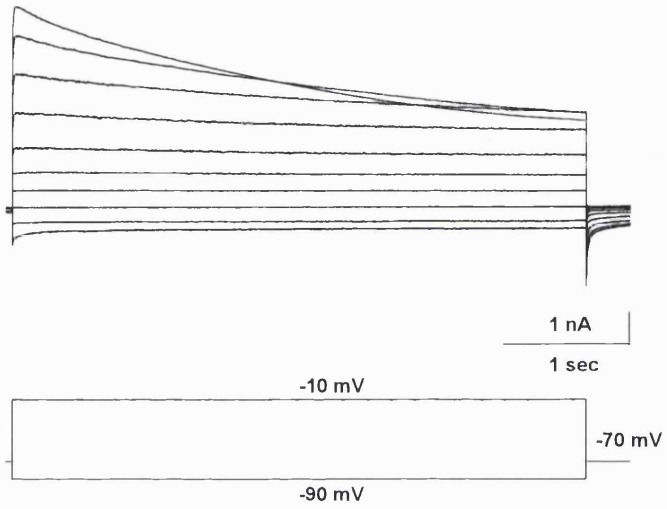

Figure 4.7 Inactivation of the outward current in T1 OHCs. Upper traces show the current responses of an OHC to prolonged step changes in potential shown below. All voltages are corrected for series resistance errors (8 MΩ).

4.3.3 The pharmacology of basal turn OHC basolateral membrane currents.

Dose-response curves for 4AP and TEA on T1 OHCs were not constructed due to the difficulty in recording from cells for long enough for such experiments. Instead, the saturating concentrations of these drugs on T4 OHCs were used as effective doses to block similar currents in T1 OHCs.

T1 OHC currents exhibit unusual pharmacology. 4AP, TEA and caesium, all applied externally to the cell and at high concentrations (1, 30 and 5 mM respectively), are able to reduce the outward current activated above -40 mV, in excess of the linear increase in current from conductances active around the zero-current potential of the cell.

4AP was applied to T1 OHCs by whole-bath perfusion. At a concentration of 5 mM, 4AP blocked the current that increased the gradient of the I-V curve around -40 mV. At 0 mV, the current was reduced by 40.5 ± 11.4 % (n = 3)(Figure 4.8). 4AP had no effect on the inward currents of T1 OHCs. The zero-current potential of the cell was unaffected in two of the three cells

where the effects of 4AP was investigated. In the third cell (shown in Figure 4.8), the zero-current potential was shifted by +14 mV (Figure 4.8). This observed shift is unlikely to be a true reflection of the effect of 4AP on T1 OHC currents. The activation kinetics of the currents remaining in the presence of 4AP were indistinguishable from the capacitative currents activated at the onset of the change in potential. This result suggests that the currents activated above -30 mV have slower kinetics, as observed in the control traces and that the conductance active around the zero-current potential of the cell has faster kinetics. It was not possible to subtract the control currents from the test currents to confirm this suggestion as the large, outward currents were activated at different voltages having compensated for errors due to series resistance.

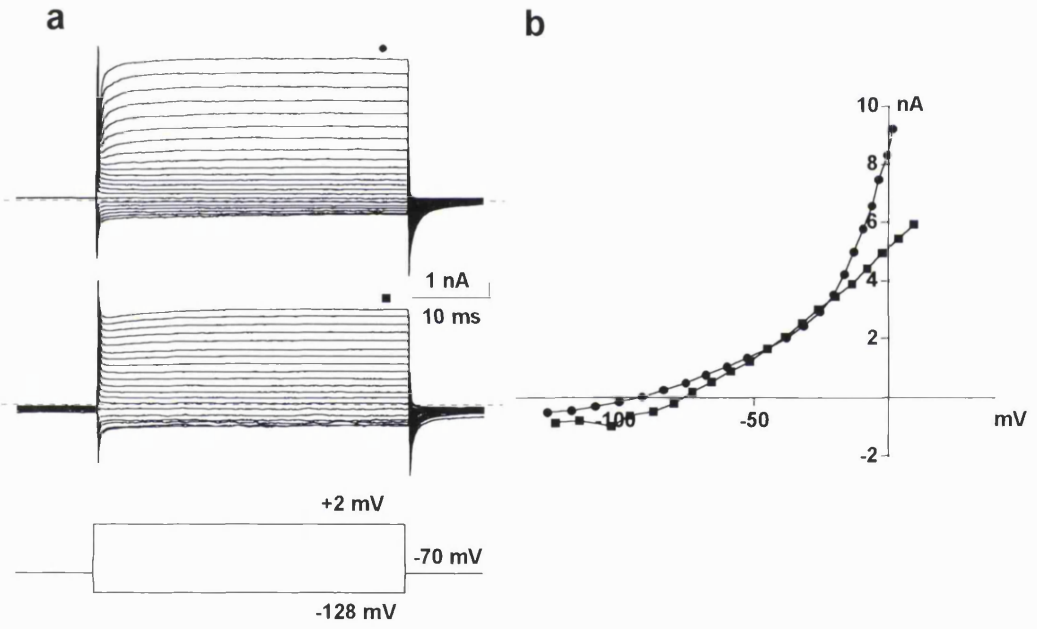

Figure 4.8 Effects of 4AP on T1 OHC currents. a, control currents (●) and currents recorded in the presence of 5 mM 4AP (■) applied by whole bath perfusion to the cell. The voltages shown at the bottom of this panel represent the most positive and the most negative voltages reached after series resistance compensation for the control recordings. For the currents recorded in the presence of 4AP, the most negative and the most positive voltages were -125 and +23 mV respectively. b, the current-voltage relationship for the control currents and the currents recorded in the presence of 4AP.

30 mM TEA was applied to T1 OHCs by whole-bath perfusion. Like the effects of 4AP, the extra current activated beyond -40 mV was almost completely removed by 30 mM TEA (Figure 4.9). The inward current and the zero-current potential of the cell were not significantly affected by the TEA. The kinetics of the residual current were faster than the control current, adding further evidence to the notion that the slower kinetics of current activation

observed in the control traces are associated with the current activated above -30 mV.

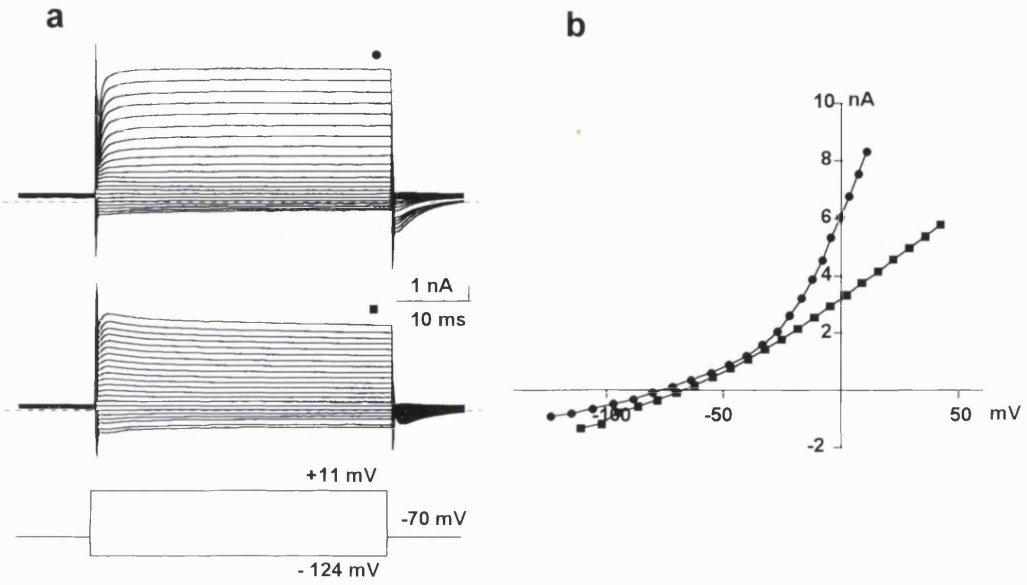

Figure 4.9 The effect of 30 mM TEA on T1 OHC currents. a, currents in the absence (●) and presence (■) of 30 mM TEA. The voltages shown below represent the most positive and the most negative voltage steps achieved in the absence of TEA. In the presence of TEA, the minimum and maximum voltages were -111 and +42 mV respectively. b, current-voltage relationship for the currents shown in a.

Finally, the effects of 5 mM caesium, applied externally to a T1 OHC via a puff pipette, were investigated (Figure 4.10). Extracellularly applied caesium is a very potent inhibitor of the outward current in T1 OHCs. At 0 mV, the outward current was reduced by 75.4 ± 2.85 % (n = 2). It is clear from the current-voltage relationship in Figure 4.10 that caesium also affects the current activated at more negative potentials. If caesium was a true inhibitor of this current, both the inward and the outward current would be expected to decrease without any change in the zero-current potential, unless a full block was achieved. However, this was not observed. Instead, the zero-current potential of the cell shifted in the positive direction by 26 ± 6 mV (n = 2) and the inward current clearly increased in size. The former observation suggests that the residual currents is less K^+ selective. The latter observation could suggest that a cation conductance has been activated by caesium. This suggests that the net current observed around the zero-current potential of the cell in the presence of caesium is a combination of a cation conductance and a par-blocked K^+ conductance. The residual currents remaining in the presence of

caesium exhibit very fast activation kinetics. The unusual tail currents associated with T1 OHC currents are also completely removed.

Neither the effects of 4AP nor TEA were reversible over a wash-out period of 20 minutes. However, the effects of caesium were partially so.

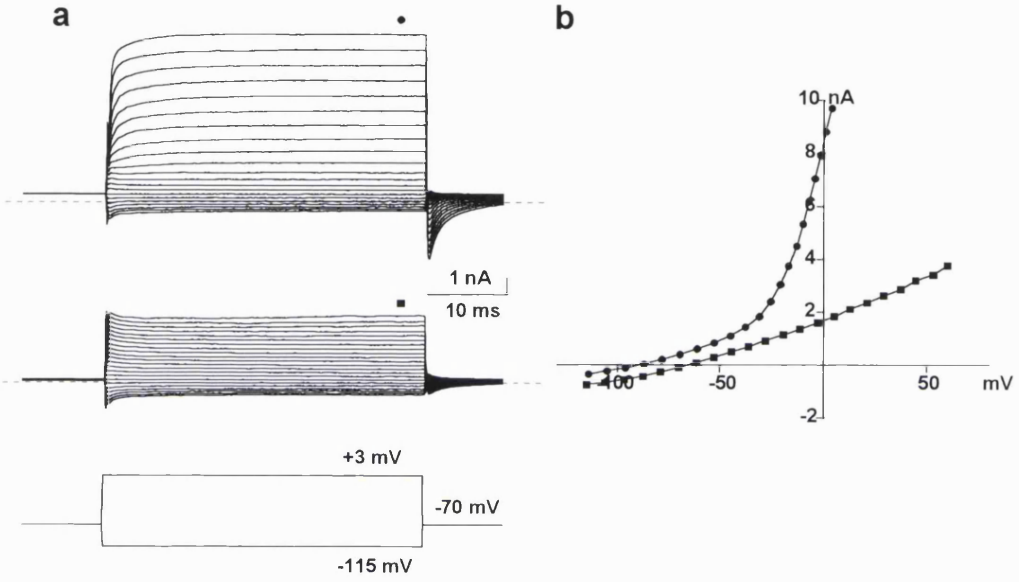

Figure 4.10 The effects of 5 mM extracellular caesium on T1 OHC currents. Caesium was applied to the cell via a puffer pipette. a, control currents (●) and currents recorded in the presence of caesium (■). The voltages shown below refer to the minimum and maximum voltages reached in the control situation. For the traces in the test situation, the minimum and maximum voltages reaches were -155 and +60 mV respectively. b, the current-voltage relationship for the currents in a.

The results of pharmacological studies confirm the existence of at least two types of potassium channels in T1 OHCs, one active around the zero-current potential of the cell, the other active at potentials >-40 mV. The former current will now be termed $I_{k,n}$, as it appears to exhibit certain kinetic and pharmacological similarities to $I_{k,n}$ in T4 OHCs. The current activated at potentials >-40 mV will be termed I_{kT1}.

4.3.4 The Ca^{2+} sensitivity of basal turn OHC basolateral membrane currents.

The Ca^{2+} sensitivity of the voltage-dependent currents in T1 OHCs was investigated using the photolabile Ca^{2+} chelator DM-Nitrophen, described in Section 3.2.1. Basal turn OHCs were patched with an intracellular solution containing KF and DM-Nitrophen. Currents were recorded before and during

the exposure of the cell to 5 seconds of UV light. However, increased intracellular Ca^{2+} had no effect on T1 OHC currents. Control experiments were conducted on T4 OHCs to ensure that the solutions were not photolysed before their use. Normal Ca^{2+} responses were observed. It seems highly unlikely that the series resistance was preventing DM-Nitrophen getting into the cell as the currents recorded from these cells are very large. Thus, the tentative conclusion appears to be that basolateral membrane conductances of basal turn OHCs are insensitive to raised intracellular Ca^{2+} concentrations.

4.4 Discussion

This study is the first to investigate in detail the kinetic and pharmacological properties of basolateral membrane currents in clearly identified basal turn OHCs. It shows that the zero-current potential of these cells is very negative, a feature also observed *in vivo* (Cody and Russell, 1987) and that the currents are large and outwardly rectifying (Raybould and Housley, 1997). In addition, this study demonstrates that the activation kinetics of the currents are extremely fast and their pharmacology unusual.

4.4.1 How physiological is the preparation?

Interestingly, no other investigations into the properties of basal turn OHCs have acknowledged problems with maintaining cells in a viable state for recording or with run-down of the currents in the whole-cell recording configuration (Housley and Ashmore, 1992; Raybould and Housley, 1997).

In vitro, T1 OHCs may appear to survive longer because the population of cells available to work on is being drawn from all three rows of the whole basal turn of the cochlea. Thus, the probability of finding a healthy cell to work on is greatly increased. *In situ*, the number of cells available to record from is limited to a sample of ~100 outer row OHCs, due to the logistical difficulties of visualizing and accessing the preparation. In addition, OHCs *in vitro* may survive longer because the potassium effluxed from the hair cells is rapidly dissipated by the efficient perfusion of solution through the recording chamber. *In situ*, perfusion will be less efficient due to the much larger volume of solution in the chamber and due to the more sheltered location of the cells within the bulla. Thus, potassium efflux from the hair cell may accumulate in the spaces of

Nuel and maintain the cells in a depolarized state. *In vivo*, potassium buffering has traditionally been associated with Hensen's cells (Mammano, Goodfellow and Fountain, 1996) but these cell are removed *in situ* to improve access to the basolateral membrane of hair cells for patching. Thus, one improvement that could perhaps be made to T1 OHC preparations is to have a much higher perfusion rate to avoid potassium accumulation or to find a way of accessing OHCs through this layer of Hensen's cells.

Fluoride was used as the main intracellular anion in these experiments to avoid the rapid run-down of currents observed when chloride was used. Although an unphysiological anion, basal turn OHCs *in situ* patched with KF solution exhibited stable zero-current potentials of -76 mV, comparable to the resting membrane potential of T1 OHCs *in vivo* (Cody and Russell,1987). Additionally, the amplitude of the currents recorded from *in situ* OHCs compared favourably with those observed *in vitro* where cells had been patched with a KCl based solution (Raybould and Housley, 1997; Rennie and Ashmore, 1991). This suggests that KF stops the rapid deteoriation of T1 OHCs without significantly affecting the major voltage-dependent basolateral membrane currents.

4.4.2 Potassium currents in basal turn OHCs

The results presented in this chapter provide considerable evidence for at least two types of potassium currents in basal turn OHCs, one that activates at very negative potentials around the zero-current potential of the cell ($I_{k,n}$), the other activating at potentials more positive than -40 mV (I_{kT1}). However, with maximum receptor potentials of 10 mV in basal turn OHCs (Cody and Russell, 1987), it is unlikely that this second conductance would be activated physiologically. The amplitude and activation kinetics of the outward currents are very similar to those observed in IHCs *in vitro* (Kros and Crawford, 1990). However, the pharmacology of the currents is quite different. Where 4AP and TEA were able to cleanly distinguish between a slow and fast conductance respectively in IHCs, such distinctions were not obvious in basal turn OHCs. Instead, 4AP, TEA and caesium all reduced the outward current activated above -40 mV. Only caesium may have affected the more negatively activating potassium current. Potassium currents with such unusual pharmacology have not previously been identified. However, kinetically, the current activated above

-40 mV, shows similarities to the current carried by Kv3.1 (Grissmer, Nguyen, Aiyar, Hanson, Mather, Gutman, Karmilowicz, Auperin and Chandy, 1994; Salkoff, Baker, Butler, Covarrubias, Pak, Wei, 1992), part of the *Shaw* family of potassium channel genes. This channel has been shown to be expressed at high levels throughout the auditory pathway, including the rat anterior ventricular nucleus and the medial nucleus of the trapezoid body (Wang, Gan, Forsythe, Kaczmarek, 1998) where they contribute to the relatively high frequency firing of mouse auditory neurones. Thus, Kv3.1, or perhaps another subunit from the *Shaw* family may be responsible for the rapid activation kinetics of channels seen in T1 OHCs.

The tentative results presented in this chapter suggest that T1 OHC currents are Ca^{2+} insensitive. These results oppose those of Raybould and Housley (1997) who observed that by removing extracellular Ca^{2+}, the conductance of basal turn OHCs decreased by 25 %, reflecting a Ca^{2+} dependence to the conductances in basal turn OHCs. In fact, the results presented in this this thesis do not rule out the possibility that these currents are Ca^{2+} sensitive. With F^- as the main intracellular anion, Ca^{2+} released from the cage is unlikey to end up as free Ca^{2+} but instead, will form the insoluable precipitate CaF_2. Under these circumstances, Ca^{2+} will be prevented from affecting OHC basolateral membrane ion channels. Thus, the issue of Ca^{2+} dependence of T1 currents has yet to be resolved.

One unusual feature of T1 OHC currents were the tails currents observed on stepping the membrane potential of the cell back to the holding potential from a positive test potential. In explaining why these tail current arise, it is worth pointing out an observation made by Cody and Russell (1987). When recording the membrane potential of basal turn OHCs during intense tone stimulations, it was observed that OHC membrane potentials did not return instantly to the pre-stimulus level at the off-set of the tone. Instead, it returned to a level more positive than this. The time taken for full repolarization appeared to be governed by the intensity and duration of the stimulus, but for a 50 ms, 600 Hz tone at 114 dB s.p.l., full recovery of the membrane potential took 50 ms. This observation could be explained if potassium accumulation occurred in the spaces of Nuel. If the rate limiting step in repolarization is the removal of potassium from this space, the resulting increase in the concentration of extracellular potassium will depolarize the OHC. As mentioned above,

potassium buffering *in vivo* is a role typically associated with Hensen's cells. In their absence, potassium efflux from OHCs is not well buffered and is only dissipated by other supporting cells and/or the rate of perfusion of new solution around the hair cell. *In situ*, perhaps these tail currents result from the slow buffering of potassium around the OHCs, as a result of removing the Hensen's cells. These tail currents caused as a result of potassium accumulation around the hair cells may underlie the depolarized receptor potential observed *in vivo*.

4.4.3 Membrane filtering by basal turn OHCs

OHCs are able to change length according to the potential across their basolateral membrane. It is generally assumed that this property provides the force to amplify the motion of the basilar membrane to which the organ of Corti is attached. To be effective, OHC length changes must act on a cycle-by-cycle basis. Thus, for an OHC located at a point along the basilar membrane tuned to 12.5 kHz, length changes and thus potential changes across the basolateral membrane, must work on a 80 μs timescale. One of the major problems facing an OHC is that at high frequencies, changes in potential across the basolateral membrane are limited due to the charging of the membrane capacitance. Thus, the basolateral membrane of the OHC appears as a low-pass filter. Concern has been expressed about whether enough of a change in potential across the basolateral membrane of the cell can be generated to force OHC length changes on a physiological time scale (Dallos and Evans, 1995; Kolston, 1995; Santos-Sacchi, 1992).

The corner frequency of the basal turn OHCs used in this study was calculated to be 2.4 kHz. This is well below 12.5 kHz, the frequency to which this part of the basilar membrane is tuned (Greenwood, 1990). Nevertheless, the maximum receptor potential generated in basal turn OHCs was observed to be 10 mV at 90 dB s.p.l. (Cody and Russell, 1987). For every doubling of the stimulus frequency above the cut-off frequency of the basolateral membrane, the intracellular potential generated will halve (Kolston, 1995). Thus, the receptor potential generated in this basal turn OHC will be 2.2 mV. The sensitivity of the motor protein is 2 nm/mV (Santos-Sacchi, 1989). Thus, OHCs would be expected to generate a movement of 4.4 nm. Even at the threshold of hearing, OHCs can generate a movement of 0.4 nm. Thus, even above the cut-off frequency of the OHC basolateral membrane, it appears that OHC length

changes can affect basilar membrane motion. Whether this is a physiologically relevant movement has yet to be determined.

4.4.4 Summary and Model

A model of the ionic currents thought to be present in basal turn OHCs is presented in Figure 4.11. Experiments described in this chapter show that these currents have extremely fast on-set kinetics and unusual pharmacology. They also suggest that basal turn OHCs are able to influence the motion of the basilar membrane even at frequencies above the cut-off frequency of the basolateral membrane of the hair cell.

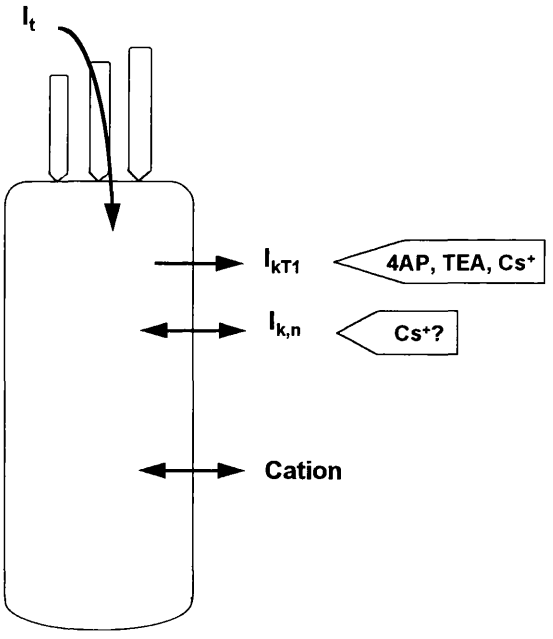

Figure 4.11 Proposed model for ionic conductance present in T1 *in situ* OHCs. I_{kT1} represents the 4AP, TEA and Cs^+-sensitive current activated above -40 mV. $I_{k,n}$ is the current activated around the zero-current potential of the cell.

Chapter 5

A comparison of T4 and T1 OHC currents

5.1 Introduction

Variations in the expression of OHC potassium conductances along the tonotopic gradient of the adult mammalian cochlea have been investigated (Housley and Ashmore, 1992; Mammano and Ashmore, 1996). However, these investigations have never been satisfactorily completed due to a paucity of information regarding potassium conductances in true T1 OHCs. Raybould and Housley (1997) were the first to record from clearly identified T1 OHCs using the whole-cell voltage-clamp technique. They demonstrated a position-dependent increase in basolateral membrane conductances from apex to base along the length of the mammalian cochlea. However, their results did not attempt to explain to what extent this variation is explained by a single class of potassium channels or by the change in expression of an ensemble of potassium channels. Using the more extensive T1 OHC data presented in Chapter 4 of this thesis and comparing it to the T4 OHC data presented in Chapter 3, the primary goal of this chapter is to determine whether there are variations in the expression of potassium currents along the tonotopic axis of the cochlea. A comparison is possible because of the very precise nature of the investigations into T4 and T1 OHCs. Suggestions are presented as to how these variations may affect the generation of the receptor potential and thus the activity of the cochlear amplifier along the length of the adult mammalian cochlea.

5.2 Discussion

5.2.1 Morphology

The *in situ* preparation allows unambiguous identification of the site of origin of the OHC along the length of the basilar membrane and within the three rows of OHCs. This is an important advantage over isolated OHC preparations, where the location of the OHC is determined by length alone. This can lead to errors in locating the OHC, as cells of 30-50 μm may belong either to the inner row of T4 or the outer row of T3 of the cochlea (Pujol, Lenoir, Ladrech, Trebillac,

Rebillard, 1992). The *in situ* preparation therefore allows the properties of OHCs to be closely correlated with the frequency of sound transduced at a specified point along the basilar membrane.

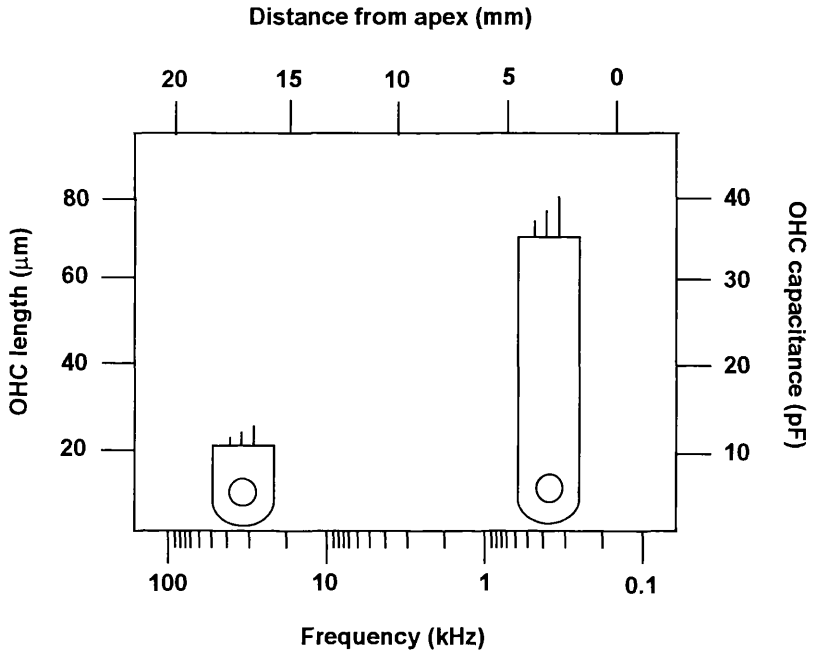

Figure 5.1 A frequency-place map for guinea-pig outer row OHC length and capacitance.

OHC length varies by a factor of 3.5 between the recording positions in the apex and base of the cochlea (Figure 5.1). However, the cylindrical shape and diameter of the outer row OHC is almost invariable. This difference in cell length is reflected in the capacitative measurements of the OHCs between the apex and base of the cochlea which measured 35 and 10 pF respectively (Sections 3.3.2 and 4.2.4).

Do variations in OHC length affect the motor activity of the cell? It might be expected that for a short hair cell to have the same influence on basilar membrane mechanics as long OHCs, there would be a greater density of motor proteins packed into its basolateral membrane. Alternatively, the sensitivity of the motor protein may be increased towards the base of the cochlea allowing T1 OHCs to generate a greater movement for the same change in potential. However, neither morphological nor electrophysiological investigations have investigated these ideas. Indirect evidence comes from observing the capacitative transients, observed at the onset and offset of a step change in voltage during whole-cell recordings. The non-linear component of these

transients, thought to arise from charge displacements within the motor molecule, appears to increase towards the base of the cochlea (Mammano and Ashmore, 1996). This suggests an increased density of motor molecules in short OHCs. However, the contribution from uncancelled stray capacitance towards the total transient capacitance should not be underestimated. In contrast to these observations, Ashmore (1987) observed that the absolute magnitude of OHC length changes reduced from apex to base, although the change as a percentage of total OHC length was a constant 4 %. This latter information does not support the hypothesis that there is a greater density of motor molecules in the basolateral membrane of short OHCs. Interestingly, all three rows of OHCs at the base of the cochlear are the same length (Pujol, Lenoir, Ladrech, Tribillac, Rebillard, 1992). This characteristic may impart a more effective active mechanism to the cochlear partition compared to the apex, where a steep gradient in OHC length across the organ of Corti is observed.

5.2.2 Kinetics of T4 and T1 OHC basolateral membrane currents

T4 and T1 OHCs exhibit similarities in so far as the currents recorded from both sets of cells under voltage-clamp exhibited outward rectification and the slope of the current-voltage relationship increased around -40 mV (Figure 5.2). These results suggest that both T4 and T1 OHCs express at least two voltage-activated conductances. However, they do not uncover whether the two conductances responsible for these characteristics are the same or different in OHCs located at the apex and base of the cochlea.

T4 and T1 OHCs exhibited significant differences with regards to their zero-current potentials, slope conductances and onset kinetics. Zero-current potentials of T1 OHC were significantly more negative than T4 OHCs, their slope conductances were significantly larger at each of the potentials tested (Figure 5.3) and the onset kinetics of their currents were significantly faster than those observed in T4 OHCs. The significance of these differences were tested using a two-tailed Student t-test. In all cases, it was possible to be more than 99 % sure that the differences observed between the two set of data were real and not due to chance variation among samples from a single population. Information regarding these significance tests can be found as tests h, I, j, k and l in Table1, Appendix 1.

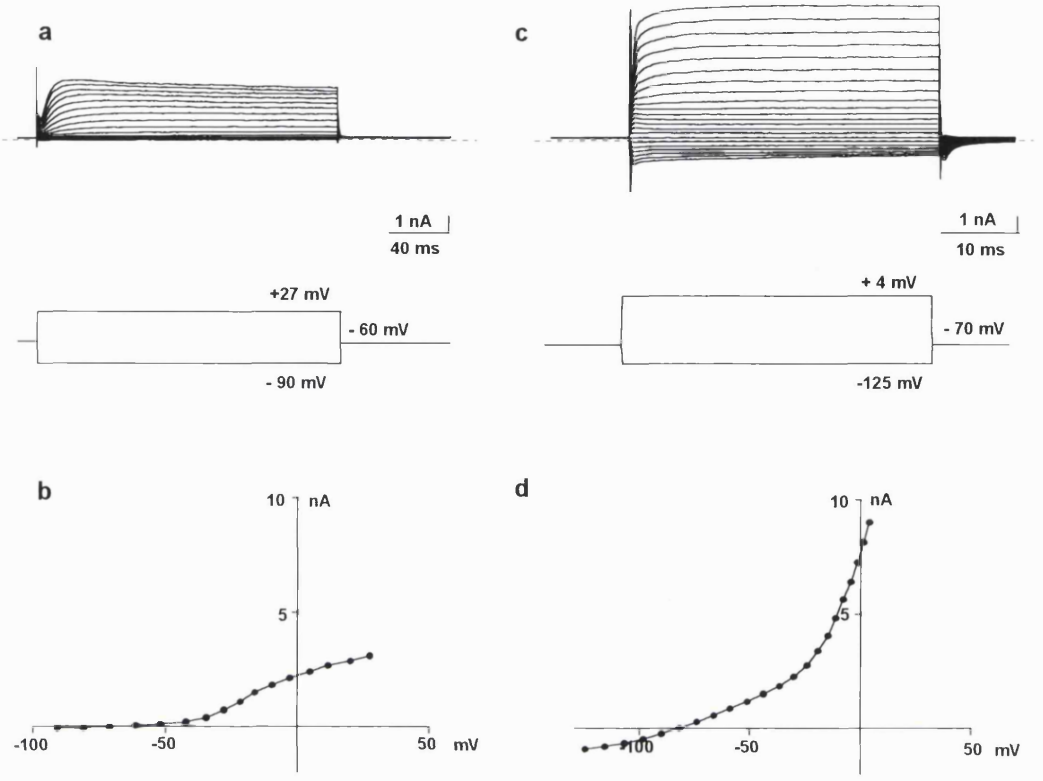

Figure 5.2 A comparison of T1 and T4 OHC currents. a and c, whole-cell voltage-clamp recordings from T4 and T1 OHCs respectively. b and d, current-voltage relationships for the data in a and c. All voltages are corrected for errors due to uncompensated series resistance. The data presented in this figure has been taken from figures 3.5 and 4.5.

The difference in the zero-current potential between T4 and T1 OHCs does not contribute towards an understanding of whether different currents are expressed in these two populations of OHCs. A more negative zero-current potential in T1 OHCs could be explained purely by an increased expression of the same ion channels as found in T4 OHCs, leading to an increased potassium conductance and a more negative zero-current potential (Goldman-Hodgkin-Katz theory). This feature of T1 OHCs does contribute positively towards their function as it increases the driving force of the transducer conductance across the apical membrane of the cells, maximizing the change in potential across the basolateral membrane of the OHC to activate the motor protein. However, the actual change in potential generated as a result of the transducer conductance is subject to filtering by the low-pass filter of the basolateral membrane (Section 5.4).

A comparison of the kinetics and time constant of current activation in T4 and T1 OHCs provides some indication that ion channel expression changes

along the length of the cochlea. At 0 mV, T1 OHC currents activate with exceptionally fast onset kinetics that include at least two time constants, a fast

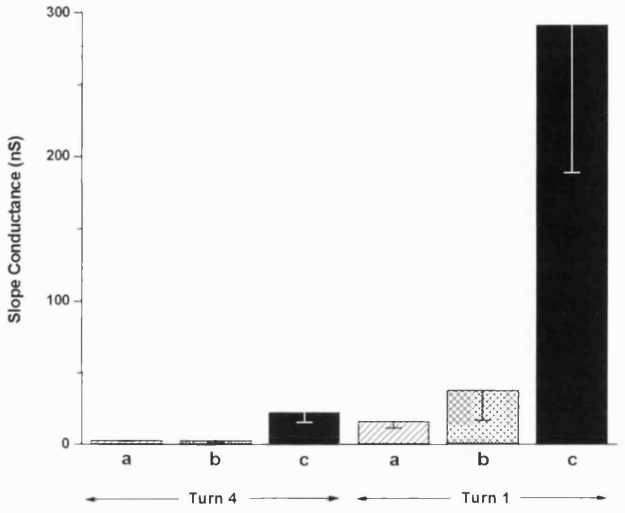

Figure 5.3 A comparison of the slope conductances of T4 and T1 OHCs. a) g_{in} at -110 mV, b) g_{in} at the zero-current potential of the cell and c) g_{in} at the point of maximum conductance. For clarity, standard deviation bars have only been added in the negative direction.

and a slower component (Section 4.3.2). In comparison, T4 OHC currents activate at 0 mV with much slower kinetics with just one time constant (Figure 5.4 and Section 3.3.2). Unless there is a variation in channels isoform along the length of the cochlea as observed with the calcium-activated potassium conductance in the chick cochlea (Rossenblatt, Sun, Heller and Hudspeth, 1997; Navaratnam, Bell, Tu, Cohen, Oberholtzer, 1997), it is highly unlikely that the same ion channels are responsible for such different kinetic properties at the apex and base of the cochlea.

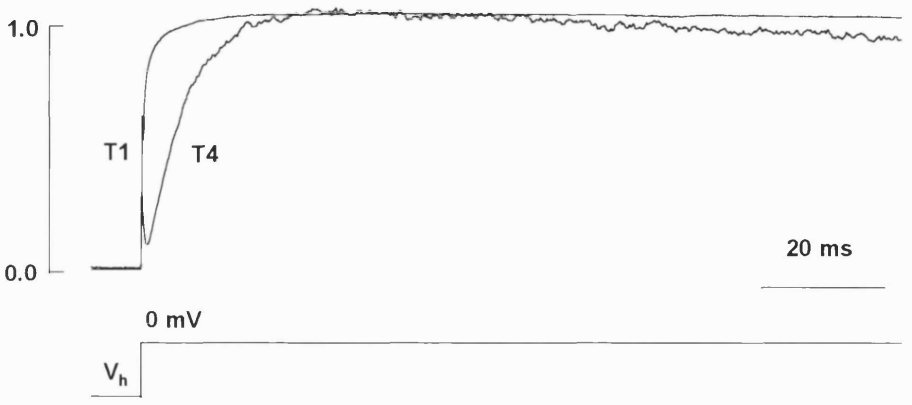

Figure 5.4 A comparison of the activation kinetics of T4 and T1 OHC currents at 0 mV, after series resistance compensation. The T4 current amplitude has been normalized to the T1 OHC current amplitude. V_h for a T4 OHC = -60 mV. V_h for a T1 OHC = -70 mV.

5.2.3 A comparison of the pharmacology of T4 and T1 OHC basolateral membrane currents

Pharmacological studies uncovered ion channels with different sensitivities to potassium channel antagonists activated above -40 mV in T4 and T1 OHCs (Table 5.1). The outward current in T4 OHCs was blocked by 77 % at 0 mV with micromolar concentrations of 4AP (IC_{50} = 6 μm) (Section 3.3.3.2). An additional 10 % of the outward current in T4 OHCs could be blocked by TEA (Section 3.3.3.2). However, extracellular Cs^+ did not affect this current. In contrast, millimolar concentrations of 4AP were required to inhibit just 40 % of the outward current at 0 mV in T1 OHCs. In addition, this current was substantially inhibited by TEA and Cs^+ (Section 4.3.3). Although the outward current in T1 OHCs exhibits very unusual pharmacology, it is quite different to that observed in T4 OHCs, confirming that different ion channels carry the outward current activated above -40 mV in T4 and T1 OHCs.

The currents activated around the zero-current potential of T4 and T1 OHCs could not be separated by pharmacological means. Neither 4AP, TEA nor Cs^+ at concentrations of 1, 30 and 5 mM respectively affected this current in either population of cells. A tentative conclusion that can be drawn from this evidence is that the ion channel carrying the current activated around the zero-current potential of T4 and T1 OHCs is the same, varying only in the number ion channels expressed in the two locations.

	T4		T1	
	(-110 mV)	(0 mV)	(-110 mV)	(0 mV)
4AP		77.1 ± 13.1 %		40.5 ± 11.4 %
	(n = 8)	(n = 8)	(n = 3)	(n = 3)
TEA		9 %		50 %
	(n = 1)	(n = 1)	(n = 1)	(n = 1)
Cs^+				75.4 ± 2.85 %
	(n = 2)	(n = 2)	(n = 2)	(n = 2)

Table 5.1 A summary of the effects of extracellular 4AP, TEA and Cs^+ on the currents activated at -110 mV and 0 mV in both T4 and T1 OHCs. Dashes indicate no effect of the drug on the current activated at that potential.

5.2.4 A comparison of the Ca^{2+} sensitivity of T4 and T1 OHC basolateral membrane currents

The Ca^{2+} sensitivity of T4 and T1 OHCs currents cannot be used as a means of confirming the similarity or otherwise of the current activated around the zero-current potential of the OHC. Although this current was observed to be Ca^{2+} sensitive in T4 OHCs (Section 3.3.4), technical difficulties limited the conclusions that could be drawn from similar experiments on T1 OHCs.

So far, no mention has been made of the cation conductance occasionally observed in OHCs (Housley and Ashmore, 1992). This conductance was rarely observed in OHCs *in situ*. Its expression was almost exclusively associated with a deleterious action on the cell such as increasing the intracellular Ca^{2+} concentration in T4 OHCs (Section 3.3.4) or perfusing Cs^{+} around the extracellular surface cell in T1 OHCs (Section 4.3.3). As its expression does not appear to coincide with a healthy, *in situ* preparation, it will not be discussed further.

5.3 Conclusions

Both the type and extent of potassium channel expression changes between the apex and base of the cochlea. This conclusion has been reached on the basis of investigations into the kinetic and pharmacological properties and Ca^{2+} sensitivity characteristics of T4 and T1 OHC currents. These changes are summarized in Figure 5.5. T4 OHCs express at least three different potassium conductances, I_{kT4}, I_{kca} and $I_{k,n}$ (Figure 3.16) In contrast, evidence for just two types of potassium conductances have been observed in T1 OHCs, I_{kT1} and $I_{k,n}$. If $I_{k,n}$ is the same conductance in T4 and T1 OHCs, the extent rather than the type of conductance activated around the zero-current potential of OHCs varies between the base and apex of the cochlea.

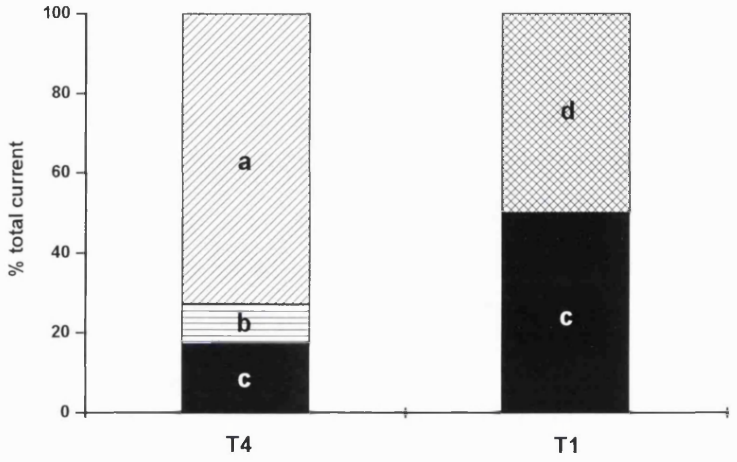

Figure 5.5 Summary of the different types of potassium channels expressed in T4 and T1 OHCs. a - I_{kT4}, b - I_{kca}, c - $I_{k,n}$, d - I_{kT1}

Based on the evidence presented in this and the preceding two chapters, Figure 5.6 shows a model of how potassium channel expression may change along the length of the adult, mammalian cochlea. The predictions for potassium channel expression in turns 3 and 2 are based partly on hypothesis and partly on the data presented in Mammano and Ashmore (1996) who show whole-cell patch-clamp data for *in situ* OHCs in these two turns of the cochlea. Their data shows a clear increase in the inward current and the speed and amplitude of the outward current from T4 towards T2 of the cochlea. On a purely qualitative basis, the characteristics of T1 OHC currents observed in this thesis fit well with the trends observed by Mammano and Ashmore (1996). The model put forward in this thesis implies that the ensemble of potassium currents in turns 3 and 2 of the mammalian cochlea are even more complex than those observed in T4 and T1. However, without further investigation, it is impossible to know whether changes in potassium channel expression along the tonotopic axis of the cochlea are as linear as predicted by this model.

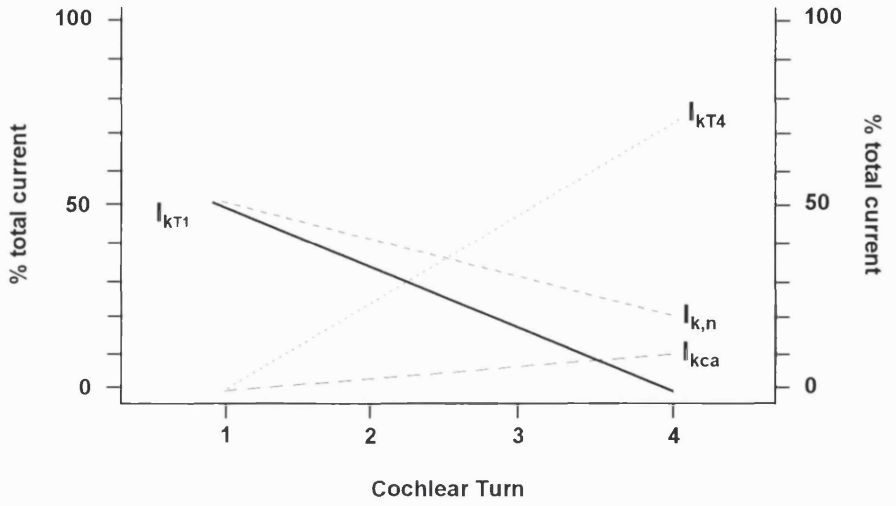

Figure 5.6 A prediction of the change in potassium channel expression along the length of the cochlea.

5.4 Implications

To affect the mechanics of the basilar membrane, OHC length changes must be able to work at acoustic frequencies. With a sufficient change in potential, the motor molecule of OHCs has been shown to operate at frequencies upto 25 kHz (Gale and Ashmore, 1997). However, due to the low-pass filtering of the OHC receptor potential by the basolateral membrane, it is questionable whether potential changes *in vivo* are large enough and fast enough to activate the motor molecule on a microsecond timescale. Thus, the physiological relevance of the cochlear amplifier has been questioned (Dallos and Evans, 1995; Kolston,1995). Interestingly, OHCs appear to have attempted to optimise themselves to respond to the frequency of sound to which the basilar membrane is tuned at that point. Strangely, this optimization is not sufficient. This may suggest that the change in potential generated by the transduction current, even in the face of low-pass filtering by the OHC basolateral membrane, is sufficient or that a different mechanism activates the motor protein of OHCs. As there are no such frequency limits to the action of the motor which has been shown to operate upto 25 kHz (Gale and Ashmore, 1997), one alternative theory that explains how OHCs respond to such high stimulus frequencies relative to the cut-off frequency of their basolateral membrane is proposed by Dallos and Evans (1995) and amended by Kolston (1995). This mechanism proposes that OHC motor activity is determined both by changes in the extracellular potential of the cell and changes in the intracellular potential.

Chapter 6

Ca^{2+} buffering in T4 OHCs of the *in situ* cochlea

6.1 Introduction

Ca^{2+} has evolved as a ubiquitous regulator of intracellular processes. Its efficiency as a signalling agent relies heavily on controlling the spatial and temporal spread of Ca^{2+} rises and falls throughout a cell. Ca^{2+} buffers are molecules that resist changes in the concentration of Ca^{2+} in a solution. They bind or release Ca^{2+} according to their K_d for the ion. The endogenous Ca^{2+} buffers of a cell control the spread of Ca^{2+} throughout the cytosol. They will avoid crosstalk between different Ca^{2+} modified pathways and allow Ca^{2+} to regulate fast, precisely timed actions.

The aim of this study was to estimate the equivalent concentration of endogenous Ca^{2+} buffer within T4 OHCs of the adult mammalian cochlea. This was achieved by comparing the time constant of voltage-dependent current activation in whole-cell recordings, containing various concentrations of BAPTA, with the time constant of current activation in perforated-patch recordings. Perforated-patch recordings retain the endogenous Ca^{2+} buffer within the cytoplasm.

6.2 Methods

6.2.1 Whole-cell patch-clamp recordings

The preparation and recording techniques used to investigate T4 OHCs *in situ* have been described in Chapter 2. OHCs were recorded from using the tight seal, whole-cell patch-clamp technique. The preparation was maintained in standard PBS solution (Table 2.1) containing 1 mM $CaCl_2$ and was continuously perfused at a rate of 450 µl/min. 4-5 MΩ soda glass pipettes were filled with basic PBS solution containing either 0, 5 or 10 mM tetrapotassium-BAPTA

(Table 6.1). The concentration of KCl was reduced by an amount equal to the concentration of added BAPTA to maintain a constant osmolarity. T4 OHCs were patched at the base of the cell, around the nucleus. Averaged series resistance values of 8.5 ± 2.2 MΩ (n = 10) were obtained. To ensure that the contents of the patch pipette had completely dialyzed the cell, a period of 5 minutes was allowed to elapse between achieving the whole-cell configuration and the start of recording. In theory, the time constant of 'wash-in' for a substance the size of BAPTA is 21 seconds, as calculated from the following equation (Pusch and Neher, 1988):

$$\tau = 0.6R_sM^{(1/3)} \qquad \textbf{Equation 6.1}$$

where τ = Time constant of equilibrium of a substance (s)

R_s = Series resistance of pipette tip = 4.5 MΩ

M = Molecular mass of the diffusing species = 500 Da for BAPTA

The delay of 5 minutes before recording whole-cell currents was chosen to allow the high molecular weight constituents of the cytoplasm to 'wash-out' of the cell. The voltage error due to uncompensated series resistance was corrected off-line.

	0 mM BAPTA (mM)	5 mM BAPTA (mM)	10 mM BAPTA (mM)
KCl	144	124	104
$MgCl_2$	2	2	2
Na_2HPO_4	8	8	8
NaH_2PO_4	1	1	1
K^+_4-BAPTA	0	5	10
Mg-ATP	2.5	2.5	2.5
D-Glucose	30	30	30
pH	7.25	7.25	7.25

Table 6.1 Ionic composition of the basic PBS solutions used to patch T4 OHCs.

6.2.2 Perforated-patch recordings

The technique used for perforated-patch recordings was similar to that described by Rae, Cooper, Gates and Watsky (1991). For each experiment, 10

mg of Amphotericin-B was dissolved in 1 ml dimethyl sulfoxide and sonicated briefly. This stock solution was diluted 1:1000 with the 10 mM BAPTA patch pipette solution (Table 6.1). Both the stock and the diluted solution were kept on ice in the dark and used for up to 2 hours before being replaced.

Patch pipettes were tip-filled with antibiotic-free solution and back-filled with the Amphotericin-B solution. This maximized the time window available to patch the OHC before Amphotericin-B reached the pipette tip and inhibited seal formation. Tip-filling was achieved by dipping the pipette tip into the antibiotic-free solution for 10 seconds, allowing enough solution to enter the pipette by capillary action such that it was just visible with the naked eye. Care was taken when back-filling the pipette not to disturb the tip-solution with the Amphotericin-B solution. This was ensured by forming a bubble at the interface between the two solutions when back filling the pipette. This bubble could be removed by gently tapping the side of the pipette. This technique ensured relatively gentle mixing of the two solutions. No positive pressure was applied to the patch pipette on approaching the cell to avoid premature filling of the pipette tip with the antibiotic.

Once a high resistance seal (> 10^9 Ω) had been obtained between the OHC membrane and the patch pipette, the degree of perforation was monitored by following changes in the capacitative transients generated in response to +10 mV step change in pipette potential. As perforation proceeded, so the series resistance between the pipette and the cell interior decreased. This allowed the size of the capacitative transients to increase and the time constant of the transients to decrease as greater proportions of the cell capacitance were charged during the voltage pulse. The holding potential at the start of perforation was -30 mV to ensure that the cell did not depolarize. As perforation proceeded, the holding potential was readjusted to follow the negative shift in the zero-current potential of the cell. Full perforation took up to 10 minutes to achieve and was identified by a stable series resistance values of 16 ± 9.9 MΩ, (n = 4, max. = 33 MΩ, min. = 7 MΩ). Series resistance remained extremely constant throughout the period of recording. It was assumed that the patch had not ruptured to a whole-cell configuration because:

a) there was no spontaneous change in the capacitative transients

b) the series resistance values were almost double that observed during normal whole-cell recording with the same pipettes

The same cells were never ruptured to form a whole-cell recording configuration following a perforated-patch recording (Ricci, Wu and Fettiplace, 1998; Tucker and Fettiplace, 1996). This ensured that Amphotericin-B did not perforate OHCs from the inside and produce artificial channels.

Data were analyzed using 'Patch and Voltage Clamp Software' (Version 6.0, Cambridge Electronic Design Ltd, UK).

6.3 Results

6.3.1 The effects of intracellular BAPTA on the whole-cell currents of T4 OHCs.

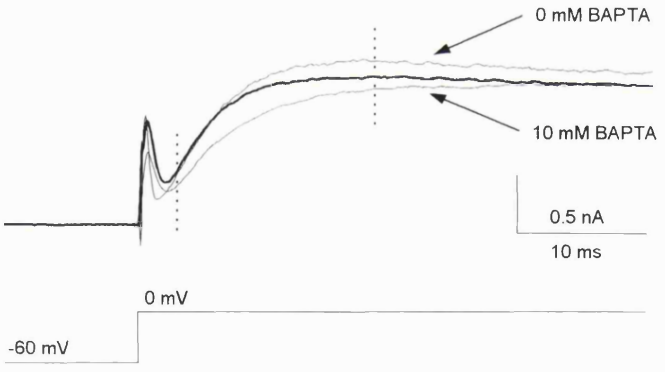

Figure 6.1 Currents activated in response to voltage steps from -60 mV to 0 mV in three different T4 OHCs. These current traces represent those traces with amplitudes and time constants nearest to the means values. For clarity, the current trace recorded in the presence of 5 mM BAPTA has not been included. All voltages are corrected for errors due to series resistance. The perforated-patch recording is shown in bold. Single exponential curves were fitted to the data between the dotted lines.

Both the steady-state current amplitude and the time constant of activation of T4 OHCs currents were affected by the concentration of BAPTA dialyzing the cell from the patch pipette (Figure 6.1). As the concentration of BAPTA increased from 0 to 10 mM, so the current amplitude decreased from 1.51 ± 0.42 nA (n = 6) to 1.1 ± 0.22 nA (n = 4) and the time constant of

activation slowed from 3.33 ± 0.62 ms (n = 6) to 4.9 ± 0.51 ms (n = 4). The difference between the time constant of current onset between 0 and 5 mM BAPTA and between 5 and 10 mM BAPTA was not significant at the 1 % level (P = 0.06 and 0.08 respectively). However, the difference between the time constant of current onset between 0 mM and 10 mM BAPTA was significant (P = 0.003). There was no significant difference in the mean zero-current potential (V_z) between the two sets of data (0 mM BAPTA; V_z = -66.2 ± 8.3, (n = 6); 10 mM BAPTA; V_z = -65.7 ± 13.3, (n = 4); P = 0.46).

The relationship between the time constant of current activation and the concentration of intracellular BAPTA is shown in Figure 6.2. It could be described by the following equation:

$$\tau_{onset} = 3.18 + 0.161[\text{BAPTA}] \text{ ms} \qquad \textbf{Equation 6.2}$$

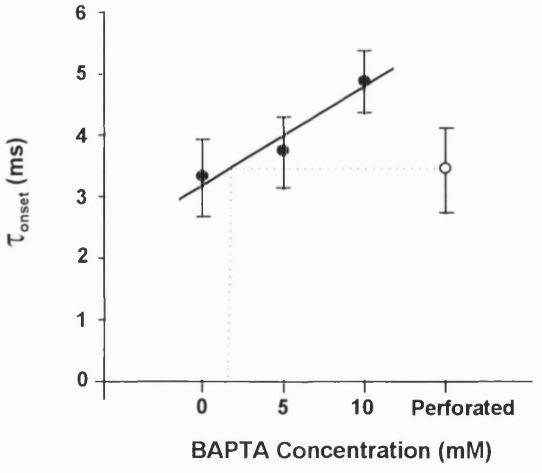

Figure 6.2 Estimation of the equivalent concentration of endogenous Ca^{2+} buffer in T4 OHCs at 0 mV. The effects of three intracellular BAPTA concentration on the onset kinetics of OHC whole-cell currents at 0 mV were investigated (filled circles) and compared to the kinetics observed during perforated-patch recordings (open circle).

Currents recorded using the perforated-patch technique activated with a time constant of 3.4 ± 0.69 ms (n = 4). As the perforated-patch technique maintains the endogenous Ca^{2+} buffer within the cytoplasm of the cell, this time constant can use equation 6.2 to establish the concentration of intracellular BAPTA. This generates an interpolated estimate of the concentration of endogenous Ca^{2+} buffer in T4 OHCs. At 0 mV, this was equivalent to 1.6 mM

BAPTA. The difference between the time constant of current onset in 0 mM BAPTA and in the perforated patch configuration was not significantly different (P = 0.38). For more information regarding these significance tests performed in this chapter, see tests m, n, o and p, Table 1, Appendix 1.

6.3.2 Voltage dependent Ca^{2+} buffering?

a

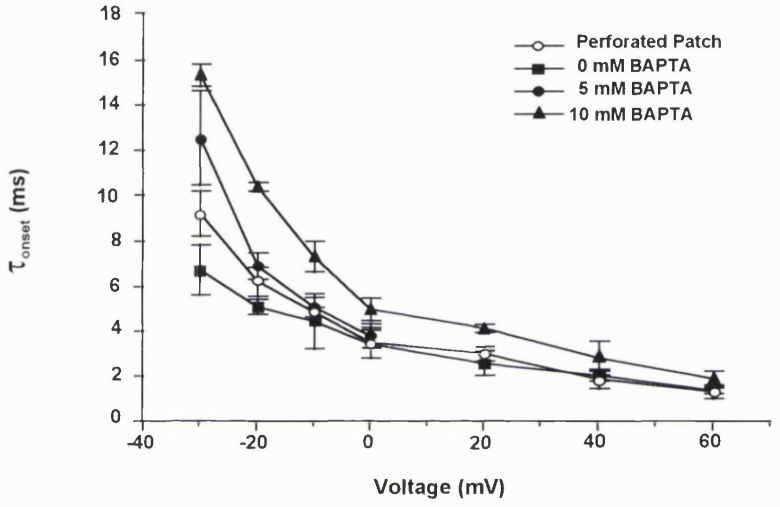

b

Voltage (mV)	-30	-20	-10	0	+20	+40	+60	Mean
Ca^{2+} buffering power (mM)	2.1	2.6	2.4	1.6	2.5	1.9	1.7	2.1

Figure 6.3 Calculated concentration of endogenous Ca^{2+} buffer over a range of voltages from -30 to +60 mV. a) Changes in the time constant of current activation with voltage at three concentrations of intracellular BAPTA. These are compared to the current onset kinetics observed during perforated-patch recordings. Mean and standard deviation values are shown. b) The equivalent concentration of endogenous Ca^{2+} buffer over a range of voltages from -30 to +60 mV in T4 OHCs. Calculated from the data in part a.

The time constant of current activation changed exponentially with changes in voltage. This was true for cells patched with either 0, 5 or 10 mM BAPTA and for cells patched using the perforated-patch technique (Figure 6.3a). For each of the voltages investigated between -30 and +60 mV, the relationship between the concentration of intracellular BAPTA dialyzing the cell from the patch pipette and the time constant of current onset was established (as for Figure 6.2). The value for the time constant of current onset measured using the perforated patch technique at the same voltage was then interpolated to this relationship to establish the equivalent concentration of endogenous Ca^{2+}

buffer at that voltage. Figure 6.3b tabulates the results of this study. No voltage dependent change in the concentration of endogenous Ca^{2+} buffer in T4 OHCs was observed. On that assumption, the mean equivalent concentration of endogenous Ca^{2+} buffer in T4 OHCs was 2.1 mM.

6.4 Discussion

6.4.1 Ca^{2+} buffering in T4 OHCs

Voltage-dependent currents expressed in T4 OHCs of the adult mammalian cochlea were used as a tool for measuring the equivalent concentration of endogenous Ca^{2+} buffer of T4 OHCs. Changes in the concentration of intracellular BAPTA affected both the amplitude and activation of the ensemble of voltage-dependent currents. BAPTA is certainly a fast enough buffer to mediate these changes, having a binding rate constant of 10^8 M^{-1} s^{-1} (Wang and Thompson, 1995). These changes are most likely to reflect changes I_{kCa} and $I_{k,n}$, currents that are both voltage and Ca^{2+} sensitive (Chapter 3). These results suggest that a component of the endogenous Ca^{2+} buffer of T4 OHCs is cytoplasmic and mobile and can be replaced by exogenous buffers, such as BAPTA, from the patch pipette. This mobile component is equivalent to the Ca^{2+} buffering capacity of 2.1 mM BAPTA.

The equivalent concentration of endogenous Ca^{2+} buffer in these cells is larger than the 1.6 mM BAPTA estimate for bullfrog saccular hair cells (Roberts 1993) and the 1 mM estimate made for mid-frequency turtle hair cells (Tucker and Fettiplace, 1995). This result seems fairly surprising. It is known that lower vertebrate hair cells require closely controlled rises and falls in the concentration of intracellular Ca^{2+} to control electrical tuning (Ashmore, 1983, Crawford and Fettiplace, 1981, Roberts, Jacobs and Hudspeth, 1990). No mechanism has so far been identified in OHCs of the adult mammalian cochlea that is so critically dependent on rapid rises and falls in the concentration of Ca^{2+}. Thus, the higher concentration of endogenous Ca^{2+} buffer in mammalian OHCs seems to conflict with the dependence of the respective cells on Ca^{2+}. Nevertheless, there may be various reasons why these OHCs have such high Ca^{2+} buffering. For example, in controlling the Ca^{2+} modification of $I_{k,n}$ and I_{kCa} channels (Chapter 3; Jagger and Ashmore, 1999), the P2X receptor (Raybould and Housley, 1997) and the mechanoelectric transduction apparatus (G. Géléoc, personal

communication). In addition, it will certainly prevent crosstalk between different pathways that rely on Ca^{2+} as a second messenger and may avoid regions of exccessively high Ca^{2+} concentration that may have serious consequences on cell functioning, such as the increasing activation of a leak conductance (Housley and Ashmore, 1992).

The Ca^{2+} binding capacity, β, of a buffer, B, can be calculated from (Tucker and Fettiplace, 1996):

$$\beta = d[Ca^{2+}\text{-}B]/d[Ca^{2+}] \qquad \textbf{Equation 6.3}$$

In the Ca^{2+} concentration range below K_d, $\beta \approx [B]/K_d$, where [B] is the concentration of the buffer and K_d is its affinity for Ca^{2+}. The K_d for BAPTA = 0.2 μM. Therefore, the binding capacity for 1 mM BAPTA is 10500. This indicates that for every 10499 Ca^{2+} ions in the cytosol, there is 1 that contributes to the free intracellular Ca^{2+} concentration. The Ca^{2+} binding capacity for a variety of neurones and neuroendocrine cells is far less than this value. For example, the Ca^{2+} binding capacity of adrenal chromaffin cells is 40 (Zohu and Neher, 1993), in neurohypophysial nerve endings it is 174 (Stunkel, 1994) and in neurones in the nucleus basalis it is ~126 (Tatsumi and Katayama, 1993). The nearest non-hair cell based preparation to the value reported in this study is in Purkinje cells from the rat cerebellum that estimates a Ca^{2+} binding ration of 2000 (Ferrio and Llano, 1996). This result indicates that OHCs posess an enormous Ca^{2+} binding capacity, have a low free intracellular Ca^{2+} concentration and a huge pool of bound Ca^{2+} within their cytosol.

Candidate mobile Ca^{2+} buffers include calbindin-28D, calretinin calmodulin and parvalbumin, all of which have been observed in mammalian OHCs using immunohistochemical techniques (Pack and Slepecky, 1995).

It is not clear what Ca^{2+} sources would generate rises and falls in the concentration of intracellular Ca^{2+} in mammalian OHCs. The existence of Ca^{2+} channels in OHCs has not been fully established. The investigations conducted so far present leak subtracted currents that are small and have slow activation kinetics (Chen, Nenov, Norris, Bobbin, 1995; Nakagawa, Kakehata, Akaike, Komune, Takasaka, Uemura, 1994; Nakagawa, Kakehata, Akaike, Takasaka, Uemura, 1991) unlike conventional L-type Ca^{2+} channels (Hille, 1992).

However, the putative Ca^{2+} currents do show typical voltage dependence and pharmacology and so the existance of such channels cannot be ruled out. Other sources of intracellular Ca^{2+} may be via the mechanoelectric transducer channel, non-selective cation channels (Corey and Hudspeth, 1979) located in the membrane of the stereocilia or by the release of Ca^{2+} from intracellular stores.

6.4.2 Voltage dependent Ca^{2+} buffering?

Mobile buffers are unlikely to be the only means of regulating the concentration of intracellular Ca^{2+}. Previous studies have provided evidence for the presence of Ca^{2+}-ATPases and Na^{+}-Ca^{2+} exchangers in OHCs (Apicella, Chen, Bing, Penniston, Llinas and Hillman, 1997; Ikeda, Saito, Nishiyama and Takasaka, 1992; Kozel, Firedman, Erway, Yamoah, Liu, Riddle, Duffy, Doetschman, Miller, Cardell and Shull, 1998; Schulte, 1993). Both of these may contribute to the total endogenous Ca^{2+} buffer of T4 OHCs. Being located in the plasma membrane of the cell, it was hypothesized that their activity may be modified by changes in intracellular voltage. This, in turn, may change the estimated concentration of endogenous Ca^{2+} buffer. However, consistent variations in the concentration of endogenous Ca^{2+} buffer with voltage were not observed. This may be because the change in activity of these pumps and exchangers is not enough over this voltage range to significantly affect the total equivalent concentration of Ca^{2+} buffer. This would seem a reasonable explanation based on the observed voltage dependence of the Na^{+}-Ca^{2+} exchanger observed in cardiac myocytes by Niggli and Lip (1994). No evidence of the voltage-dependence of the Ca^{2+}-ATPase has yet been published.

These results do not rule out the possibility that these and other fixed components, such as intracellular organelles, contribute to the buffering of intracellular Ca^{2+} in T4 OHCs. However, the technique used in these experiments to estimate the equivalent concentration of endogenous Ca^{2+} buffer was not sensitive enough to investigate their contribution to the total Ca^{2+} buffering of the cell.

6.4.3 Model of Ca^{2+} recruitment and regulation in T4 OHCs

Figure 6.4 shows the suggested effects and mechanisms of buffering of intracellular Ca^{2+} by T4 OHCs. Either before or following the effect of Ca^{2+} on either ion channels or downstream processes, Ca^{2+} will be buffered. Buffering may be via either mobile or fixed components. This study has estimated that the mobile component has a Ca^{2+} binding capacity equivalent to 2.1 mM BAPTA. Mobility is an important property of the endogenous Ca^{2+} buffer as it avoids saturation of the mechanism and prevents the Ca^{2+} transient travelling into the cell interior (Roberts, 1994). The contribution of fixed components to the endogenous Ca^{2+} buffering of T4 OHCs has not been estimated.

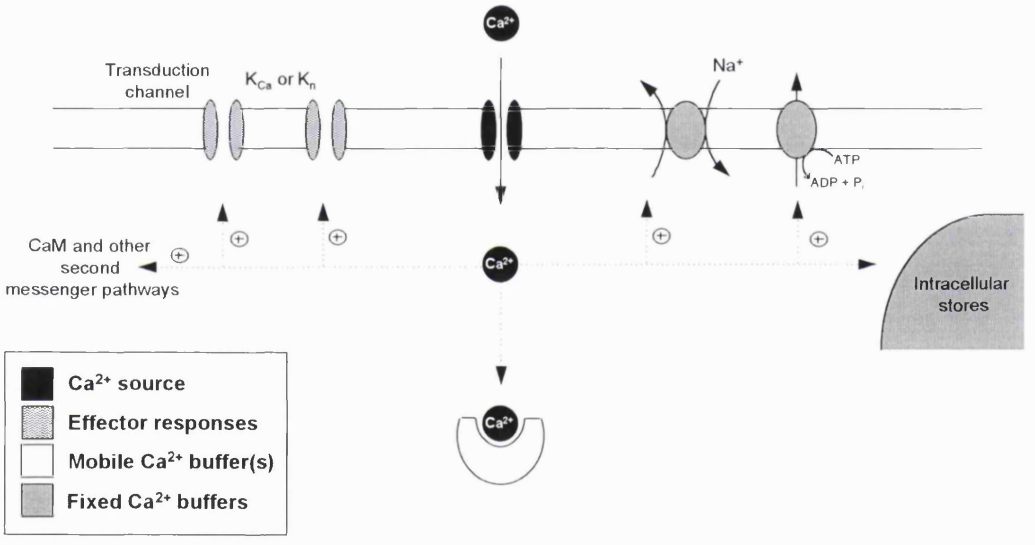

Figure 6.4 Schematic representation of the regulation of increases in intracellular Ca^{2+} in T4 OHCs. Following an increase, Ca^{2+} may effect a response such as the activation of an ion channel or a second messenger pathway. Either following this effect or before it is able to have this effect Ca^{2+} is buffered back to control levels either via a mobile or a fixed Ca^{2+} buffer.

Future experiments may aim investigate whether there are changes in the concentration of mobile Ca^{2+} buffer between apical and basal OHCs, cells that responed to very different stimulus frequencies. In support of such variations, Pack and Slepecky (1995) demonstrate immunohistochemically that Ca^{2+} binding proteins, such as Calbindin-28D, exhibit regional gradients throughout the mammalian sensory epithelium. In addition, Ricci and Fettiplace (1997) provide evidence for a gradient in the endogenous Ca^{2+} buffering of hair cells along the length of the turtle basilar papilla.

Chapter 7

Mechanoelectric transduction in OHCs of the adult mammalian cochlea

7.1 Introduction

OHCs are thought to use the mechanical energy of sound-related vibrations to generate a receptor potential that acts as the stimulus for cell length changes. The conversion of mechanical energy into an electrical response is termed mechanoelectric transduction (MET) and is the subject investigated in this chapter.

MET relies on the sound-induced deflection of the stereocilia bundle to open transducer channels. In the adult mammalian cochlea, the 100 or so stereocilia within a hair bundle are located in 3 rows of decreasing height (Lim, 1980). Transducer channels are located at the tips of the stereocilia (Hudspeth, 1982; Ohmori, 1985; Kroese, Das and Hudspeth, 1989) and are suggested to be gated by the tension in attached, elastic elements termed gating springs (Hudspeth, 1989). The morphological correlate of these gating springs is thought to be tip-links, fine, filamentous links that run from the tops of the shorter stereocilia to the side of adjacent, taller stereocilia (Pickles, Comis and Osborne, 1984). The integrity of these tip-links is removed if the Ca^{2+} concentration of the saline surrounding the hair bundle is less than 50 μM (Assad, Shepherd and Corey, 1991; Zhao, Yamoah and Gillespie, 1996). Transducer channels may be located at either one (Crawford, Evans and Fettiplace, 1991; Howard and Hudspeth, 1988) or both ends (Denk, Holt, Shepherd and Corey, 1995) of the tip-link.

Increased tension in these tip-links, caused by bundle deflection towards the tallest row of stereocilia, leads an increased probability of channel opening. Deflection in the opposite direction decreases the tension in the tip-links. This shuts the transducer channels and reduces the flow of current in to the hair cell (Shotwell, Jacobs and Hudspeth, 1981).

Transducer channels are non-selective cation channels (Corey and Hudspeth, 1979) that can be blocked by antibiotics such as streptomycin (Kimitsuki and Ohmori, 1993, Kroese, Das and Hudspeth, 1989). *In vivo*, the transduction current will be carried by K^+, the predominant cation in the endolymph, the fluid within the scala media of the cochlea (Bosher and Warren, 1968). The driving force for the movement of K^+ into the hair cell via the transduction channels is not only due to the concentration gradient for K^+ but also due to the negative potential inside the hair cell (-70 mV) as well as the positive endocochlear potential of +80 mV (Dallos, 1985). The flow of current into the cell via the transduction channels leads to a change in voltage inside the hair cells that is termed the receptor potential (Hudspeth and Corey, 1977). For OHCs, the receptor potential is thought to be the physiological stimulus that activates the motile response of the cell. For IHCs, it is thought to be the stimulus that initiates transmitter release from the basal pole of the cell to the afferent nerve with which it synapses, allowing timing and intensity information regarding a particular sound frequency to be encoded in the auditory nerve.

The mammalian auditory system is a specialized high frequency detector. Thus, the mechanism of MET in both IHCs and OHCs must be effective beyond 10 kHz if OHC length changes and IHC transmitter release are to be effective on a cycle-by-cycle basis. However, the above description of the mechanisms of MET have been almost exclusively developed on hair cells of lower vertebrates. These are specialized low frequency detectors (<1 kHz). Relatively little is known about MET in the adult mammalian auditory system. A limited number of studies have attempted to characterize the properties of the MET current in adult mammalian OHCs (Ashmore, Kolston and Mammano, 1993; Ashmore, 1987; Meyer, Furness, Zenner, Hackney and Gummer, 1998). However, the properties of the recorded currents may not be representative of their properties *in vivo* if the mechanosensitive hair bundles have been damaged by the isolation procedure. An alternative preparation, cultures of the auditory and vestibular systems of neonatal mice, has generated a substantial body of information regarding mammalian MET (Kros, Rüsch and Richardson, 1992; Géléoc, Lennan, Richardson, Kros, 1997). However, extrapolation of these results to the adult mammalian cochlea may be limited due to ambiguities from culturing immature hair cells in perilymph-like solutions.

The aim of this study was to characterize the biophysical properties of adult mammalian MET currents and to investigate whether mammalian transduction mechanisms are specialized to operate beyond 10 kHz. The *in situ* preparation used for these investigations avoided enzymatic and mechanical dissociation of hair cells, culturing and the use of neonatal tissue.

7.2 Methods

Dissection of the guinea-pig cochlea has been described in Section 2.1.3. The procedure is unchanged in this set of experiments except for the following points. OHC stereocilia were accessed by removing the overlying tectorial membrane. This was achieved by gently peeling away the tectorial membrane with an etched tungsten wire (TW10-3, Clark Electromedical Instruments, UK) at a point either basal or apical to the site of recording. Once a small section of tectorial membrane had been removed, whole sections of membrane tended to follow very easily.

Stereocilia were visualized when the bulla was mounted such that the reticular laminar of T4 was horizontal. This maintained the stereocilia in a vertical position which maximized the contrast that could be achieved with light from the fibre optic and improved the visual clarity of the preparation. Thus, the effectiveness of stereocilia stimulation could be more accurately monitored. No attempt was made to calibrate the deflection.

7.2.1 Electrophysiological recording and mechanical stimulation

Transduction currents were measured in voltage-clamped OHCs using the whole-cell recording technique (Section 2.3). The preparation was dissected and maintained in standard PBS solution with a reduced Ca^{2+} concentration (1 mM to 250 μM) (Table 2.1). It was perfused as detailed previously (Section 2.2.6) but the rate of perfusion was reduced from 450 μl/min to 100 μl/min to minimize movement of the stereocilia. Cells were patched using soda glass pipettes (3-4 MΩ) filled with basic PBS solution containing 1 mM Mg-ATP (Table 2.1).

Stereocilia were stimulated by force with a fluid-jet generated by the movement of a plunger connected to a piezo-electric stack (P-840.20, Physik Instruments, Germany). A puffer pipette was used to direct this stimulus towards OHC stereocilia (Figure 7.1). Maximum voltage steps of ±0.01 V applied to the piezo stack generated stimuli sufficient to move OHC stereocilia. Voltage steps applied to the piezo electric stack were low-pass filtered at 500 Hz by a 4-pole Bessel filter to avoid excitation of the piezo stack's first resonance (14 kHz). The time constant for the onset and offset of the step change in voltage applied to the piezo stack was 0.91 ms.

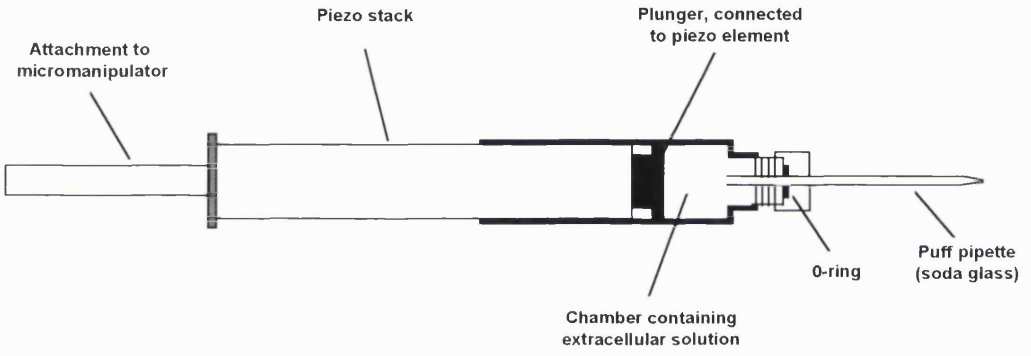

7.1 Piezo-electric stack used to generate fluid-jets that displaced OHC stereocilia by force.

The puffer pipette, used to direct the stimulus towards the stereocilia, was an over-sized soda glass patch pipette pulled to generate a tip diameter of ~10 μm. Both the puffer pipette and the chamber associated with the stimulator mechanism were filled with the same low Ca^{2+} concentration standard PBS solution as used to perfuse the preparation. To avoid resonance of the fluid jet stimulus, care was taken to avoid trapping bubbles within the puffer pipette or chamber when filling them with solution. The piezo electric stack was isolated from the solution in the chamber by an O-ring surrounding the plunger. The puffer pipette approached the OHCs from the modiolar side of the organ of Corti and was positioned 10-20 μm from the stereocilia bundle. The angle of approach of the puffer pipette was maximised within the confines of the microscope objective and the recording chamber, to avoid it touching the organ of Corti and vibrating the preparation. Fluid movement out the puffer pipette displaced the hair bundle in the direction of the tallest stereocilia (excitatory stimulus) whereas fluid movement in to the pipette displaced the hair bundle towards the shortest stereocilia (inhibitory stimulus). To ensure that no bias was being applied to the position of the hair bundle prior to recording MET currents

from OHCs, the puffer pipette was placed next to cellular debris in a distant part of the preparation and the position of the particles monitored for any movement. Any bias was off-set by applying a positive or negative DC-voltage to the piezo stack.

Control experiments ensured that the currents recorded were due to the MET current and not due to the activation of ion channels in the basolateral membrane of the OHC or leak conductances caused by a decrease in the resistance of the pipette seal. The fluid jet stimulus was first applied to the basolateral membrane of the OHC around its basal pole and second to the area of membrane forming the seal with the patch pipette. No change in conductance was observed in either case.

A fluid-jet was chosen to stimulate OHC stereocilia rather than a probe coupled to a piezo-electric bimorph because the visual resolution of *in situ* OHC stereocilia was not of a high enough quality to know precisely where the tip of the probe lay relative to the hair bundle. However, simulation of OHC stereocilia with a fluid-jet had two disadvantages:

a) The force of stimulus being applied to the stereocilia was not known.
b) Stereocilia movement was difficult to monitor in a preparation where the quality of visualization of the preparation is poor.

7.2.2 Attempts to increse the number of MET current recordings from T4 OHCs.

The frequency with which MET currents of adult mammalian OHCs were recorded was low. Many attempts were made to maximize the number of recordings obtained from the preparations. For completeness, the series of adjustments made to the experimental protocol are listed below. None of them made a difference to the probability of recording a MET current from a T4 OHC.

a) To ensure that Ag^+ ions from the Ag^+/AgCl reference electrode were not blocking the MET channel, a salt bridge (1% agar in 0.15 M NaCl) was used to connect the bath solution with an adjoining chamber containing the reference electrode. The salt bridge was located downstream of the preparation, close to

the perfusion outlet to avoid changes in the ionic composition of the extracellular solution.

b) The perfusion system was switched off for the duration of a sub-set of experiments to ensure that over-stimulation of the stereocilia through perfusion of the preparation was not affecting the probability of recording a MET current. For the same reason, the movement of the microscope objective lens in the solution of the recording chamber was kept to a minimum.

c) Dental acrylic and superglue were both used on occasions as alternatives to wax for mounting the bulla in the recording chamber. Neither method increased the likelihood of recording a MET current from OHCs. In hindsight they were probably worse options to choose as they took up to 10 minutes to dry and being cyano-acrylates, had the potential to leach Cs^+ in to the bath.

d) Light from the fibre optic illuminating the preparation was filtered at 510 nm to ensure that the stereocilia were not being damaged by the accumulation of energy from this light source in the form of heat.

e) Intracellular solutions containing 1 mM ATP were snap frozen in liquid nitrogen to avoid the breakdown of ATP to ADP and adenosine. Thus, the concentration of ADP, a compound known to inhibit adaptation (Gillespie and Hudspeth, 1993), was minimized.

f) To focus the fluid-jet stimulus more accurately towards the OHC stereocilia, the tip of the stimulus pipette was reduced from ~10 μm to ~ 5 μm and the voltage applied to the piezo stack reduced.

g) The holding potential of the cell was kept as negative as possible, without the OHC becoming unstable, to increase the driving force across the stereocilia and maximize the size of the MET current.

h) The concentration of intracellular Ca^{2+} was reduced from 1 mM to 250 μm to minimize slipping of the tip-link insertion via the adaptation motor mechanism and maximize the size of the transduction current (Crawford, Evans an Fettiplace, 1991). The concentration of intracellular Ca^{2+} was never taken

below 250 μm for fear of breaking the OHC tip-links when the patch pipette approached the cell with a minimal amount of positive pressure (Assad, Shepherd, Corey, 1991).

i) To ensure that the MET apparatus was not being damaged during the removal of Hensen's cells, these supporting cells were left in place and OHC patched by penetrating the layer of cells with increased positive pressure on the patch pipette.

j) Stereocilia were stimulated via the tectorial membrane which had been left in place to reduce mechanical disruption to the hair bundle. Gentle movement of the membrane produced no MET current. Stronger stimulation caused the patch on the OHC to be lost.

k) To mimic the method of stimulation *in vivo*, attempts were made to displace the stereocilia with a stimulus probe (Ashmore, Kolston and Mammano, 1993). However, the quality of illumination of the stereocilia in this preparation was so variable, this method of stimulation was almost impossible to use.

l) The tectorial membrane was loosened from OHC stereocilia by incubating the preparation in extracellular solution containing either 75 μg/ml trypsin or protease XXIV for up to 5 minutes. Although the removal of the tectorial membrane was considerably easier following enzyme treatment, there was no improvement in the frequency of recording MET currents.

Although none of the above adjustments increased the probability of recording a MET current, they did start to confine the source of the problem.

7.2.3 Data collection, analysis and presentation

MET currents were recorded and signal averaged on-line using Signal Averager (Version 6.15, Cambridge Electronic Design, UK). Data were stored as an average of 30 traces. In the figures that follow, the driver voltage to the piezo-electric stack is shown as the stimulus monitor.

7.3 Results

7.3.1 MET currents in T4 OHCs of the guinea-pig cochlea

Averaged MET currents recorded from a T4 OHC can be seen in Figure 7.2a. The extracellular solution bathing these cells contained Na^+ as the major cation with Mg^{2+} and Ca^{2+} present at concentrations of 1.5 mM and 250 μM respectively. Excitatory stimuli, movement of the hair bundle towards the tallest row of stereocilia, generated an increase in the inward current. This was denoted as a downward deflection of the current trace. Movements of the hair bundle in the opposite direction caused a decrease in the total amount of inward current. The maximum MET current generated in this OHC was 59.4 pA at -60 mV. This translates in to a conductance of 0.99 nS, assuming the MET conductance is a non-selective cation conductance (Ashmore, Kolston and Mammano, 1993; Crawford, Evans and Fettiplace, 1991; Kros, Rüsch and Richardson, 1992).

Figure 7.2b shows the relationship between the MET current and the voltage applied to the piezo stack. Current was measured at the peak of each trace and was plotted relative to the current value obtained with the largest negative deflection, where all the transducer channels were assumed to be closed. The relationship between the MET current and the voltage applied to the piezo stack was sigmoidal and symmetrical and was fitted by a first order Boltzmann function. This suggests that adult mammalian MET channels have just one closed state and one open state, the transition between the two being mechanically sensitive. Although the fit of a first order Boltzmann function to the data presented in this study correlates well with previous studies of OHC MET currents (Ashmore, Kolston and Mammano, 1993), it is inconsistent with most other studies where the transfer function is best fitted by a second order Boltzmann function (eg Crawford, Evans and Fettiplace, 1989; Géléoc, Lennan, Richardson and Kros, 1997). Attempts were made to fit a second order Boltzmann function to the data presented in Figure 7.2. However, too few data points at the positive voltages made it impossible to fit the function accurately.

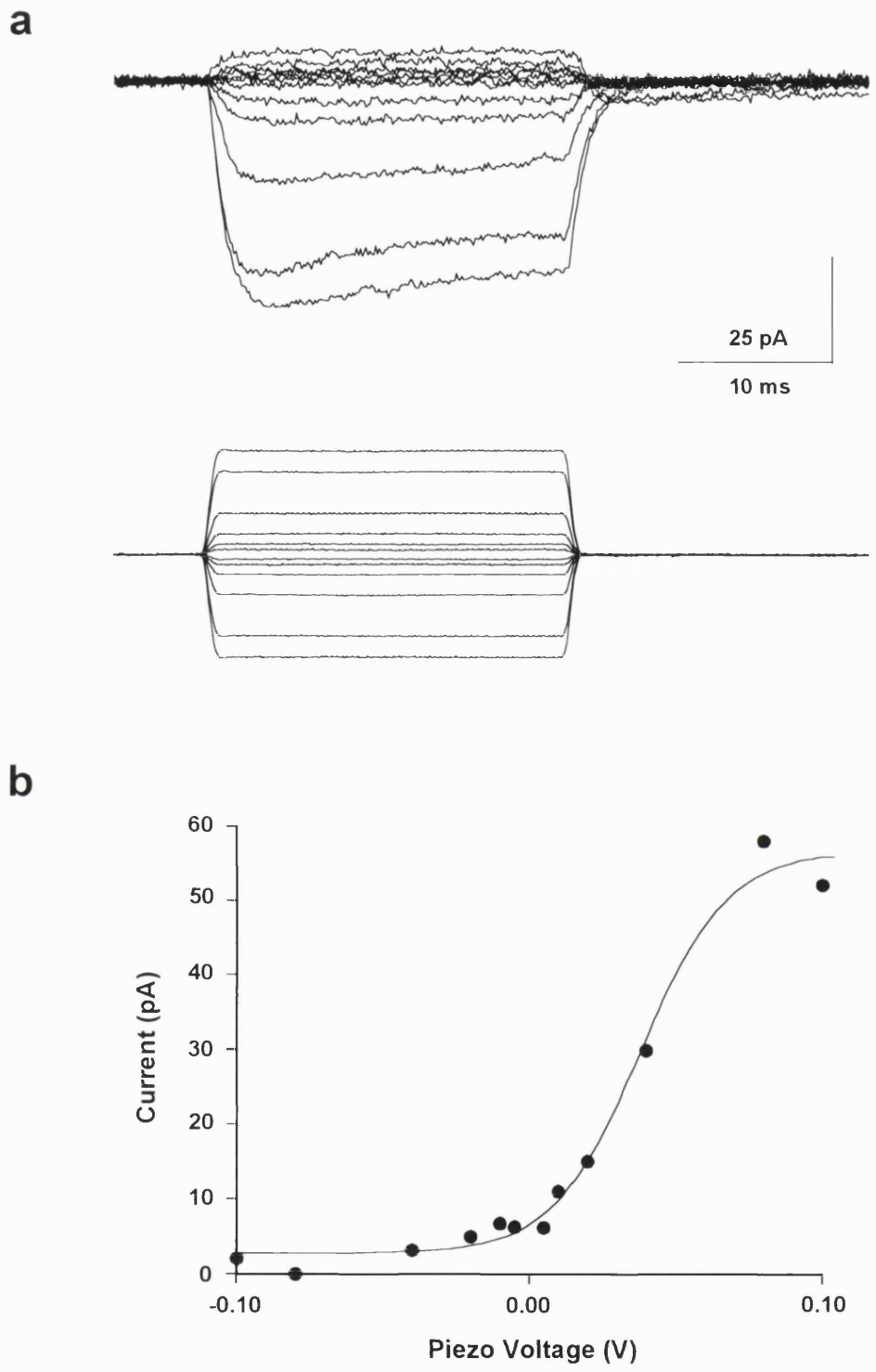

7.2 Averaged MET currents in T4 OHCs of the adult guinea-pig cochlea. a, MET currents recorded in response to force stimulation by a fluid jet. Each trace is an average of 30 responses. Voltage steps applied to the piezo of the fluid jet shown below the current traces. b, current-displacement curve for the currents shown in a. The smooth curve fitted to the data was a first-order Boltzmann function of the form $y = A_2 + ((A_1-A_2)/(1+e(x-x0)/dx))$ where $A_1 = 2.7$, $A_2 = 56.6$, $x0 = 0.03$ and $dx = 0.01$. Holding potential = -60 mV. Stimulus pipette positioned 20 μm from hair bundle. Tip diameter = 10 μm. The intracellular solution was defrosted immediately before use in the experiment to minimise the break-down of ATP to ADP and adenosine.

Mammalian OHCs have a very low ratio of MET channels to tip links. Assuming the single channel conductance of MET channels is 112 pS (Géléoc, Lennan, Richardson and Kros, 1997), adult mammalian OHCs posess 8 functioning channels per hair bundle. Alternatively, a single channel conductance of 50 pS (Ohmori, 1985), predicts that hair bundles posess 20 functioning channels. These calculations suggest that adult mammalian OHCs have a ratio of MET channels to tip-links somewhere between 1:8 and 1:3. Both values are less than the 1:1 ratio calculated by Géléoc, Lennan, Richardson and Kros (1997). However, as the single channel conductance of adult mammalian MET channels is unknown, it is premature to suggest that there are so few MET channels per hair bundle.

To determine the upper frequency limit for the adult mammalian MET apparatus, the time constant of the onset and offset kinetics of the MET current were measured. For the maximum inward deflection, these could be fitted with single exponential curves with time constants of 1.03 ms and 1.47 ms for the onset and offset of the stimulus respectively. These values correspond closely to the kinetics of the voltage step applied to the piezo stack and suggest that the kinetics of the current response are limited by the fluid-jet stimulus which has a corner frequency of 1.09 kHz (see section 7.2).

MET currents generated by the largest excitatory stimuli were characterized by a time-dependent reduction in the total amount of current in response to a maintained stimulus. It was not possible to confirm whether this reduction in current was an artefact of the stimulus as neither the position of the stereocilia nor the cell body were monitored. However, this observation does exhibit similarities to adaptation, a process observed in hair cells of both mammalian and non-mammalian species (Eatock, Corey and Hudspeth, 1987; Crawford, Evans and Fettiplace; 1989, Kros, Rüsch and Richardson, 1992). Adaptation of the second largest inward current could be fitted by a single exponential function with a time constant of 8.5 ms. This is slower than the speed of adaptation observed in turtle hair cells and neonatal OHCs where the time constant was 3-5 mS (Crawford, Evans and Fettiplace, 1989; Kros, Rüsch and Richardson, 1992). The kinetics of adaptation have been shown to be sensitive to the concentration of Ca^{2+} in the extracellular solution (Crawford, Evans and Fettiplace, 1989; Eatock, Corey and Hudspeth, 1987). Thus, the observed differences in the time constant of adaptation between the different

preparations may reflect the variations in Ca^{2+} concentrations used in the different studies. Adaptation of the MET current in adult mammalian OHCs was faster than that observed in lower vertebrate vestibular hair cells where the time constant for adaptation was ~30 ms (Eatock, Corey and Hudspeth, 1987). These differences may result, in part, from the high concentration of extracellular Ca^{2+} concentration used in these experiments (4 mM). However, they may also reflect functional differences between vestibular and auditory hair cells.

In the absence of a stimulus, 6 % of the MET channels were open. This is far less that that predicted by the AC responses of T4 OHC receptor potentials recorded *in vivo*. These recordings show that at the characteristic frequency, 25-30 % of the MET channels are open at in the absence of stimulation (Dallos, 1986). One explanation for these differences in the resting position of the hair bundle may reflect be that *in vivo*, the tectorial membrane biases the position of the stereocilia.

Sensitivity can only be expressed in terms of the volts applied to piezo stack as the movement of the OHC stereocilia was not monitored. At the resting position of the bundle, the sensitivity of current activation was 212 pA/V. This compares to a maximum sensitivity of 375 pA/V, corresponding to position on the current-stimulus curve where 40% of the channels are open. Although the position of the hair bundle at rest is not at the steepest part of the current-stimulus curve, it does appear to be positioned at or near the point where the rate of change of sensitivity is maximal. Unfortunately, comparisons to other hair cell MET currents cannot be made.

The results presented above are based on the analysis of a family of MET currents recorded from an individual T4 OHC. It should be noted that the conclusions are limited by:

a) the low number of recordings
b) the variability in the characteristics of the MET currents recorded.

The complete results of this study are summarized in Table 7.1.

Cell	Maximum conductance (nS)	Channels open at rest (%)	Kinetics of channel activation (ms)	Maximum sensitivity (pA/V)	Filtered '*in vivo*' receptor potential (mV)	Total number of MET channels 50 pS	100 pS
a	1.2	6	1.03	375	4.75	20	10
b	1.95	60	0.89	625	9.37	33	16
c	1.15	0	0.95	523	5.5	20	10
d	0.43	17	--	310	4.14	8	4

Table 7.1 Summary information regarding the MET currents recorded from T4 OHCs

7.3.2 Time-dependent changes in the MET current

MET currents were observed to run-down with time in the whole-cell recording configuration (Figure 7.3). Run-down was characterized by a decrease in the total amount of current, a slowing of the activation kinetics, a loss of adaptation, a change in the maximum sensitivity of the current and a decrease in the number of channels open at rest. The reduction in the total amount of current with time could be explained if the transduction apparatus was damaged during stimulation. However, this does not explain why the sensitivity of MET changes with time, unless there is significant co-operativety between stereocilia in a hair bundle. The possibility that these effects come about through run-down of a second messenger system and/or a change in the phosphorylation state of the MET channel cannot be ruled out. However, there is no evidence for such regulation of this channel in the literature. These results can be most easily explained if, with repeated stimulation, the cytoplasm of the stereocilia is overloaded with Ca^{2+} and the endogenous Ca^{2+} buffer is saturated. According to the mechanism of adaptation, raised intracellular Ca^{2+} will cause the tip-link insertion to slide down the stereocilia. Under these circumstance, further stimulation may not generate sufficient tension in the tip-links to open the MET channels.

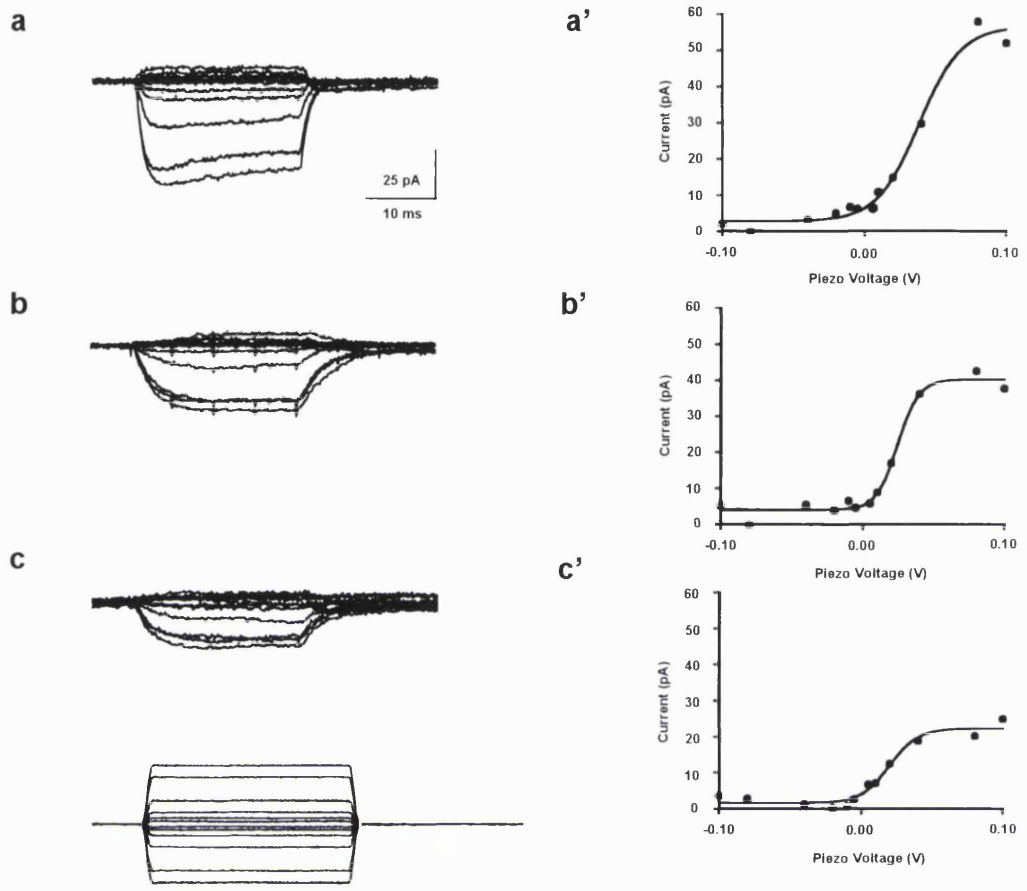

7.3 Time-dependent changes in the MET current. a) MET currents recorded 4 minutes after the whole-cell configuration achieved. a') current-displacement curve for the currents shown in a. b) MET currents recorded 10 minutes after the whole-cell configuration had been achieved. b') current-displacement curve for the currents shown in b. c) MET currents recorded 18 minutes after the whole-cell configuration had been achieved. c') current-displacement curve for the currents shown in c. Holding potential = -60 mV. The increased noise observed in the current traces of b and c are due to electrical interference from the perfusion pump.

Changes in the properties of the MET current with time in the whole-cell recording configuration can be used to predict the properties of the current at the start of the recording (Figure 7.4). Using the data from the traces shown in Figure 7.3, a plot of the changes in the maximum MET current and the time constant of activation of the largest inward current have been plotted against the time at which they were recorded after the start of the patch. The regression lines predict that at the start of the recording, the amplitude of the MET current was 66 pA at -60 mV and the time constant of current activation was 0.91 ms. Using the methodology set out in Section 7.4.1, a current of 66 pA would translate in to a change in potential of 2.4 mV, generating a change in OHC length of 4.8 nm. The predicted time constant of current activation of 0.91 ms

confirms that the frequency response of the MET current is limited by the kinetics of the fluid-jet stimulus.

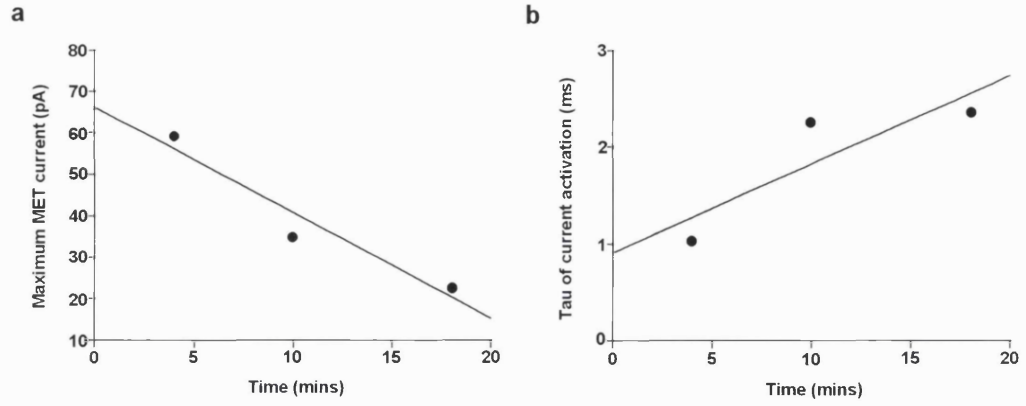

7.4 Time-dependent changes in the characteristics of the MET current in a T4 OHC. Data from MET currents shown in Figure 7.3. The straight line filled to the two sets of data is a linear regression line of the form y = Ax + B where for a) A = 66.23 and B = -2.54 and for b) A = 0.91 and B = 0.09.

7.4 Discussion

The results presented in this chapter describe some of the biophysical properties of MET currents in adult mammalian OHCs *in situ*. Qualitatively, these currents exhibited many features seen in hair cells from other systems; only a small proportion of the total number of MET channels are open at the resting position of the bundle, some adaptation-like process was observed in response to a maintained stimulus and the relationship between the displacement of the stereocilia and the MET current was sigmoidal. Quantitatively, the MET currents of adult mammalian OHCs are quite distinct from other MET current recordings.

7.4.1 Biophysical characteristics of the adult mammalian MET current

MET currents of the adult mammalian cochlea are substantially smaller the transduction currents recorded from any other system. They are 5-6 times smaller than those observed in OHCs of neonatal mice (Géléoc, Lennan, Richardson, Kros; 1997, Kros, Rüsch, Richardson, 1992) and 3-4 times smaller than those observed in hair cells of the turtle basilar papilla (Crawford, Evans and Fettiplace, 1989 & 1991). However, they are very similar in size to the currents previously recorded in isolated adult mammalian OHCs (Ashmore,

Kolston and Mammano, 1993; Meyer, Furness, Zenner, Hackney, Gummer, 1998). The small size of the MET current in adult mammalian OHCs does not render them un-physiological. This is in large part due to the small input conductance of *in situ* OHCs. This plays an important role in maximizing the receptor potential generated in response to the MET current. The receptor potential generated in response to this MET current can be calculated from the following equation:

$$\Delta V_{RP} = (\phi g_T)/(g_{in} + \phi g_T) \times (V_{EP} - V_r) \qquad \textbf{Equation 7.1}$$

where

ΔV_{RP}	the change in receptor potential generated by MET current
g_T	MET conductance
ϕ	conversion factor for MET current recorded in endolymph (see below)
g_{in}	input conductance of T4 OHC, assuming it to be a pure K^+ conductance
V_{EP}	endocochlear potential
V_r	resting potential of T4 OHC

This equation assumes that the transducer conductance will be increased in endolymph, the solution bathing the hair cell stereocilia *in vivo*. In turtle hair cells, the MET current was increased threefold in endolymph (Crawford, Evans and Fettiplace, 1991). This equation ignores the voltage-dependence of the K^+ conductances in the basolateral membrane of the cell. Thus, a maximum receptor potential of 75 mV will be generated '*in vivo*' assuming g_T = 0.99 nS, ϕ = 3, g_{in} = 2.9 nS (Table 3.2), V_{EP} = +80 mV and V_r = -60 mV. However, the low-pass filter of the basolateral membrane of T4 OHCs will filter this receptor potential according to the following equation:

$$\Delta V_{RP} = 75 \text{ mV} \cdot 1/(1+(f/f_o)^2)^{1/2} \qquad \textbf{Equation 7.2}$$

where f = 400 Hz, the stimulus frequency to which the basilar membrane best responds for this hair cell location and f_0 = 13 Hz, the cut-off frequency for the low-pass filter of the basolateral membrane of this OHC (see section 3.4.2). Thus, the effective voltage change following filtering is 2.4 mV (Sections 3.3.2 and 3.4.2). Assuming a minimum motor sensitivity of 2 nm/mV (Santos-Sacchi,

1989), T4 OHCs will undergo a maximum length change of 4.8 nm in response to the predicted change in potential inside the cell generated '*in vivo*'. Thus, these relatively small mechanosensitive conductances, recorded in perilymph-like solutions, appear to be physiologically reasonable.

From equation 7.1, it can be seen that as the input resistance of the cell decreases, so the size of the receptor potential increases. Although the size of the MET current is very similar *in vitro* and *in situ*, the resulting receptor potential is much larger *in situ* as the input conductance of the cell is considerably smaller. This may be one reason why the viability of small MET currents *in vitro* have been questioned previously (eg, Kros, 1996).

There does not appear to be a 1:1 ratio between the number of tip-links per hair bundle the number of MET channels present in adult mammalian OHCs. The best estimate suggests that there is one MET channel for every 3 tip-links or a total of 20 functional channels. The hypothesis that each tip-link is the morphological correlate of the gating spring that regulates the opening of the MET channel (Howard, Roberts and Hudspeth, 1988), suggests that the number of MET channels will equal the number of tip-links. The minimum number of MET channels present in the hair bundle of OHCs from the adult mammalian cochlea should be ~66. Given that the single channel conductance of MET channels from OHCs have not been experimentally determined, it is premature to suggest that the conductance will be the same as previous estimates from chick hair cells and neonatal OHCs. If there were one channel per tip-link, the predicted single channel conductance would be 15 pS. What seems rather unusual from this discussion is that MET channels are down-regulated from 100 pS to 15 pS during development. However, such changes are not inconceivable when there are such obvious alterations to the basolateral conductances during development.

It has not been possible to determine the upper frequency limit of the transduction apparatus in adult mammalian OHCs. The frequency limit of the fluid-jet was 1 kHz and the results presented in this chapter suggest that the kinetics of the current are limited by the fluid-jet stimulus. This could not be substantially increased without causing the stimulus to resonate. Thus, substantial readjustments would be made to the fluid-jet stimulator to probe the frequency limits of the adult mammalian MET further. There is no information to

date regarding the temperature sensitivity of the adult mammalian transduction process. However, the temperature sensitivity of the onset kinetics of the transduction current in turtle hair cells has been investigated and a Q_{10} value of 1.9 was found (Crawford, Evans and Fettiplace, 1989). Assuming that the Q_{10} value is the same for the adult mammalian transduction apparatus, the upper frequency limit estimated for the transduction apparatus in these experiments can be adjusted for physiological temperatures. Under these circumstances, an upper frequency limit of 2 kHz was calculated. This still generates a 4 fold difference between the maximum frequency in these experiments and the characteristic frequency for hair cells located at that point along the length of the cochlea (12.5 kHz).

This study should not detract from the fact that very little data has ever been published on adult mammalian MET currents. This is presumably because the frequency with which such currents are recorded is very low. During the course of this study, many control experiments were conducted to try and identify why it is so difficult to record MET currents from adult mammalian OHCs. Although the problem was not clearly identified, the control experiments did imply, albeit indirectly, that mechanical disruption to the hair bundle through the removal of the tectorial membrane was the most likely source of the problem. This is presumably because the tallest row of stereocilia in adult mammalian OHCs are embedded in to the tectorial membrane (Lim, 1980). This is not true of neonatal or lower vertebrate hair cells where MET currents are much more easily recorded.

The *in situ* preparation was possibly not the best preparation to use for these investigations. Although it avoided mechanical and enzymatic dissociation of the hair cells, it limited the sample of cells available to record from to ~100 outer row OHCs. In comparison, isolated OHC preparations draw on all three rows of OHCs from all four turns of the cochlea. If the problem with these experiments is not so much the dissociation procedure but more the removal of the tectorial membrane, then isolated OHC preparations will provide an increased probability of choosing a cell where the transduction apparatus is relatively undamaged.

7.4.2 Future improvements

Future attempts to study adult mammalian MET should consider the following improvements to the present experimental protocol. First, OHCs should be patched using the perforated patch technique (Rae, Cooper, Gates, Watsky, 1991). This will help to avoid run-down of the MET current with time in the whole-cell recording configuration. Second, a mechanism should be developed to monitor the movement of the stereocilia in response to a stimulus. This is important, not only for information such as the absolute displacement of the stereocilia but also to investigate the mechanics of the bundle movement. Whatever adjustments are made to the experimental protocol, they should still enable the experimenter to investigate possible changes in the properties of the MET currents along the length of the cochlea. These could be extremely interesting investigations. For example, with input conductances of 37.4 nS, T1 OHCs would be predicted to have very large MET currents in order to produce a receptor potential large enough to activate the electromotile response.

Appendix 1

Statistical tests

The statistical test chosen to compare the means of two sets of data was a Student t-test. This test is based on the assumption that the samples to be compared have been randomly selected from populations with a t-distribution, a parametric distribution whose dispersion varies according to size of the sample. This makes it suitable for use on small sample sizes ($n \leq 30$). Before comparing the means of the two samples, the Student t-test first investigates the significance of the difference between the standard deviations (SDs) of the two samples. If the SDs of the samples are very different, this alone suggests that the samples come from two different populations. Under these circumstances, a comparison of the means is not appropriate. However, if the difference between the SDs is not significant, a comparison of the means of the samples is justified. Two-tailed Student t-tests were performed on the data. The null hypothesis put forward for each test was: There is no significant difference between the means of the two samples, suggesting that the samples are from the same population. The alternative hypothesis, accepted if the difference between the means was significantly different, was: x is significantly larger/smaller than y. This suggests that the samples come from different populations. Significance is presented as a P-value, the smallest significance level possible for which the null hypothesis is rejected. Significance was measured to the 1 % level. The results of the Student t-tests are presented in Table 1.

If the difference between the SDs of two samples is significantly different, a Mann-Whitney U-test can be performed to test the significance of the difference between the two samples. This is an unpaired, non-parametric test that ranks the observations across the two samples in order of magnitude from 1 to n. The ranks for each set of observations are then summed and the difference between these values tested for significance. If the samples were very similar, the rank sums would be nearly equal. For very different samples, the rank sums would be correspondingly different and may indicate a difference between the two populations. However, it was felt

that the information gleaned from a significant difference between the SDs using the Student t-test was sufficient information regarding the difference between the two samples for the purposes of this investigation.

Test	Samples	Unit	Sample a	Sample b	Result
a	In vivo vs in situ V_z for T4 OHCs	(mv)	-65.6 ± 8.85 mV (n = 20)	-76.7 ± 11.2 (n = 12)	SD: n.s.d. mean: s.d. P = 0.002
b	In situ vs in situ V_z for T4 OHCs	(mV)	-65.6 ± 8.85 mV (n = 20)	-70 ± 5 (n = 14)	SD: n.s.d. mean: n.q.s.d. P = 0.05
c	In situ vs in vitro V_z for T4 OHCs	(mV)	-65.6 ± 8.85 mV (n = 20)	-56.9 ± 15.5 (n = 50)	SD: s.d P < 0.004
d	In situ vs in situ C_m for T4 OHCs	(pF)	35.5 ± 5.08 (n = 20)	37.5 ± 3.1 (n = 14)	SD: n.s.d. mean: n.s.d. P = 0.09
e	V_z with I_{kt} vs V_z without I_{kt}	(mV)	-56.8 ± 7.82 (n = 5)	-64.2 ± 3.19 (n = 5)	SD: n.s.d. mean: n.s.d. P = 0.04
f	τ_{onset} without Ca^{2+} vs τ_{onset} with Ca^{2+}	(ms)	8.95 ± 0.5 (n = 9)	8.67 ± 0.43 (n = 5)	SD: n.s.d. mean: n.s.d. P = 0.15
g	In vivo vs in situ V_z for T1 OHCs	(mV)	-76.7 ± 11.2 (n = 12)	-83 ± 12.8 (n = 20)	SD: n.s.d. mean: n.s.d. P = 0.08
h	T4 vs T1 V_z	(mV)	-65.6 ± 8.85 (n = 20)	-76.7 ± 11 (n = 12)	SD: n.s.d. mean: v.s.d. P = 0.002
i	T4 vs T1 γ at -110 mV	(nS)	-2.7 ± 0.88 (n = 10)	16.1 ± 4.9 (n = 11)	SD = e.s.d P < 0.001
j	T4 vs T1 γ at V_z	(nS)	-2.92 ± 1.73 (n = 20)	37.4 ± 21.0 (n = 20)	SD: e.s.d. P < 0.001
k	T4 vs T1 γ max	(nS)	22.01 ± 6.90 (n = 20)	291.0 ± 102.5 (n = 5)	SD: e.s.d P < 0.001

Table continued on next page.

Test	Samples	Unit	Sample a	Sample b	Result
l	T4 vs T1 τ_{onset} at 0 mV	(ms)	8.13 ± 2.60 (n = 20)	1.05 ± 0.72 (n = 8)	SD: e.s.d. P < 0.001
m	T_{onset}: 0 mM BAPTA vs perforated patch	(ms)	3.33 ± 0.62 (n = 6)	3.4 ± 0.69 (n = 4)	SD: n.s.d mean: n.s.d P = 0.38
n	T_{onset}: 0 vs 10 mM BAPTA	(ms)	3.33 ± 0.62 (n = 6)	4.9 ± 0.51 (n = 4)	SD: n.s.d mean: v.s.d P = 0.003
o	T_{onset}: 0 vs 5 mM BAPTA	(ms)	3.33 ± 0.62 (n = 6)	4.13 ± 0.53 (n = 4)	SD: n.s.d mean: n.s.d P = 0.06
p	T_{onset}: 5 vs 10 mM BAPTA	(ms)	4.13 ± 0.53 (n = 4)	4.9 ± 0.51 (n = 4)	SD: n.s.d mean: n.s.d P = 0.08

Table A1: A summary of the data used and the results obtained in two-tailed Student t-tests conducted to compare the means of two sets of data. e.s.d. = extremely significantly different, v.s.d. = very significantly different, s.d. = significantly different, n.q.s.d. = not quite significantly different, n.s.d = not significantly different. All data in the above table is from this thesis except in: test a, sample a - Dallos, (1986); test b, sample b - Mammano and Ashmore, (1996); test c, sample b - Housley and Ashmore, (1992); test g, sample a - Dallos, (1986).

Appendix 2

Calculation of K^+ depletion during a voltage step

The mathematical steps required to calculate the concentration of K^+ leaving a T1 OHC during a 40 ms step change in potential from -70 mV to 0 mV are shown below.

1) Number of mols of K^+ leaving the cell during a voltage pulse

8 nA of current flow out of the T1 OHC for 40 ms.

Therefore, 8 nA . 40 ms = $3.2\ 10^{-10}$ C flow in the interval or equivalently, using F = $9.64\ 10^4$ culombs.mol^{-1} = $\underline{3.2\ 10^{-15}\ mol}$

2) Volume of T4 OHC

volume of OHC = $l\pi r^2$ = 20 μm . π . 5 μm^2 = 1570 μm^3
= $1.57\ 10^{-15}\ m^3$ = $\underline{1.57\ pl}$

3) Concentration of K^+ leaving the OHC

concentration = mols/vol = $3.2\ 10^{-15}$ mols/$1.57\ 10^{-12}$ l = $\underline{2.03\ 10^{-3}\ mols}$

4) Effect of depleting the intracellular K^+ concentration by 2 mM on the equilibrium potential for K^+.

a) Control $E_k = 58 \log_{10} 144/4 = -90$ mV

b) K^+ depletion $E_k = 58 \log_{10} 142/4 = -89.9$ mV

Note: Refilling of the cell with $K^+$from the patch pipette was ignored in these calculations.

References

Adams, SR, Kao, JPY, Grynkiewicz, G, Tsien, RY (1988) Biologically useful chelators that release Ca^{2+} upon illumination *J. Am. Chem. Soc.* **110** 3212-3220

Apicella, S, Chen, S, Bing, R, Penniston, JT, Llinas, R, Hillman, DE (1997) Plasmalemmal ATPase calcium pump localizes to inner and outer hair bundles *Neuroscience* **79** 1145-1151

Art, JJ, Fettiplace, R (1987) Variation in the membrane properties in hair cells isolated from the turtle cochlea *J. Physiol.* **385** 207-242

Ashmore, JF (1992) Mammalian hearing and the cellular mechanisms of the cochlear amplifier In: *Sensory Transduction* Ed, COREY, DP, ROPER, SD pp 396-412 Rockefeller University Press

Ashmore, JF (1990) Forward and reverse transduction in the mammalian cochlea *Neurosci. Res.* **12** (suppl) 39-50

Ashmore, JF (1987) A mechanically evoked current in outer hair cells isolated from guinea-pig cochlea *J. Physiol.* **392** 37P

Ashmore, JF (1987) A fast motile response in guinea-pig outer hair cells: the cellular basis of the cochlear amplifier *J. Physiol.* **388** 323-347

Ashmore, JF (1983) Frequency tuning in the frog vestibular organ *Nature* **304** 536-538

Ashmore, JF, Kolston, PJ (1994) Hair cell based amplification in the cochlea *Current Biol.* **4** 503-508

Ashmore, JF, Kolston PJ, Mammano, F (1993) Dissecting components of the outer hair cell feedback loop In: *Biophysics of hair cell sensory systems* Ed, DUIFHUIS, H, HORST, JW, VAN DIJK, P, VAN NETTEN, SM pp 151-158 World Scientific

Ashmore, JF, Meech, RW (1986) Ionic basis of membrane potential in outer hair cells of guinea pig cochlea *Nature* **322** 368-371

Ashmore, JF, Ohmori, H (1990) Control of intracellular calcium by ATP in isolated outer hair cells of the guinea pig cochlea *J. Physiol* **428** 109-133.

Assad, JA, Shepherd, GMG, Corey, DP (1991) Tip-link integrity and mechanical transduction and vertebrate hair cells *Neuron* **7** 985-994

Atkinson, NS, Robertson, GA, Ganetzky, B (1991) A component of calcium-activated potassium channels encodod by the *Drosophila Slo* locus *Science* **253** 551-555

Barnes, S, Hille, B (1989) Ionic channels of the inner segment of tiger salamander cone photoreceptors *J. Gen. Physiol.* **91** 421-443

Baro, DJ, Levini, RM, Kim, MT, Willms, AR, Lanning, CC, Rodriguez, HE, Harris-Warrick, RM (1997) Quantitative single-cell-reverse transcription-PCR demonstrates that A-current magnitude varies as a linear function of *shal* gene expression in identified stomatogastric neurones *J. Neurosci.* **17** 6597-6610

Barry, PH, Lynch, JW (1991) Liquid Junction Potentails and small cell effects in patch-clamp analysis *J. Membrane Biol.* **121** 101-117

Boscher, SK, Warren, RL, (1978) Very low calcium content of cochlear endolymph, an extracellular fluid *Nature* **273** 377-378

Bosher, SK, Warren, RL (1968) Observations on the electrochemistry of the cochlear endolymph of the rat: a quantitative study of its electrical potential and ionic composition as determined by means of flame spectrophotometry *Proc. R. Soc. Lond. B* **171** 227-247

Brown, MC (1987a) Morphology of labeled afferent fibres in the guinea-pig cochlea *J. Comp. Neurol.* **260** 591-604

Brown, MC, Nuttall, AL (1984) Efferent control of cochlear inner hair cell responses in the guinea pig *J. Physiol.* **354** 625-646

Brownell, WE, Bader, CR, Bertrand, D, de Ribaupierre, Y (1985) Evoked mechanical responses of isolated cochlear hair cells *Science* **227** 194-196

Butler, A, Tsunoda, S, McCobb, DP, Wei, A, Salkoff, L (1993) *mSlo*, a complex mouse gene encoding 'maxi' calcium-activated potassium channels *Science* **261** 221-224

Chen, C, Nenov, A, Norris, CH, Bobbin, RP (1995) ATP modulation of L-type calcium channels currents in guinea pig outer hair cells *Hear. Res.* **86** 25-33

Cody, AR, Russell, IJ (1987) The responses of hair cells in the basal turn of the guinea-pig cochlea to all turns *J. Physiol.* **383** 551-569

Corey, DP, Hudspeth, AJ (1979) Ionic basis of the receptor potential in a vertebrate hair cell *Nature* **281** 675-677

Crawford, AC, Evans, MG, Fettiplace, R (1991) The actions of calcium on the mechano-electrical transducer current of turtle hair cells *J. Physiol.* **434** 369-398

Crawford, AC, Evans, MG, Fettiplace, R (1989) Activation and adaptation of transducer currents in turtle hair cells *J. Physiol.* **419** 405-434

Crawford, AC, Fettiplace, R (1981) An electrical tuning mechanism in turtle cochlear hair cells *J. Physiol.* **312** 377-412

Currie, KPM, Wootton, JF, Scott RH (1995) Activation of Ca^{2+}-depandent Cl^- currents in cultured rat sensort neurones by flash photolysis of DM-Nitrophen *J. Physiol.* **482** 291-307

Dallos, P (1996) Overview: Cochlear Neurobiology In: *The Cochlea* Ed, DALLOS, P, POPPER, AN, FAY, PP pp 1-43 Springer

Dallos, P (1986) Neurobiology of cochlear inner and outer hair cells: intracellular recordings *Hear. Res.* **22** 185-198

Dallos, P (1985) Response characteristics of mammalian cochlear hair cells *J. Neurosci.* **5** 1591-1608

Dallos, P, Billone, MC, Durrant, JD, Wong, CY, Raynor, S (1972) Cochlear inner and outer hair cells: functional differences *Science* **177** 356-358

Dallos, P, Evans, BN (1995) High-frequency motility of outer hair cells and the cochlear amplifier *Science* **267** 2006-2009

Dallos, P, Evans, BN, Halliworth, R (1991) Nature of the motor element in electrokinetic shape changes of cochlear outer hair cells *Nature* **350** 155-157

Davis, H (1983) An active process in cochlear mechanics *Hear. Res.* **9** 79-90

Denk, W, Holt, JR, Shepherd, GMA, Corey, DP (1995) Calcium imaging of single stereocilia in hair cells: localization of transduction channels at both ends of tip links *Neuron* **15** 1311-1321

Duszyk, M, Liu, D, Kamosinska, B, French, AS, Paul Man, SF (1995) Characterization and regulation of a chloride channel from bovine tracheal epithelium *J. Physiol.* **489** 81-93

Eatock, RA, Corey, DP, Hudspeth, AJ (1987) Adaptation of mechanoelectrical transduction in hair cells of the bullfrog's sacculus *J. Neurosci.* **7** 2821-2836

Eckert, R, Chad, JE (1984) Inactivation of Ca *channels* *Prog. Biophys. Mol. Biol.* **44** 215-267

Edwards, FA, Konnerth, A, Sakmann, B, Takahashi, T (1989) A thin slice preparation for patch clamp recordings from neurones of the mammalian central nervous system *Pflügers Arch.* **414** 600-612

Feng, J, Wible, B, Li, G-R, Wang, Z, Nattel, S (1997) Antisense oligodeoxynucleotides directed against Kv1.5 mRNA specifically inhibit ultrarapid delayed rectifier K^+ current in cultured adult human atrial myocytes *Circ. Res.* **80** 572-579

Fierro, L, Llano, I (1996) High endogenous calcium buffering in Purkinji cells from rat cerebellar slices *J. Physiol.* **496** 617-625

Fuch, PA, Evans, MG (1990) Potassium currents in hair cells isolated from the cochlear of the chick *J. Physiol.* **429** 529-551

Galambos, R, Davis, H (1943) The response of single audotory-nerve fibres to acoustic stimulation *J. Neurophys.* **6** 39-57

Gale, JE, Ashmore, JF (1997) An intrinsic frequency limit to the cochlear amplifier *Nature* **389** 63-66

Géléoc, GSG, Ashmore, JF (1998) Interaction between sugar transport and the mechanism of fast motility in guinea-pig outer hair cells *J. Physiol.* **511** 120P

Géléoc, GSG, Lennan, GWT, Richardson, GP, Kros, CJ (1997) A quantitative comparison of mechanoelectrical transduction in vestibular and auditory hair cells of neonatal mice *Proc. R. Soc. Lond.* B **264** 611-621

Gofa, A, Davidson,RM (1996) NaF potentiates a K^+-selective ion channel in G292 osteoblastic cells *J. Membrane Biol.* **149** 211-219

Greenwood, DD (1990) A cochlear frwquency-position function for several species - 29 years later *J. Acoust. Soc. Am* **87** 2592-2605

Grissmer, S, Nguyen, AN, Aiyar, J Hanson, DC, Mather, RJ, Gutman, GA, Karmilowicz, MJ, Auperin, DD, Chandy, KG (1994) Pharmacological characterization of five cloned voltage-gated K^+ channels, types Kv1.1, 1.2, 1.3, 1.5 and 3.1, stably expressed in mammalian cell lines *Mol. Pharm.* **45** 1227-1234

Guo, W, Kamiya, K, Liu, W, Toyama, J (1997) Developmental changes of the ultrarapid delayed rectifier K+ current in rat ventricular myocytes *Pflügers Arch.* **433** 442-445

Gurney, AM (1991) Photolabile calcium buffers to selectively activate calcium-dependent processes In *Cellular Neurobiology: a practical approach.* Eds: Chad, J, Wheal, H IRL Press at Oxford University Press pp 153-177

Hamill, OP, Marty, A, Neher, E, Sakmann B, Sigworth FJ (1981) Improved patch-clamp techniques for high-resolution current recording from cells and cell-free membrane patches *Pflügers Arch.* **391** 85-100

Helmholtz, H (1954) On the Sensations of Tone. Unabridged and unaltered republication of the second edition (1885) of the Ellis translation *'Die Lihre von den Tonempfindungen'* pp 146 Dover

Hille, B (1992) Potassium channels and chloride channels In: *Ionic channels of excitable membranes, second edition.* pp 62, pp116-121, pp 434-435 and pp 467 Sinauer Associates Inc

Hirose, K, Hockenbery, DM, Rubel, EW (1997) Reactive oxygen species in chick hair cells after gentamicin exposure in vitro *Hear. Res.* **104** 1-14

Holley, M (1990) Cell biology of hair cells *Seminars in the Neurosciences* **2** 41-48

Hoshi, T, Zagotta, WN, Aldrich, RW (1990) Biophysical and molecular mechanisms of *Shaker* potassium channel inactivation *Science* **250** 533-558

Housley, GD, Ashmore, JF (1992) Ionic conductances of outer hair cells isolated from the guinea-pig cochlea *J. Physiol.* **448** 73-98

Howard, J, Hudspeth, AJ (1988) Compliance of the hair bundle associated with gating of mechanoelectric transduction channels in the bullfrog's saccular hair cell *Neuron* **1** 189-199

Howard, J, Roberts, WM, Hudspeth, AJ (1988) Mechanoelectrical transduction by hair cells *Ann. Rev. Biophys. Biophys. Chem.* **17** 99-124

Huang, G, Santos-Sacchi, J (1993) Mapping the distribution of the outer hair cell motility voltage sensor by electrical amputation *Biophys. J.* **65** 2228-2236

Hudspeth, AJ (1989) How the ear's works work *Nature* **341** 397-404

Hudspeth, AJ (1982) Extracellular current flow and the site of transduction by vertebrate hair cells *J. Neurosci.* **2** 1-10

Hudspeth, AJ, Corey, DP (1977) Sensitivity, polarity and conductance change in the responses of vertebrate hair cells to controlled mechanical stimuli *Proc. Natl. Acad. Sci. USA* **74** 2407-2411

Hudspeth, AJ, Gillespie, PG (1994) Pulling springs to tune transduction: Adaptation by hair cells *Neuron* **12** 1-9

Hudspeth, AJ, Lewis, RS (1988) Kinetic analysis of and voltage- and ion-dependent conductances in saccular hair cells of the bull-frog, *Rana Catesbeiana* *J. Physiol.* **400** 237-274

Hudspeth, AJ, Markin, VS (1994) The ear's gears: Mechanoelectrical transduction by hair cells *Physics Today* **47** 22-28

Ikeda, K, Saito, Y, Nishiyama, A, Takasaka, T (1993) Na^{+}-Ca^{2+} exchange in the isolated cochlear outer hair cells if the guinea-pig studied by flourescence image microscopy *Pflügers Arch.* **420** 493-499

Iwasa, KH, Chadwick, RS (1992) Elasticity and active force generation of cochlear outer hair cells *J. Acoust. Soc. Am.* **92** 3169-3173

Jagger, DJ, Ashmore, JF (1999) Regulation of ionic currents by protein kinase A and interacellular calcium in outer hair cells isolated from the guinea-pig cochlea *Pflügers Arch.* **437** 409-416

Jan, LY, Jan, YN (1990) How might the diversity of potassium channels be generated? *TINS* **13** 415-419

Johnston, BM, Patuzzi, R, Yates, GK (1986) Basilar membrane measurements and the travelling wave *Hear. Res.* **22** 147-153

Kalinec, F, Holley, M, Iwasa, KH, Lim, DJ, Kachar, BA (1992) A membrane-based force generation in auditory sensory cells *Proc. Natl. Acad. Sci. USA* **89** 8671-8657

Kanis, LJ (1995) Cochlear Nonlinearity: a computational model of the cochlea solved in the frequency domain Thesis

Kaplan, JH, Ellis-Davies, GCR (1988) Photolabile chelators for the rapid photorelease of divalent cations *Proc. Natl. Acad. Sci. USA* **85** 6571-6575

Khanna, SM, Leonard, DG (1982) Basilar membrane tuning in the cat cochlea *Science* **215** 305-306

Khanna, SM, Willemin, J-F, Ulfendahl, M (1989) Measurement of optical reflectivity in cells of the inner ear. *Acta Otolaryngol (Stockh)* **467** (suppl.) 69-75

Kimitsuki, T, Ohmori, H (1993) Dihydrostreptomycin modifies adaptation and blocks the mechano-electric transducer in chick cochlear hair cells *Brain Res.* **624** 143-150

Kimura, R, Wersäll, J (1962) Termination fothe olivocochlear bundle in relation to the outer hair cells of th organ of Corti in guinea-pig *Acta Otolaryngol. (Stockh)* **55** 11-32

Kolston, PJ (1995) A faster transduction mechanism for the cochlear amplifier? *TINS* **18** 427-429

Kozel, PJ, Friedman, RA, Erway, LC, Yamoah, EN, Liu, LH, Riddle, T, Duffy, JJ, Doetschman, T, Miller, ML, Cardell, EL, Shull, GE Balance and hearing deficits in mice with a null mutation in the gene encoding plasma membrane Ca^{2+}-ATPase isoform 2 *J. Biol. Chem.* **273** 18693-18696

Krose, ABA, Das, A, Hudspeth, AJ (1989) Blockages of the transduction channels of hair cells in the bullfrog's sacculus by aminoglycoside antibiotics *Hear. Res.* **37** 203-218

Kros, CJ (1996) Physiology of mammalian cochlear hair cells In: The Cochlea: Springer handbook of auditory research Ed, DALLOS, P, POPPER, AN, FAY, RR pp 318-385 Springer

Kros, CJ, Crawford, AC (1990) Potassium currents in inner hair cells isolated from the guinea-pig cochlea *J. Physiol.* **421** 263-291

Kros, CJ, Rüsch, A, Richardson, GP (1992) Mechano-electrical transducer currents in hair cells of the cultured neonal mouse cochlea *Proc. R. Soc. Lond.* B **249** 185-193

Lancaster, B, Zuker, RS (1993) Photolytic manipulation of Ca^{2+} and the time course of slow, Ca^{2+}-activated K^+ current in rat hippocampal neurones *J. Physiol.* **475** 229-239

Lim, DJ (1980) Cochlear anatomy related to cochlear micromechanics. A review. *J. Acoust. Soc. Am.* **67** 1686-1695

Liu, TC (1997) Measurement of $[Ca^{2+}]_i$ and $[Na^+]_i$ in outer hair cells isolated from gerbil cochlea *J. Oto-Rhino-Laryng. And Rel. Species* **56** 322-325

Locke, RE, Nerbonne, JM (1997) Three kinetically distinct Ca^{2+}-independent depolarization-activated K^+ currents in callosal-projecting rat visual cortical neurones *J. Neurophysiol.* **78** 2309-2320

Mammano, F, Ashmore, JF (1996) Differential expression of outer hair cell potassium currents in the isolated cochlea of the guinea-pig *J. Physiol.* **496** 639-646

Mammano, F, Ashmore, JF (1995) A laser interferometer for sub-nanometer measurements in the cochlea *J. Neurosci. Meth.* **60** 89-94

Mammano, F, Ashmore, JF (1993) Reverse transduction measured in the isolated cochlea by Michaelson interferometry *Nature* **365** 838-841

Mammano,F, Goodfellow, SJ, Foutain, E (1996) Electrophysiological properties of Hensen's cells investigated *in situ* *Neuroreport* **7** 537-542

Mammano, F, Kros, CJ, Ashmore, JF (1995) Patch clamped responses from outer hair cells in the intact adult organ of Corti *Pflügers Arch.* **430** 745-750

Marty, A (1981) Ca-dependent K channels with large unitary conductance in chromaffin cell membranes *Nature* **291** 497-500

Maruyama, Y, Gallacher, DV, Petersen, OH (1983) Voltage and Ca^{2+}-activated K^+ channel in baso-lateral acinar cell membranes of mammalian salivary glands *Nature* **302** 827-829

Massengill, JL, Smith, MA, Son, DI, O'Dowd, DK (1997) Differential expression of K4-AP currents and Kv3.1 potassium channel transcripts in cortical neurones that develop distinct firing phenotypes *J. Neurosci.* **17** 3136-3147

Meech, RW (1974) The sensitivity of *Helix Aspersa* neurones to injected calcium ions *J. Physiol.* **237** 259-277

Meyer, J, Furness, DN, Zenner, H-P, Hackney, CM, Gummer, AW (1998) Evidence for opening of hair-cell transducer channels after tip-link loss *J. Neurosci.* **18** 6748-6756

Miledi, R (1982) A calcium-dependent transient outward current in Xenopus laevis oocytes *Proc. R. Soc. Lond. B* **215** 491-497

Miyamoto, K, Tatsumi, S, Sonoda, T, Yamamoto, H, Minami, H, Taketani, Y, Takeda, E (1995) Cloning and functional expression of a Na(+)-dependent phosphate co-transporter from human kidney: cDNA cloning and functional expression *Biochem.J.* **305** 81-85

Nakagawa, T, Kakahata, S, Akaike, N, Komune, S, Takasaka, T, Uemura, T (1994) Voltage-dependent channels in dissociated outer hair cells of the guinea pig *Eur. Arch. Otorhinolaryngol.* **251** S57-S60

Nakagawa, T, Kakahata, S, Akaike, N, Komune, S, Takasaka, T, Uemura, T (1991) *Neurosci. Lett.* **125** 81-84

Natall, AL, Dolan, DF (1993) Basilar membrane velocity responses to acoustiv and intracochlear electrical stimuli In: *Biophysics of hair cell sensory systems* Ed, DUIFHUIS, H, HORST, JW, VAN DIJK, P, VAN NETTEN, SM pp 288-295 World Scientific

Navaratnam, DS, Bell, TJ, Tu, TD, Cohen, EL, Oberholtzer, CJ (1997) Differential distribution of Ca^{2+}-activated K^+ channel splice varients among hair cells along the tonotopic axis of the chick cochlea *Neuron* **19** 1077-1085

Nenov, AP, Norris, C, Bobbin, RC (1997) Outwardly rectifying currents in guinea-pig outer hair cells *Hear. Res.* **105** 146-158

Niggli, E, Lipp, P (1994) Voltage dependance of Na-Ca exchanger conformational currents *Biophys. J.* **67** 1516-1524

Nobili, R, Mammano, F (1996) Biophysics of the cochlea II: Stationalry nonlinear phenomenology *J. Acoust. Soc. Am.* **99** 2244-2255

Ohmori, H (1985) Mechano-electrical transduction currents in isoltaed vestibular hair cells of the chick *J. Physiol.* **359** 189-217

Ohmori, H (1984) Studies of ionic currents in the isolated vestibular hair cell of the chick *J. Physiol.* **350** 561-581

Pack, AK, Slepecky, NB (1995) Cytoskeletal and calcium-binding proteins in the mammalian organ of Corti; cell type-specific proteins displaying longitudinal and radial gradients *Hear. Res.* **91** 119-135

Parsons, TD, Ellis-Davies, GCR, Almers, W (1996) Millisecond studies of calcium-dependent exocytosis in pituitary melanotrophs: comparison of the photolabile calcium chelators nitrophenyl-EGTA and DM-Nitrophen *Cell Calcium* **19** 185-192

Paton, JFR (1996) A working heart-brainsten preparation of the mouse *J. Neurosci. Methods* **65** 63-68

Pickles, JO (1988) An introduction to the physiology of hearing 2^{nd} Ed. pp 27 Academic Press

Pickles, JO, Comis, SD, Osborne, MD (1984) Cross-links between stereocilia in the guinea-pig organ of Corti and their possible relation to sensory transduction *Hear. Res.* **15** 103-112

Pujol, R, Lenoir, M, Ladrech, S, Tribillac, F, Rebillard, G (1992) Correlation between the length of outer hair cells and the frequency coding of the cochlea In: *Auditory Physiology and Perception*, Ed, CAZALS, Y, DEMENY, L, HORNER, K pp 45-52 Pergamon Press

Pusch, M, Neher, E (1988) Rates of diffusional exchange between small cells and a measuring patch pipette *Pflügers Arch.* **411** 204-211

Rae, J, Cooper, K, Gates, P, Wataky, M (1991) Low access resistance perforated patch recordings using amphotericin B *J. Neurosci. Methods* **37** 15-26

Raybould, NP, Housley, GD (1997) Variation in expression of the outer hair cell P2X receptor conductance along the guinea-pig cochlea *J. Physiol.* **498** 717-727

Rennie, KJ, Ashmore, JF (1991) Ionic currents in isolated vestibular hair cells from the guinea-pig crista ampullaris *Hear. Res.* **51** 279-292

Ricci, AJ, Fettiplace, R, (1997) The effects of calcium buffering and cyclic AMP on mechanoelectric transduction in turtle auditory hair cells *J. Physiol.* **501** 111-124

Ricci, AJ, Wu, Y-C, Fettiplace, R (1998) The endogenous calcium buffer and the time course of transducer adaptation in auditory hair cells *J. Neurosci.* **18** 8261-8277

Roberts, WM (1994) Localization of calcium signals by a mobile calcium buffer in frog saccular hair cells *J. Neurosci.* **14** 3246-3262

Roberts, WM (1993) Spatial calcium buffering in saccular hair cells *Nature* **363** 74-76

Roberts, WM, Jacobs, RA, Hudspeth, AJ (1991) The hair cell as a presynaptic terminal *Ann. NY Acad. Sci.* **635** 221-233

Rosenblatt, KP, Sun, Z-P, Heller, S, Hudspeth, AJ (1997) Distribution of Ca^{2+} activated K^+ channel isoforms along the tonotopic gradient of the chicken's cochlea *Neuron* **19** 1061-1075

Rüsch, A, Eatock, RA (1996) A delayed rectifier conductance in type I hair cells of the mouse utricle *J.Neurophysiol.* **76** 995-1004

Ryan, A, Dallos, P (1975) Absence of cochlear outer hair cells: effect on behavioral auditory threshold *Nature* **253** 44-46

Salkoff, L, Baker, K, Butler, A, Covarrubias, M, Pak, MD, Wei, A (1992) An essential 'set' of K^+ channels conserved in flies, mice and humans *TINS* **15** 161-166

Santos-Sacchi, J (1992) On the frequency limit and phase of outer hair cell motility: the effects of the membrane filter *J. Neurosci.* **12** 1906-1916

Santos-Sacchi, J (1989) Asymmetry in voltage-dependent movements of isolated outer hair cells from the Organ of corti *J. Neurosci.* **9** 2954-2962

Santos-Sacchi, J, Diliger, JP (1988) Whole cell currents and mechanical responses of isolated outer hair cells *Hear. Res.* **35** 143-150

Santos-Sacchi, J, Huang, G-J, Wu, M (1997) Mapping the distribution of outer hair cell voltage-dependent condutances by electrical amputation *Biophys. J.* **73** 1424-1429

Schmiedt, RA, Zwislocki, JJ, Hamemik, RP (1980) Effects of hair cell lesions on responses of cochlear nerve fibres. I. Lesions, tuning curves, two-tone inhibition and responses to trapezoid wave patterns *J. Neurophysiol.* **43** 1367-1389

Schulte, BA (1993) Immunohistochemical localization of intracellular Ca-ATPase in outer hair cells, neurones and fibrocytes in the adult and developing inner ear *Hear. Res.* **65** 262-273

Sellick, PM, Patuzzi, RB, Johnstone, BM (1982) Measurement of basilar membrane motion in guinea-pig using the Mössbauer technique *J. Acoust. Soc. Am.* **72** 131-141

Shotwell, SL, Jacobs, R, Hudspeth, AJ (1981) Directional sensitivity of individual vertebrate hair cells and controlled deflections of their hair bundles *Ann. N. Y. Acad. Sci.* **374** 1-10

Slepecky, NB (1996) Cochlear Structure In: *The Cochlea* Ed, DALLOS, P, POPPER, AN, FAY, PP pp 44-129 Springer

Song, W-J, Tkatch, T, Baranauskas, G, Ichinohe, N, Kitai, ST, Surmeier, DJ (1998) Somatodendritic depolarization-activated potassium currents in the rat neostrital cholinergic interneurones are predominantly of the a type and attibutable to coexpression of Kv4.2 and Kv4.1 subunits *J. Neurosci.* **18** 3124-3137

Spoendlin, H (1972) Innervation densities of the cochlea *Acta Otolaryngol.* **73** 235-248

Storm, JF (1988) Temporal integration by a slowly inactivating K+ component in hippocampal neurones *Nature* **336** 379-381

Sugihara, I (1994) Calcium-activated potassium channels in goldfish hair cells *J. Physiol.* **476** 373-390

Tucker, T, Fettiplace, R (1995) Confocal imaging of calcium microdomains and calcium extrusion in turtle hair cells *Neuron* **15** 1323-1335

Todorovic, SM, Lingle, CJ (1998) Pharmacological properties of T-type Ca^{2+} current in adult rat sensory neurones: Effects of anticonvulsant and anesthetic agents *J. Neurophys.* **78** 240-252

Tunstall, MJ, Gale, JE, Ashmore, JF (1995) Action of salicylate on membrane capacitance of outer hair cells from the guinea-pig cochlea *J. Physiol.* **485** 739-752

Van den Abbeele, T, Tran Ba Huy, P, Teulon, J (1994) A calcium-activated nonselective cationic channel in the basolateral membrane of outer hair cells of the guinea-pig cochlea *Pflügers Arch.* **417** 56-63

Von Békésy (1960) Experiments in Hearing Translated and edited by Weaver, EG Chapter11 The pattern of vibrations in the cochlea McGraw-Hill Book Company

Wang, L-Y, Gan, L, Forsythe, ID, Kaczmarek, LK (1998) Contribution of the Kv3.1 potassium channel to high-frequency firing in mouse auditory neurones *J. Physiol.* **509** 183-194

Wang, SSH, Thompson, SH (1995) Local positive feedback by calcium in the propogation of intracellular calcium waves *Biophys. J.* **69** 1683-1697

Wu, R-L, Barish, ME Two pharmacologically and kinetically distinct transient potassium currents in cultured embryonic mouse hippocampal *neurones* *J. Neurosci.* **12** 2235-2246

Xue, S, Moutain, DC, Hubbard, AE (1993) Direct measurement of electrically evoked basilar membrane motion In: *Biophysics of hair cell sensory systems* Ed, DUIFHUIS, H, HORST, JW, VAN DIJK, P, VAN NETTEN, SM pp 361-369 World Scientific

Yamoah, EN, Lumpkin, EA, Dumont, RA, Smith, PJS, Hudspeth, AJ, Gillespie, PG (1998) Plasma membrane Ca^{2+}-ATPase extrudes Ca^{2+} from hair cell stereocilia *J. Neurosci.* **18** 610-624

Yue, L, Feng, J, Li, G-R, Nattel, S (1996) Characterization of an ultradelayed rectifier potassium channel involved in canine atrial repolarization *J. Physiol.* **496** 647-662

Zhao, Y, Yamoah, EN, Gillespie, PG (1996) Regeneration of broken tip-links and restoration of mechanical transduction in hair cells *Proc. Natl. Acad. Sci. USA* **93** 15469-15474

Zhou, Z, Neher, E (1993) Mobile and immobile calcium buffers in bovine adrenal chromaffin cells *J. Physiol.* **469** 245-273